CERN-EP/2016-284
2017/05/22

CMS-SUS-16-008

Searches for pair production of third-generation squarks in $\sqrt{s} = 13$ TeV pp collisions

The CMS Collaboration*

Abstract

Searches are presented for direct production of top or bottom squark pairs in proton-proton collisions at the CERN LHC. Two searches, based on complementary techniques, are performed in all-jet final states that are characterized by a significant imbalance in transverse momentum. An additional search requires the presence of a charged lepton isolated from other activity in the event. The data were collected in 2015 at a centre-of-mass energy of 13 TeV with the CMS detector and correspond to an integrated luminosity of 2.3 fb^{-1} . No statistically significant excess of events is found beyond the expected contribution from standard model processes. Exclusion limits are set in the context of simplified models of top or bottom squark pair production. Models with top and bottom squark masses up to 830 and 890 GeV, respectively, are probed for light neutralinos. For models with top squark masses of 675 GeV, neutralino masses up to 260 GeV are excluded at 95% confidence level.

Published in the European Physical Journal C as doi:10.1140/epjc/s10052-017-4853-2.

1 Introduction

The standard model (SM) has been extremely successful at describing particle physics phenomena. Nevertheless, it suffers from shortcomings such as the hierarchy problem [1–6], the need for fine-tuned cancellations of large quantum corrections to keep the Higgs boson mass near the electroweak scale. Supersymmetry (SUSY), based on a symmetry between bosons and fermions, is an attractive extension of the SM. A key feature of SUSY is the existence of a superpartner for every SM particle with the same quantum numbers, except for spin, which differs by one half unit. In R-parity conserving SUSY models [7, 8], supersymmetric particles are created in pairs, and the lightest supersymmetric particle (LSP) is stable [9, 10] and considered to be a candidate for dark matter [11]. Supersymmetry can potentially provide a “natural”, i.e. not fine-tuned, solution to the hierarchy problem through the cancellation of quadratic divergences in particle and sparticle loop corrections to the Higgs boson mass. In natural SUSY models light top and bottom squarks with masses close to the electroweak scale are preferred.

This paper presents three complementary searches for direct production of a pair of top ($\tilde{t}_1\tilde{t}_1$) or bottom squarks ($\tilde{b}_1\tilde{b}_1$), where the subscript here denotes the less massive partner of the corresponding SM fermion’s chirality states. The first search targets top squark pair production in the all-jet final state, while the second focuses on the single-lepton final state. These two analyses were explicitly designed for complementarity, allowing for a combination of the results to enhance the sensitivity. The third search targets bottom squark pair production in the all-jet final state. The searches are performed using the data collected in proton-proton collisions at a centre-of-mass energy of 13 TeV with the CMS detector at the CERN LHC in 2015, corresponding to an integrated luminosity of 2.3 fb^{-1} . The results of similar searches were previously reported by the ATLAS and CMS collaborations using proton-proton collisions at 7 and 8 TeV [12–25] and by the CDF and D0 collaborations in $p\bar{p}$ collisions at 1.96 TeV at the Fermilab Tevatron [26–30]. With the increase in LHC collision energy from 8 to 13 TeV, the cross section to produce signal events is enhanced by a factor of 8–12 for a top or bottom squark mass in the range 700–1000 GeV [31, 32]. Therefore, new territory can be explored even with the relatively small amount of data collected in 2015. The CMS and ATLAS collaborations have already provided first exclusion results for these models in the all-jet and single-lepton final states [33–36]. Unlike the more generic searches for new phenomena presented by the CMS collaboration in Refs. [33–35], the searches described in this paper directly target top and bottom squark production through the design of search regions that exploit the specific characteristics of these signal models, for instance through the use of a top quark tagging algorithm in the top squark search in the all-jet final state to identify boosted hadronically decaying top quarks originating from top squark decays.

The decay modes of top squarks depend on the sparticle mass spectrum. Figure 1 illustrates the top and bottom squark decay modes explored in this paper. The simplest top squark decay modes are $\tilde{t}_1 \rightarrow t^{(*)}\tilde{\chi}_1^0$ and $\tilde{t}_1 \rightarrow b\tilde{\chi}_1^\pm \rightarrow bW^{\pm(*)}\tilde{\chi}_1^0$, with $\tilde{\chi}_1^\pm$ representing the lightest chargino, and with intermediate particles that can be virtual marked by asterisks. In these decay modes, the neutralino and charginos are mixtures of the superpartners of electroweak gauge and Higgs bosons, and $\tilde{\chi}_1^0$ is considered to be an LSP that escapes detection, leading to a potentially large transverse momentum imbalance in the detector. The two analyses of top squark pair production in the all-jet and single-lepton final states probe both of these \tilde{t}_1 decay modes. In the $\tilde{t}_1 \rightarrow t^{(*)}\tilde{\chi}_1^0$ decay mode, the top quark is produced off-shell when $\Delta m \equiv m_{\tilde{t}_1} - m_{\tilde{\chi}_1^0} < m_t$, while in the $\tilde{t}_1 \rightarrow b\tilde{\chi}_1^\pm$ decay mode, the experimental signature is affected by the mass of the chargino. We consider a model in which both top squarks decay via the $\tilde{t}_1 \rightarrow t^{(*)}\tilde{\chi}_1^0$ decay mode. A second model in which the branching fraction for each of the two top squark decay modes is 50%

is also considered, under the assumption of a compressed mass spectrum in which the mass of $\tilde{\chi}_1^\pm$ is only 5 GeV greater than that of $\tilde{\chi}_1^0$, with the W bosons resulting from chargino decays consequently being produced heavily off-shell. If $\Delta m < m_W$, \tilde{t}_1 can decay through a four-body decay involving an SM fermion pair $f\bar{f}$ as $\tilde{t}_1 \rightarrow f\bar{f}\tilde{\chi}_1^0$, or through a flavour changing neutral current decay $\tilde{t}_1 \rightarrow c\tilde{\chi}_1^0$. The analysis of bottom squark pair production considers the decay mode $\tilde{b}_1 \rightarrow b\tilde{\chi}_1^0$ within the allowed phase space, and also probes top squark pair production in the $\tilde{t}_1 \rightarrow c\tilde{\chi}_1^0$ decay scenario.

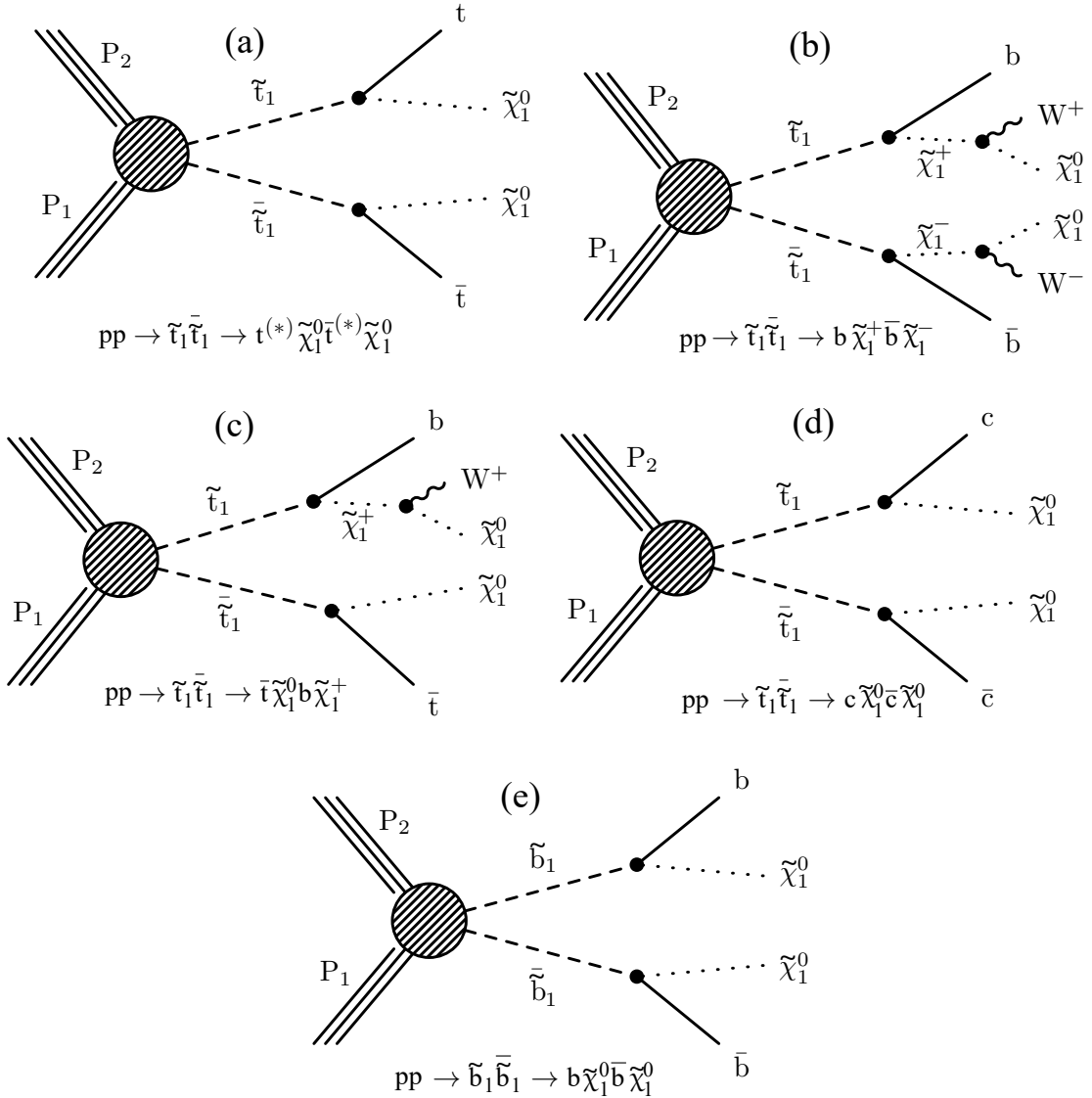


Figure 1: Feynman diagrams for pair production of top and bottom squarks via the decay modes considered in this paper. The model with 50% branching fractions for $\tilde{t}_1 \rightarrow t^{(*)} \tilde{\chi}_1^0$ and $\tilde{t}_1 \rightarrow b \tilde{\chi}_1^\pm \rightarrow b W^{\pm*} \tilde{\chi}_1^0$ decays leads to the final states in diagrams (a)–(c).

This paper is organized as follows. Section 2 contains a brief description of the CMS detector, while Section 3 discusses the event reconstruction and simulation. Sections 4, 5, and 6 present details for the all-jet top squark search, the single-lepton top squark search, and the all-jet bottom squark search, respectively. Section 7 describes the systematic uncertainties affecting the

results of the three analyses. The interpretation of the results in the form of exclusion limits on models of top or bottom squark pair production is discussed in Section 8, followed by a summary in Section 9.

2 The CMS detector

The central feature of the CMS apparatus is a superconducting solenoid of 6 m internal diameter, providing a magnetic field of 3.8 T. Within the solenoid volume are an all-silicon pixel and strip tracker, a lead tungstate crystal electromagnetic calorimeter (ECAL), and a brass and scintillator hadron calorimeter (HCAL), each composed of a barrel and two endcap sections. Forward calorimeters extend the pseudorapidity (η) coverage provided by the barrel and endcap detectors. Muons are measured in gas-ionization detectors embedded in the steel flux-return yoke outside the solenoid. The first level of the CMS trigger system, composed of custom hardware processors, uses information from the calorimeters and muon detectors to select the most interesting events in a fixed time interval of less than 4 μ s. The high-level trigger processor farm further decreases the event rate from around 100 kHz to around 1 kHz, before data storage. A more detailed description of the CMS detector, together with a definition of the coordinate system used and the relevant kinematic variables, can be found in Ref. [37].

3 Reconstruction algorithms and simulation

Event reconstruction uses the particle-flow (PF) algorithm [38, 39], combining information from the tracker, calorimeter, and muon systems to identify charged hadrons, neutral hadrons, photons, electrons, and muons in an event. The missing transverse momentum, \vec{p}_T^{miss} , is computed as the negative vector sum of the transverse momenta (\vec{p}_T) of all PF candidates reconstructed in an event, and its magnitude E_T^{miss} is an important discriminator between signal and SM background. Events selected for the searches are required to pass filters designed to remove detector- and beam-related noise and must have at least one reconstructed vertex. Usually more than one such vertex is reconstructed, due to pileup, i.e. multiple pp collisions within the same or neighbouring bunch crossings. The reconstructed vertex with the largest $\sum p_T^2$ of associated tracks is designated as the primary vertex.

Charged particles originating from the primary vertex, photons, and neutral hadrons are clustered into jets using the anti- k_T algorithm [40] implemented in FastJet [41] with a distance parameter of 0.4. The jet energy is corrected to account for the contribution of additional pileup interactions in an event and to compensate for variations in detector response [41, 42]. Jets considered in the searches are required to have their axes within the tracker volume, within the range $|\eta| < 2.4$.

Jets originating from b quarks are identified with the combined secondary vertex (CSV) algorithm [43, 44] using two different working points, referred to as “loose” and “medium”. The b tagging efficiency for jets originating from b quarks is about 80% and 60% for the loose and medium working point, respectively, while the misidentification rates for jets from charm quarks, and from light quarks or gluons are about 45% and 12%, and 10% and 2%, respectively.

The “CMS top (quark) tagging” (CTT) algorithm [45–47] is used to identify highly energetic top quarks decaying to jets with the help of observables related to jet substructure [48, 49] and mass. For a relativistic top quark with a Lorentz boost $\gamma = E/m$, the W boson and b quark produced in the top quark decay are expected to be separated by a distance $R \equiv \sqrt{(\Delta\eta)^2 + (\Delta\phi)^2} \approx 2/\gamma$ (where ϕ is the azimuthal angle in radians). In cases where the W boson subsequently

decays hadronically, the three resulting jets from the W boson decay and the hadronization of the b quark are likely to be merged into a single jet by a clustering algorithm with a distance parameter larger than $2/\gamma$. To identify hadronically decaying top quarks with $p_T > 400$ GeV, we therefore use jets reconstructed using the anti- k_T algorithm with a distance parameter of 0.8 to try to cluster the top quark decay products into a single jet. The next step of top quark reconstruction is an attempt to decompose the candidate jet into at least three subjets with the help of the Cambridge-Aachen jet clustering algorithm [50, 51], the invariant mass of which is required to be consistent with the top quark mass (140–250 GeV). The final requirement of top quark identification is that the minimum invariant mass of any pair of the three subjets with the highest p_T must exceed 50 GeV. The efficiency of the CTT algorithm to identify jets originating from top quark decays is measured to be about 30–40% while the misidentification rate is found to be about 4–6%, depending on the p_T of the top quark candidates. No disambiguation is performed between top quark candidates and jets reconstructed with a distance parameter of 0.4.

Electron candidates are reconstructed by first matching clusters of energy deposited in the ECAL to reconstructed tracks. Selection criteria based on the distribution of the shower shape, track-cluster matching, and consistency between the cluster energy and track momentum are then used in the identification of electron candidates [52]. Muon candidates are reconstructed by requiring consistent hit patterns in the tracker and muon systems [53]. Electron and muon candidates are required to be consistent with originating from the primary vertex by imposing restrictions on the size of their impact parameters in the transverse plane and longitudinal direction with respect to the beam axis. The relative isolation variable I_{rel} for these candidates is defined as the scalar sum of the transverse momenta of all PF candidates, excluding the lepton, within a p_T -dependent cone size of radius R around the candidate's trajectory, divided by the lepton p_T . The size R depends on lepton p_T as follows:

$$R = \begin{cases} 0.2, & p_T \leq 50 \text{ GeV}, \\ 10 \text{ GeV} / p_T, & 50 < p_T < 200 \text{ GeV}, \\ 0.05, & p_T \geq 200 \text{ GeV}. \end{cases} \quad (1)$$

The shrinking cone radius for higher- p_T leptons allows us to maintain high efficiency for the collimated decay products of boosted heavy objects. The isolation sum is corrected for contributions originating from pileup interactions through an area-based estimate [42] of the pileup energy deposited in the cone.

Hadronically decaying τ lepton (τ_h) candidates are reconstructed using the CMS hadron-plus-strips (HPS) algorithm [54]. The constituents of the reconstructed jets are used to identify individual τ lepton decay modes with one charged hadron and up to two neutral pions, or three charged hadrons. The presence of extra particles within the jet, not compatible with the reconstructed decay mode, is used as a criterion to discriminate τ_h decays from other jets.

Photon candidates are reconstructed from energy deposited in the ECAL, and selected using the distribution of the shower shape variable, the photon isolation, and the amount of leakage of the photon shower into the HCAL [55].

Monte Carlo (MC) simulations of events are used to study the properties of SM backgrounds and signal models. The MADGRAPH 5_aMC@NLO 2.2.2 generator [56] is used in leading-order (LO) mode to simulate events originating from $t\bar{t}$, W +jets, Z +jets, γ +jets, and quantum chromodynamics multijet processes ('QCD'), as well as signal events, based on LO NNPDF3.0 [57] parton distribution functions (PDFs). Single top quark events produced in the tW channel and

$t\bar{t}$ samples used in the single-lepton analysis are generated at next-to-leading order (NLO) with POWHEG v2 [58–61], while rare SM processes such as $t\bar{t}Z$ and $t\bar{t}W$ are generated at NLO using the MADGRAPH 5_aMC@NLO 2.2.2 program, using NLO NNPDF3.0 PDFs. Parton showering and hadronization is generated using PYTHIA8.205 [62]. The response of the CMS detector for the SM backgrounds is simulated via the GEANT4 [63] package. The CMS fast simulation package [64] is used to simulate all signal samples, and is verified to provide results that are consistent with those obtained from the full GEANT4-based simulation. Event reconstruction is performed in the same manner as for collision data. A nominal distribution of pileup interactions is used when producing the simulated samples. The samples are then reweighted to match the pileup profile observed in the collected data. The signal production cross sections are calculated using NLO with next-to-leading logarithm (NLL) soft-gluon resummation calculations [31]. The most precise cross section calculations are used to normalize the SM simulated samples, corresponding most often to next-to-next-to-leading order (NNLO) accuracy.

4 Search for top squarks in the fully-hadronic final state

The top squark search in the all-jet final state is characterized by the categorization of events into exclusive search regions based on selection criteria applied to kinematic variables related to jets and E_T^{miss} , and the use of the CTT algorithm to identify boosted top quark candidates. The main backgrounds in the search regions are estimated from dedicated data control samples.

4.1 Analysis strategy

The events in this analysis are recorded using a trigger that requires the presence of two or more energetic jets within the tracker acceptance and large E_T^{miss} . To be efficient, events selected offline are therefore required to have at least two jets with $p_T > 75$ GeV, $|\eta| < 2.4$, and $E_T^{\text{miss}} > 250$ GeV. In order to reduce SM backgrounds with intrinsic E_T^{miss} such as leptonic $t\bar{t}$ and W +jets events, we reject events with isolated electrons or muons that have $p_T > 5$ GeV, $|\eta| < 2.4$, and I_{rel} less than 0.1 or 0.2, respectively. The contribution from events in which a W boson decays to a τ lepton is reduced by rejecting events containing isolated charged-hadron PF candidates with $p_T > 10$ GeV and $|\eta| < 2.5$ that are consistent with τ_h decays. The isolation requirement applied is based on a discriminant obtained from a multivariate boosted decision tree (BDT) trained to distinguish the characteristics of charged hadrons originating from τ_h decays. The transverse mass M_T of the system comprising the charged-hadron PF candidate and \vec{p}_T^{miss} is required to be less than 100 GeV assuring consistency with τ_h originating from a W boson decay, to minimize loss of signal at high jet multiplicity. The transverse mass for a particle q (in this case, the τ_h candidate) is defined as:

$$M_T(q, \vec{p}_T^{\text{miss}}) \equiv \sqrt{2q_T E_T^{\text{miss}} (1 - \cos \Delta\phi)}, \quad (2)$$

with q_T denoting the particle transverse momentum, and $\Delta\phi$ the azimuthal separation between the particle and \vec{p}_T^{miss} .

Events selected for the search sample must also have at least five jets with $p_T > 20$ GeV, at least two of which must be b-tagged satisfying the loose working point of the CSV algorithm, with one or more of them required to additionally satisfy the medium working point. In addition, the absolute value of the azimuthal angle between \vec{p}_T^{miss} and the closest of the four highest- p_T (leading) jets, $\Delta\phi_{1234}$, must be at least 0.5. An imbalance in event p_T is produced in QCD events through a mismeasurement of jet p_T , and is often aligned with one of the leading jets in the event. The requirement on $\Delta\phi_{1234}$ therefore greatly reduces the contribution of the QCD

background. The set of selection criteria defined above will be referred to as the “baseline selection” for this search.

After imposing the baseline selection, we subdivide the event sample into categories based on kinematic observables related to jets and E_T^{miss} to improve the power of the analysis to discriminate between signal and the remaining SM background. The dominant sources of SM background are $t\bar{t}$, W +jets, and Z +jets events. The contribution from $t\bar{t}$ and W +jets processes arises from events with W bosons decaying leptonically, in which the charged lepton either falls outside of the kinematic acceptance, or, in most cases, evades identification, and may be reconstructed as a jet. Large E_T^{miss} can be generated by the associated neutrino, allowing such events to satisfy the baseline selection criteria. This background is collectively referred to as the “lost-lepton background”. Contributions arising from $t\bar{t}W$ and single top quark processes also enter this category, but with lesser importance. The contributions from Z +jets and $t\bar{t}Z$ events arise when the Z boson decays to neutrinos, producing thereby a significant amount of E_T^{miss} . The QCD background is reduced to a subdominant level by the requirements of the baseline selection.

In $t\bar{t}$ events with a lost lepton, the transverse mass of the b quark \vec{p}_T^{miss} system arising from the same top quark decay as the lost lepton has a kinematic endpoint at the mass of the top quark. The observable $M_T(b_{1,2}, \vec{p}_T^{\text{miss}})$ is defined as

$$M_T(b_{1,2}, \vec{p}_T^{\text{miss}}) \equiv \min[M_T(b_1, \vec{p}_T^{\text{miss}}), M_T(b_2, \vec{p}_T^{\text{miss}})], \quad (3)$$

where b_1, b_2 are the two selected b -tagged jets with highest values in the CSV discriminant. Imposing a minimum requirement of 175 GeV on $M_T(b_{1,2}, \vec{p}_T^{\text{miss}})$ reduces a significant portion of the $t\bar{t}$ background, but also results in a loss in signal efficiency for models with small Δm , as seen in Fig. 2, in which signal models with different top squark and neutralino mass hypotheses are shown, with the first number indicating the assumed top squark mass in units of GeV and the second the neutralino mass. To benefit from the separation power provided by this variable, we define two search categories, one with $M_T(b_{1,2}, \vec{p}_T^{\text{miss}}) \geq 175$ GeV, taking advantage of the corresponding reduction in $t\bar{t}$ background for signal models with large Δm , and another with $M_T(b_{1,2}, \vec{p}_T^{\text{miss}}) < 175$ GeV to retain the statistical power of events populating the low- $M_T(b_{1,2}, \vec{p}_T^{\text{miss}})$ region for models with small Δm .

Signal events with all-jet top quark decays should have at least six jets in the final state, although in the case of signals with compressed mass spectra these jets can be too soft in p_T to satisfy the jet selection threshold. Additional jets may be produced through initial-state radiation (ISR). The jet multiplicity is lower for the semileptonic $t\bar{t}$ background, as well as for the other backgrounds remaining after the baseline selection. A requirement of higher reconstructed jet multiplicity therefore improves the discrimination of signal events from the SM background. We consider two regions in jet multiplicity for the analysis, a high- N_j region (≥ 7 jets) that benefits from this improved discrimination, and a medium- N_j region (5–6 jets) to preserve signal events with fewer reconstructed jets. The high- N_j region in conjunction with the low threshold on the p_T of selected jets improves sensitivity for signal models with soft decay products in the final state.

In the high- $M_T(b_{1,2}, \vec{p}_T^{\text{miss}})$ category, requiring the presence of at least one top quark reconstructed by the CTT algorithm ($N_t \geq 1$) ensures a high-purity selection of signal events with highly boosted top quarks, at the sacrifice of some loss in signal efficiency. To benefit from this high-purity region, without giving up signal events that would enter the $N_t = 0$ region, we use both regions to extract the final signal. Figure 2 shows the N_t distribution for events in the high- $M_T(b_{1,2}, \vec{p}_T^{\text{miss}})$ category. Subdividing each N_t region by the number of b -tagged jets (N_b)

that satisfy the medium working point of the CSV algorithm provides even greater discrimination of signal from background. Since there are relatively few events in the $N_t \geq 1$ category, the subcategorization in N_j is not performed for these events because it provides no additional gain after the N_b subdivision.

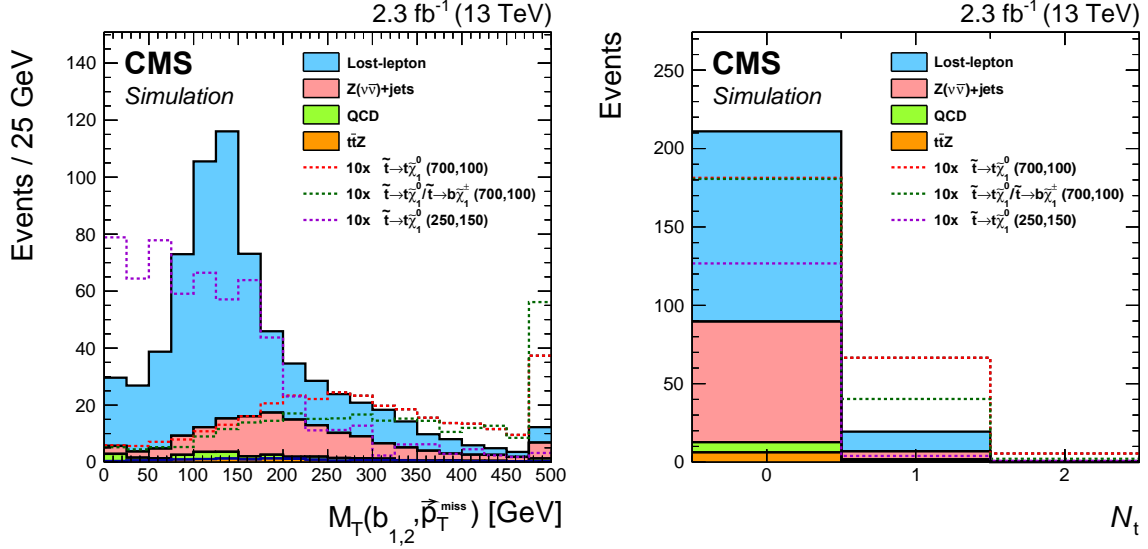


Figure 2: The $M_T(b_{1,2}, \vec{p}_T^{\text{miss}})$ distribution after the baseline selection of the top squark search in the all-jet final state (left), and the number of reconstructed top quarks for events in the high- $M_T(b_{1,2}, \vec{p}_T^{\text{miss}})$ category (right). Signal models with different top squark and neutralino mass hypotheses are shown, with the first number indicating the assumed top squark mass in units of GeV and the second the neutralino mass. The expected signal yields are scaled up by a factor of 10 to facilitate comparison of the distributions with expectations from SM backgrounds. In this and subsequent figures, the last bin shown includes the overflow events.

The event categorization according to $M_T(b_{1,2}, \vec{p}_T^{\text{miss}})$, N_j , N_b , and N_t is summarized in Table 1. In each of these categories, we use E_T^{miss} as the final discriminant to characterize and distinguish potential signal from the SM background by defining five E_T^{miss} regions. The analysis is therefore carried out in a total of 50 disjoint search regions (SRs).

Table 1: Categorization in $M_T(b_{1,2}, \vec{p}_T^{\text{miss}})$, N_j , N_b , and N_t used to define the SRs for the top squark search in the all-jet final state. Events in each category are further separated into the following E_T^{miss} regions: 250–300, 300–400, 400–500, 500–600, and >600 GeV, resulting in 50 disjoint SRs.

$M_T(b_{1,2}, \vec{p}_T^{\text{miss}}) < 175 \text{ GeV}$		$M_T(b_{1,2}, \vec{p}_T^{\text{miss}}) \geq 175 \text{ GeV}$	
$N_b = 1$	$N_b \geq 2$	$N_b = 1$	$N_b \geq 2$
$N_t = 0$			
$5 \leq N_j \leq 6$	$5 \leq N_j \leq 6$	$5 \leq N_j \leq 6$	$5 \leq N_j \leq 6$
		$N_j \geq 7$	$N_j \geq 7$
$N_j \geq 7$	$N_j \geq 7$	$N_t \geq 1$	
		$N_j \geq 5$	$N_j \geq 5$

4.2 Background estimation

4.2.1 Estimation of the lost-lepton background

The lost-lepton background is estimated from a single-lepton control sample, selected using the same trigger as the search sample, and consisting of events that have at least one lepton (ℓ) ob-

tained by inverting the electron and muon rejection criteria. Studies in simulation indicate that the event kinematics for different lepton flavours are similar enough to estimate them collectively from the same control sample. Potential signal contamination is suppressed by requiring $M_T(\ell, \vec{p}_T^{\text{miss}}) < 100 \text{ GeV}$. If there is more than one lepton satisfying the selection criteria, the lepton used to determine $M_T(\ell, \vec{p}_T^{\text{miss}})$ is chosen randomly. The events selected in the lepton control sample are further subdivided into control regions (CRs) using the same selection criteria as in the search sample, according to $M_T(b_{1,2}, \vec{p}_T^{\text{miss}})$, N_j , N_t , and E_T^{miss} . However with the requirement $N_b \geq 1$ the distribution in E_T^{miss} originating from lost-lepton processes is independent of N_b , and therefore the CRs are not subdivided according to the number of b-tagged jets. These CRs generally have a factor of 2–4 more events than the corresponding SRs.

The estimation of the lost-lepton background in each SR is based on the event count in data in the corresponding single-lepton CR ($N_{1\ell}^{\text{data}}$). We translate this event count to the SR by means of a lost-lepton transfer factor T_{LL} obtained from simulation. The lost-lepton background prediction can therefore be extracted as

$$N_{\text{LL}}^{\text{pred}} = N_{1\ell}^{\text{data}} T_{\text{LL}}, \quad T_{\text{LL}} = \frac{N_{0\ell}^{\text{sim}}}{N_{1\ell}^{\text{sim}}}, \quad (4)$$

where $N_{0\ell}^{\text{sim}}$ and $N_{1\ell}^{\text{sim}}$ are the simulated lost-lepton background yields in the corresponding zero- and single-lepton regions, respectively, taking into account contributions from $t\bar{t}$ and W +jets events, with smaller contributions from single top quark and $t\bar{t}W$ processes. The contamination from other SM processes in the single-lepton CRs is found to be negligible in studies of simulated events. Monte Carlo simulated samples are used to estimate the small component of the lost-lepton background that originates from leptons falling outside the kinematic acceptance, since this component is not accounted for in the CRs.

To improve the statistical power of the estimation, CRs with $N_t \geq 1$ are summed over E_T^{miss} bins as well as over N_b . We rely on the simulation through $N_{0\ell}^{\text{sim}}$ to provide the E_T^{miss} -dependence and to predict the yield in each of the SRs with $N_t \geq 1$. We check this procedure by computing the data-to-simulation ratios $N_{1\ell}^{\text{data}}/N_{1\ell}^{\text{sim}}$ in the higher-statistics region of $M_T(b_{1,2}, \vec{p}_T^{\text{miss}}) \geq 175 \text{ GeV}$ with $N_t = 0$, and find no evidence of a dependence on E_T^{miss} . We assign the relative statistical uncertainties of these ratios as systematic uncertainties in the SRs.

The dominant uncertainty in the lost-lepton prediction is due to the limited number of events in the CRs, and can be as large as 100%. The statistical uncertainties in the simulated samples also affect the uncertainty in the prediction via the transfer factors. The effect in the uncertainty ranges between 3% and 50%. A source of bias in the prediction can arise from a possible difference between data and simulation in the background composition, which is assessed by independently changing the cross sections of the W +jets and $t\bar{t}$ processes by $\pm 20\%$ based on CMS differential cross section measurements [65, 66]. The effect of these changes is as large as 11% for the transfer factors. The uncertainties in the measurements of correction factors in lepton efficiency that are applied to the simulation to reduce discrepancies with the data lead to a systematic uncertainty of up to 7% in T_{LL} . All other sources of systematic uncertainty, to be discussed in Section 7, have a negligible effect on the prediction.

4.2.2 Estimation of the $Z \rightarrow \nu\bar{\nu}$ background

Two methods are traditionally used to estimate the $Z \rightarrow \nu\bar{\nu}$ background in searches involving all-jet final states with large E_T^{miss} . The first method relies on a sample dominated by $Z \rightarrow \ell\ell$ +jets events, which has the advantage of accessing very similar kinematics to the $Z \rightarrow \nu\bar{\nu}$ process, after correcting for the difference in acceptance between charged-lepton pairs

and pairs of neutrinos, but is statistically limited in regions defined with stringent requirements on jets and E_T^{miss} . The second method utilizes γ +jets events that have a significantly larger production cross section than the $Z \rightarrow \ell\ell$ +jets process, but similar leading-order Feynman diagrams. The two main differences between the processes that must be taken into account, namely, different quark-boson couplings and the massive nature of the Z boson, become less important at large Z boson p_T , which is the kinematic region we are probing in this search.

We have therefore adopted a hybrid method to estimate the $Z \rightarrow \nu\bar{\nu}$ background by combining information from Z+jets, with $Z \rightarrow \ell\ell$, and γ +jets events. $Z \rightarrow \ell\ell$ events are used to obtain the normalization for the $Z \rightarrow \nu\bar{\nu}$ background in different ranges of N_b to account for potential effects related to heavy-flavour production, while the much higher yields from the γ +jets sample are exploited to extract corrections to distributions of variables used to characterize the SRs. The $Z \rightarrow \ell\ell$ events are obtained from dielectron and dimuon triggers, with the leading lepton required to have $p_T > 20$ GeV, and the trailing lepton $p_T > 15$ and > 10 GeV for electrons and muons, respectively. Both leptons must also have $|\eta| < 2.4$. The γ +jets sample is collected through a single-photon trigger, and consists of events containing photons with $p_T > 180$ GeV and $|\eta| < 2.5$. The transverse momentum of the dilepton or photon system is added vectorially to \vec{p}_T^{miss} in each event of the corresponding data samples to emulate the kinematics of the $Z \rightarrow \nu\bar{\nu}$ process. The modified E_T^{miss} , denoted by $E_T^{\text{miss},\ell\ell}$ and $E_T^{\text{miss},\gamma}$ for the $Z \rightarrow \ell\ell$ and γ +jets processes, respectively, is used to calculate related kinematic variables.

The prediction for the $Z \rightarrow \nu\bar{\nu}$ background is given by:

$$N_{Z \rightarrow \nu\bar{\nu}}^{\text{pred}} = N_{Z \rightarrow \nu\bar{\nu}}^{\text{sim}} R_Z S_\gamma, \quad (5)$$

where $N_{Z \rightarrow \nu\bar{\nu}}^{\text{sim}}$ is the expected number of $Z \rightarrow \nu\bar{\nu}$ events obtained from simulation, R_Z is the flavour-dependent Z+jets normalization factor measured with the $Z \rightarrow \ell\ell$ sample, and S_γ is the correction factor for distributions in E_T^{miss} and jet kinematic variables extracted from the γ +jets sample. The underlying assumption of this hybrid estimation method is that the differences in the E_T^{miss} (or $E_T^{\text{miss},\gamma}$) distributions between data and simulation are similar for $Z \rightarrow \nu\bar{\nu}$ and photon events. We checked this assumption by comparing the ratios of data to simulation observed in the $E_T^{\text{miss},\ell\ell}$ and $E_T^{\text{miss},\gamma}$ distributions for $Z \rightarrow \ell\ell$ +jets and γ +jets samples, respectively, and found them to agree.

The factor R_Z is calculated by comparing the observed and expected $Z \rightarrow \ell\ell$ yields for a relaxed version of the baseline selection. In particular, we remove the requirements on $\Delta\phi_{1234}$ after confirming that this does not bias the result, and relax the requirements on $E_T^{\text{miss},\ell\ell}$ from a threshold of 250 GeV to a threshold of 100 GeV. To increase the purity of the $Z \rightarrow \ell\ell$ events, we require the dilepton invariant mass to lie within the Z boson mass window of $80 < M_{\ell\ell} < 100$ GeV. The normalization of the nonnegligible $t\bar{t}$ contamination is estimated in the region outside the Z boson mass window ($20 < M_{\ell\ell} < 80$ or $M_{\ell\ell} > 100$ GeV) and taken into account. Small contributions from tZ and $t\bar{t}Z$ production, estimated from simulation, are included in the $Z \rightarrow \ell\ell$ sample when measuring R_Z . Contributions from tW and $t\bar{t}W$ are included in the simulation sample used to obtain the normalization factor for the $t\bar{t}$ contamination. As discussed previously, we calculate R_Z separately for different N_b requirements. The values obtained are 0.94 ± 0.13 and 0.84 ± 0.19 for $N_b = 1$ and ≥ 2 , respectively. The uncertainty in R_Z originates from the limited event counts in data and simulation, and from the extrapolation in E_T^{miss} .

The quantity S_γ is the correction factor related to the modelling of the distributions in the kinematic variables of $Z \rightarrow \nu\bar{\nu}$ events. It is calculated via a comparison of the $E_T^{\text{miss},\gamma}$ distributions of γ +jets events in simulation and data. The simulation is normalized to the number of events

in data after applying the baseline selection. To suppress potential contamination from signal and avoid overlap with the search sample, we only consider events with $E_T^{\text{miss}} < 200$ GeV. The S_γ factor is estimated separately for each SR to account for any potential mismodelling of the observables $M_T(b_{1,2}, E_T^{\text{miss},\gamma})$, N_j , $E_T^{\text{miss},\gamma}$, and N_t in simulation. Since no statistically significant dependence of $E_T^{\text{miss},\gamma}$ on N_b is observed, we improve the statistical power of the correction by combining the $N_b = 1$ and $N_b \geq 2$ subsets of the γ +jets sample to extract the S_γ corrections. The correction factors range between 0.3 and 2, with uncertainties of up to 100% due to the limited number of events in the data sample.

The γ +jets control data have contributions from three main components: prompt photons produced directly or via fragmentation, and other objects misidentified as photons. The prompt photon purity measured in Ref. [33] shows good agreement between data and simulation. In addition, the impact of varying the fraction of misidentified photons, or those produced via fragmentation, by 50% in simulated events results in a bias of less than 5% in the E_T^{miss} distribution from the predicted $Z \rightarrow \nu\bar{\nu}$ background. We therefore rely on simulation to estimate the relative contributions of the three different components.

The statistical uncertainty in the γ +jets control data and the uncertainty in R_Z are the main sources of uncertainty in the $Z \rightarrow \nu\bar{\nu}$ prediction. The statistical uncertainties in the simulated samples, ranging up to 50% in both the SRs and in the γ +jets CRs, also makes sizeable contributions.

4.2.3 Estimation of the QCD background

The QCD background is estimated using a data CR selected with the same trigger as the SR and enriched in QCD events by imposing a threshold on the azimuthal separation between \vec{p}_T^{miss} and the closest of the three leading jets, namely $\Delta\phi_{123} < 0.1$. After correcting for the contribution from other SM processes (i.e. $t\bar{t}$ and W +jets), estimated by applying the normalization factor obtained in the corresponding single-lepton control sample to simulation, we translate the observation in this CR to a prediction in the SR by means of transfer factors obtained from simulation. Each transfer factor is defined as the ratio of the expected QCD events satisfying $\Delta\phi_{1234} > 0.5$ to the expected QCD events with $\Delta\phi_{123} < 0.1$. The estimation is carried out in each search category. Since the distributions in key observables show little dependence on N_b , the QCD CR is summed over N_b to improve the statistical precision of the estimation.

The main source of QCD events populating the SR is from severe mismeasurement of the p_T of one or more jets in the event. Correct modelling of jet mismeasurement in simulation is therefore an important part of the QCD prediction. The level of mismeasurement of a simulated event is parameterized by the jet response of the most mismeasured jet, which is the jet with the greatest absolute difference between the reconstructed and generated p_T . The jet response, r_{jet} , is defined as the ratio of the reconstructed p_T of a jet to its generated p_T , computed without including the loss of visible momentum due to neutrinos. We use the observable $r_{\text{jet}}^{\text{pseudo}}$, defined as the ratio of the p_T of a jet to the magnitude of the vector sum of its transverse momentum and \vec{p}_T^{miss} , as an approximate measure of the true jet response in data, and extract mismeasurement correction factors for the simulation by comparing $r_{\text{jet}}^{\text{pseudo}}$ of the jet closest in ϕ to \vec{p}_T^{miss} between data and simulation. The correction factors extracted from simulation are parameterized by r_{jet} and the flavour of the most mismeasured jet. The correction factors range between 0.44 and 1.13, and are applied in the simulation on an event-by-event basis.

The largest sources of uncertainty in the QCD prediction originate from the limited event counts in data and simulated samples surviving the selection, giving rise to uncertainties of

up to 100% in the estimated QCD background contribution in some SRs. The uncertainty due to jet response corrections is up to 15%, while the uncertainty due to contributions from non-QCD processes in the data CR ranges from 7% to 35%.

4.2.4 Estimation of the $t\bar{t}Z$ background

Contributions from the $t\bar{t}Z$ process are generally small since this is a relatively rare process. However, it has a final state very similar to signal when the Z boson decays to neutrinos and both top quarks decay only into jets, which can constitute up to 25% of the total SM background in some SRs with large E_T^{miss} and $N_t \geq 1$. The $t\bar{t}Z$ prediction is obtained from simulation. We assign a 30% uncertainty to the $t\bar{t}Z$ cross section, based on the 8 TeV CMS measurement [67]. Additional theoretical and experimental uncertainties in the prediction are evaluated as will be discussed in Section 7, and range up to 25% and 20%, respectively, depending on the SR. We also take into consideration the statistical uncertainty in the simulation, which ranges from 5% to 100% for regions with small $t\bar{t}Z$ contributions.

4.3 Results

Figure 3 shows the yields in each of the SR bins, as well as the predicted SM backgrounds based on the background estimation methods discussed in Section 4.2. The results are also summarized in Table 2. Expected yields are also shown for two benchmark models for the pure $\tilde{t}_1 \rightarrow t^{(*)}\tilde{\chi}_1^0$ decay and one for the mixed ($\tilde{t}_1 \rightarrow t\tilde{\chi}_1^0$ or $\tilde{t}_1 \rightarrow b\tilde{\chi}_1^\pm$) decay. No statistically significant deviation from the SM prediction is observed in the data.

5 Search for top squarks in the single-lepton final state

We also perform a search for top squarks in events with exactly one isolated electron or muon and considerable E_T^{miss} . The main SM backgrounds originating from $t\bar{t}$ and W +jets processes are suppressed using dedicated kinematic variables. The dominant remaining backgrounds arise from lost-lepton processes and the surviving W +jets background, both of which are estimated from control samples in data.

5.1 Analysis strategy

The search sample is selected using triggers that require either large E_T^{miss} or the presence of an isolated electron or muon. The combined trigger efficiency for a selection of $E_T^{\text{miss}} > 250$ GeV and at least one lepton, as measured in a data sample with large H_T , is found to be 99% with an asymmetric uncertainty of $^{+1}_{-3}\%$. Selected events are required to have at least two jets with $p_T > 30$ GeV, at least one of which must be b -tagged using the medium working point. We require exactly one well-identified and isolated electron or muon with $p_T > 20$ GeV, $|\eta| < 1.442$ or < 2.4 , respectively, and $I_{\text{rel}} < 0.1$. Electrons in the forward region of the detector are not considered in this search due to a significant rate for a jet to be misidentified as an electron. To reduce the dilepton background originating from $t\bar{t}$ and tW production, events are rejected if they contain a second electron or muon with $p_T > 5$ GeV and $I_{\text{rel}} < 0.2$. A significant fraction of the remaining SM background originates from events with τ_h decays. This contribution is reduced by rejecting events that have an isolated τ_h candidate reconstructed using the HPS algorithm with $p_T > 20$ GeV and $|\eta| < 2.4$. A further veto is placed on events containing isolated charged-hadron PF candidates with $p_T > 10$ GeV and $|\eta| < 2.5$. Candidates are categorized as being isolated if their isolation sum, i.e. the scalar sum of the p_T of charged PF candidates within a fixed cone of $R = 0.3$ around the candidate, is less than 6 GeV and smaller than 10% of the candidate p_T .

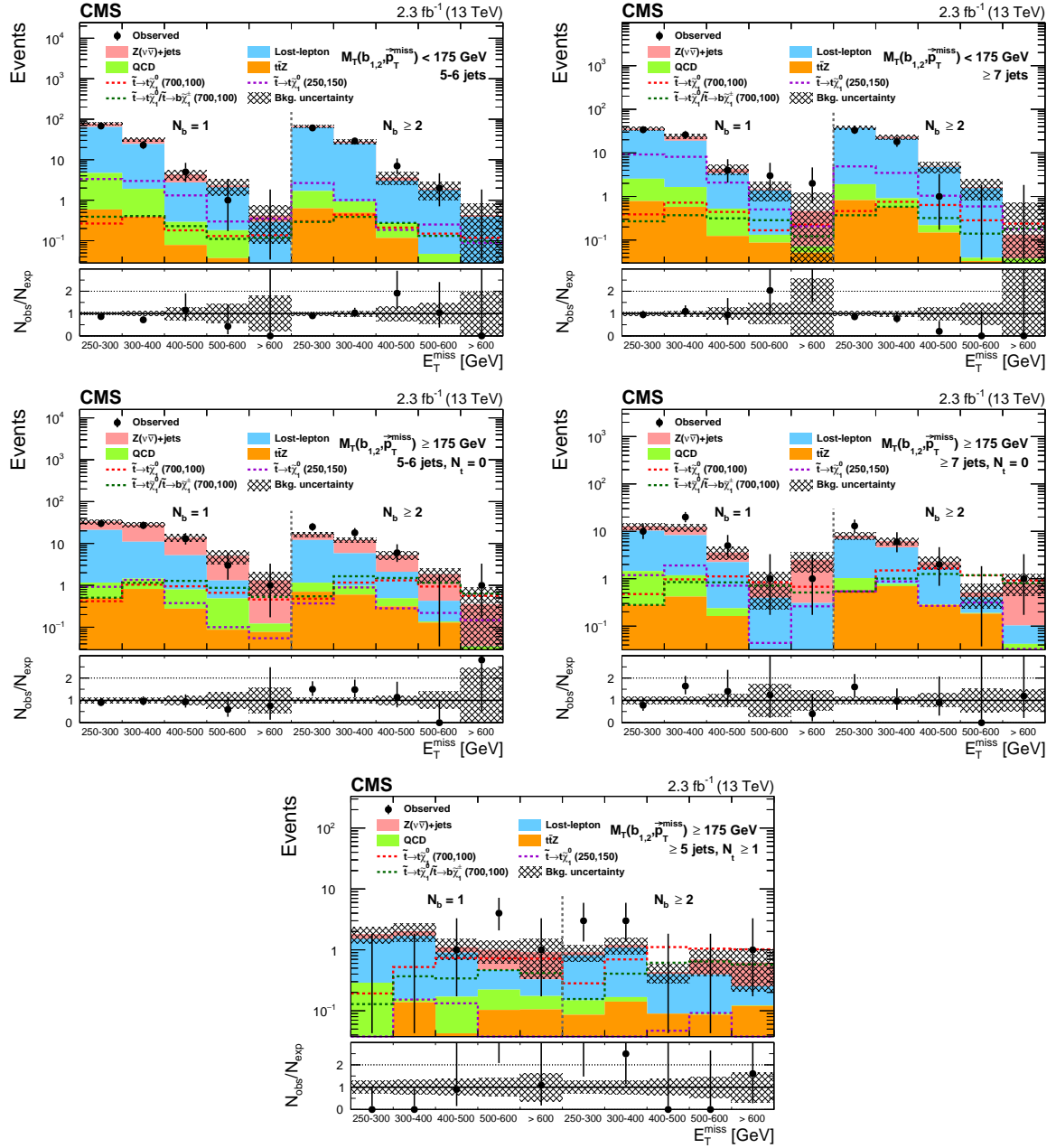


Figure 3: Observed and estimated SM background and signal yields in the SRs of the top squark search in the all-jet final state: $M_T(b_{1,2}, \vec{p}_T^{\text{miss}}) < 175 \text{ GeV}$, $5 \leq N_j \leq 6$ (upper left), $M_T(b_{1,2}, \vec{p}_T^{\text{miss}}) < 175 \text{ GeV}$, $N_j \geq 7$ (upper right), $M_T(b_{1,2}, \vec{p}_T^{\text{miss}}) \geq 175 \text{ GeV}$, $N_t = 0$, $5 \leq N_j \leq 6$ (middle left), $M_T(b_{1,2}, \vec{p}_T^{\text{miss}}) \geq 175 \text{ GeV}$, $N_t = 0$, $N_j \geq 7$ (middle right), $M_T(b_{1,2}, \vec{p}_T^{\text{miss}}) \geq 175 \text{ GeV}$, $N_t \geq 1$, $N_j \geq 5$ (bottom row). The first 5 bins in each plot correspond to E_T^{miss} ranges of 250–300, 300–400, 400–500, 500–600, $> 600 \text{ GeV}$ for $N_b = 1$, and the second 5 bins correspond to the same E_T^{miss} binning for $N_b \geq 2$. The SM background predictions shown do not include the effects of the maximum likelihood fit to the data. The ratio of the data to the SM prediction extracted from CRs is shown in the lower panel of each plot. The shaded black band represents the statistical and systematic uncertainty in the background prediction.

Table 2: Observed and predicted background yields in the different search regions for the top squark search in the all-jet final state. The total uncertainty is given for each background prediction.

E_T^{miss} [GeV]	Lost-lepton	$Z \rightarrow \nu\bar{\nu}$	QCD	$t\bar{t}Z$	Total SM	Data
$M_T(b_{1,2}, \vec{p}_T^{\text{miss}}) < 175 \text{ GeV}, 5 \leq N_j \leq 6, N_b = 1$						
250-300	60 ± 6	14 ± 3	4.1 ± 1.7	0.59 ± 0.21	79 ± 7	68
300-400	23 ± 3	7.4 ± 1.9	1.5 ± 0.8	0.39 ± 0.14	32 ± 4	23
400-500	2.5 ± 1.0	1.6 ± 0.8	0.21 ± 0.15	0.08 ± 0.04	4.3 ± 1.3	5
500-600	1.9 ± 1.0	$0.25^{+0.27}_{-0.25}$	$0.14^{+0.15}_{-0.14}$	0.04 ± 0.02	2.3 ± 1.0	1
>600	$0.28^{+0.31}_{-0.28}$	$0.13^{+0.15}_{-0.13}$	0.01 ± 0.01	<0.01	0.42 ± 0.34	0
$M_T(b_{1,2}, \vec{p}_T^{\text{miss}}) < 175 \text{ GeV}, 5 \leq N_j \leq 6, N_b \geq 2$						
250-300	61 ± 6	4.7 ± 1.4	1.1 ± 0.5	0.63 ± 0.22	68 ± 6	61
300-400	24 ± 3	3.0 ± 1.0	0.44 ± 0.23	0.50 ± 0.18	28 ± 4	29
400-500	2.8 ± 1.2	0.61 ± 0.33	0.16 ± 0.13	0.12 ± 0.06	3.7 ± 1.2	7
500-600	1.7 ± 0.9	$0.13^{+0.15}_{-0.13}$	$0.05^{+0.06}_{-0.05}$	<0.01	1.9 ± 0.9	2
>600	$0.38^{+0.41}_{-0.38}$	$0.04^{+0.06}_{-0.04}$	<0.01	0.01 ± 0.01	0.43 ± 0.41	0
$M_T(b_{1,2}, \vec{p}_T^{\text{miss}}) < 175 \text{ GeV}, N_j \geq 7, N_b = 1$						
250-300	30 ± 4	3.0 ± 1.0	1.8 ± 0.6	0.79 ± 0.28	36 ± 4	34
300-400	17 ± 3	4.6 ± 1.6	1.1 ± 0.5	0.58 ± 0.21	24 ± 3	26
400-500	2.9 ± 0.9	0.82 ± 0.64	0.40 ± 0.27	0.12 ± 0.07	4.2 ± 1.1	4
500-600	1.3 ± 0.7	$0.09^{+0.11}_{-0.09}$	0.05 ± 0.05	0.09 ± 0.05	1.5 ± 0.7	3
>600	<0.56	$0.39^{+0.46}_{-0.39}$	0.02 ± 0.02	0.05 ± 0.03	$0.46^{+0.72}_{-0.46}$	2
$M_T(b_{1,2}, \vec{p}_T^{\text{miss}}) < 175 \text{ GeV}, N_j \geq 7, N_b \geq 2$						
250-300	36 ± 4	0.96 ± 0.38	1.1 ± 0.5	0.83 ± 0.30	38 ± 4	33
300-400	20 ± 3	2.1 ± 0.9	0.34 ± 0.19	0.58 ± 0.22	23 ± 3	18
400-500	4.5 ± 1.4	0.15 ± 0.13	0.07 ± 0.05	0.15 ± 0.07	4.9 ± 1.4	1
500-600	1.5 ± 0.8	$0.09^{+0.11}_{-0.09}$	0.01 ± 0.01	0.03 ± 0.03	1.6 ± 0.8	0
>600	<0.59	$0.10^{+0.12}_{-0.10}$	0.01 ± 0.01	0.03 ± 0.02	$0.13^{+0.60}_{-0.13}$	0
$M_T(b_{1,2}, \vec{p}_T^{\text{miss}}) \geq 175 \text{ GeV}, 5 \leq N_j \leq 6, N_t = 0, N_b = 1$						
250-300	20 ± 3	12 ± 3	0.66 ± 0.37	0.50 ± 0.19	33 ± 5	30
300-400	9.6 ± 2.3	17 ± 4	0.63 ± 0.32	0.82 ± 0.27	28 ± 4	27
400-500	4.4 ± 1.9	8.6 ± 2.6	0.52 ± 0.35	0.28 ± 0.12	14 ± 3	13
500-600	0.82 ± 0.63	3.8 ± 1.8	0.40 ± 0.35	0.09 ± 0.06	5.1 ± 1.9	3
>600	<0.4	1.2 ± 0.7	0.05 ± 0.05	0.08 ± 0.04	1.3 ± 0.8	1
$M_T(b_{1,2}, \vec{p}_T^{\text{miss}}) \geq 175 \text{ GeV}, 5 \leq N_j \leq 6, N_t = 0, N_b \geq 2$						
250-300	11 ± 2	4.5 ± 1.4	0.45 ± 0.27	0.70 ± 0.24	17 ± 3	25
300-400	4.9 ± 1.2	6.3 ± 1.8	0.37 ± 0.23	0.60 ± 0.22	12 ± 2	18
400-500	1.6 ± 0.7	3.1 ± 1.1	0.18 ± 0.17	0.31 ± 0.12	5.3 ± 1.4	6
500-600	0.29 ± 0.24	1.4 ± 0.8	0.01 ± 0.01	0.13 ± 0.06	1.9 ± 0.8	0
>600	<0.49	0.32 ± 0.20	$0.01^{+0.02}_{-0.01}$	0.02 ± 0.02	$0.36^{+0.53}_{-0.36}$	1
$M_T(b_{1,2}, \vec{p}_T^{\text{miss}}) \geq 175 \text{ GeV}, N_j \geq 7, N_t = 0, N_b = 1$						
250-300	8.8 ± 1.9	2.5 ± 1.0	1.2 ± 0.6	0.29 ± 0.18	13 ± 2	10
300-400	7.1 ± 1.8	3.9 ± 1.5	0.76 ± 0.46	0.42 ± 0.18	12 ± 2	20
400-500	2.0 ± 0.8	1.3 ± 0.7	0.08 ± 0.07	0.16 ± 0.09	3.6 ± 1.1	5
500-600	$0.38^{+0.40}_{-0.38}$	$0.40^{+0.43}_{-0.40}$	0.02 ± 0.02	<0.01	0.80 ± 0.59	1
>600	$0.28^{+0.33}_{-0.28}$	2.2 ± 1.2	$0.02^{+0.03}_{-0.02}$	<0.01	2.5 ± 1.2	1
$M_T(b_{1,2}, \vec{p}_T^{\text{miss}}) \geq 175 \text{ GeV}, N_j \geq 7, N_t = 0, N_b \geq 2$						
250-300	5.9 ± 1.3	1.2 ± 0.5	0.46 ± 0.24	0.57 ± 0.21	8.1 ± 1.5	13
300-400	3.8 ± 1.0	1.6 ± 0.7	0.08 ± 0.06	0.70 ± 0.26	6.2 ± 1.2	6
400-500	1.5 ± 0.6	0.48 ± 0.27	0.01 ± 0.01	0.28 ± 0.12	2.2 ± 0.7	2
500-600	$0.22^{+0.25}_{-0.22}$	$0.11^{+0.12}_{-0.11}$	0.01 ± 0.01	0.18 ± 0.08	0.51 ± 0.29	0
>600	$0.06^{+0.07}_{-0.06}$	0.73 ± 0.44	$0.02^{+0.03}_{-0.02}$	$0.02^{+0.03}_{-0.02}$	0.84 ± 0.45	1
$M_T(b_{1,2}, \vec{p}_T^{\text{miss}}) \geq 175 \text{ GeV}, N_j \geq 5, N_t \geq 1, N_b = 1$						
250-300	1.2 ± 0.5	0.30 ± 0.25	0.26 ± 0.21	$0.02^{+0.03}_{-0.02}$	1.8 ± 0.6	0
300-400	1.5 ± 0.7	0.34 ± 0.26	0.02 ± 0.01	0.14 ± 0.06	2.0 ± 0.8	0
400-500	0.73 ± 0.40	$0.20^{+0.22}_{-0.20}$	$0.13^{+0.17}_{-0.13}$	$0.04^{+0.05}_{-0.04}$	1.1 ± 0.5	1
500-600	0.25 ± 0.22	0.54 ± 0.34	$0.12^{+0.16}_{-0.12}$	0.10 ± 0.06	1.0 ± 0.4	4
>600	$0.15^{+0.33}_{-0.15}$	0.59 ± 0.49	0.07 ± 0.07	0.11 ± 0.05	0.92 ± 0.60	1
$M_T(b_{1,2}, \vec{p}_T^{\text{miss}}) \geq 175 \text{ GeV}, N_j \geq 5, N_t \geq 1, N_b \geq 2$						
250-300	0.66 ± 0.26	0.11 ± 0.09	0.06 ± 0.05	0.09 ± 0.05	0.92 ± 0.29	3
300-400	0.92 ± 0.39	0.12 ± 0.10	0.03 ± 0.03	0.14 ± 0.08	1.2 ± 0.4	3
400-500	0.31 ± 0.17	$0.03^{+0.04}_{-0.03}$	<0.01	0.09 ± 0.06	0.43 ± 0.18	0
500-600	0.30 ± 0.30	0.30 ± 0.21	<0.01	0.09 ± 0.04	0.70 ± 0.37	0
>600	$0.13^{+0.29}_{-0.13}$	0.37 ± 0.32	<0.01	0.12 ± 0.05	0.62 ± 0.43	1

Single-lepton backgrounds originating from semileptonic $t\bar{t}$, W +jets, and single top quark processes are suppressed through the M_T of the lepton-neutrino system. Background processes containing a single lepton from W boson decay have a kinematic endpoint for M_T at the W boson mass, modulo detector resolution and off-shell W boson mass effects. In this analysis we require $M_T > 150$ GeV, which significantly reduces single-lepton backgrounds. To further reduce the $t\bar{t}$ background, we require the absolute value of the azimuthal angle between \vec{p}_T^{miss} and the closest of the two highest- p_T jets, $\Delta\phi_{12}$, to be larger than 0.8, since the events that satisfy the E_T^{miss} and M_T requirements tend to have higher- p_T top quarks, and therefore smaller values of $\Delta\phi_{12}$ than signal events.

The remaining background after the preselection is dominated by dilepton events from $t\bar{t}$ and tW production, where one of the leptons is not reconstructed or identified, and the presence of the additional neutrino from the second leptonically decaying W boson makes it possible to satisfy the M_T requirement.

Kinematic properties of signal events such as E_T^{miss} , M_T , and jet multiplicity depend on the decay modes of top squarks, as well as on the mass splittings (Δm) between the top squark, neutralino, and chargino (if present). As a basis for the search strategy in the topologies shown in Figs. 1(a) and 1(b), we require the presence of at least four jets. Events are then categorized based on the value of the M_{T2}^W variable [68], which is calculated for each event under the assumption that it originates from the dilepton $t\bar{t}$ process with a lost lepton:

$$M_{T2}^W \equiv \text{Min}\{m_y, \text{consistent with: } [p_1^2 = 0, (p_1 + p_\ell)^2 = p_2^2 = M_W^2, \vec{p}_1 + \vec{p}_\ell = \vec{E}_T^{\text{miss}}, (p_1 + p_\ell + p_{b_1})^2 = (p_2 + p_{b_2})^2 = m_y^2]\}, \quad (6)$$

where m_y is the fitted parent particle mass, and p_1 , p_ℓ , p_2 , p_{b_1} , and p_{b_2} are the four momenta of the neutrino corresponding to the visible W boson decay, the lepton from the same decay, the W boson whose decay gives rise to the undetected lepton, and the two b jet candidates, respectively. To select the b jet candidates, we examine all possible pairings with the three jets that have the highest CSV discriminator values. The pairing that gives the lowest value of M_{T2}^W defines the final estimate. The reconstruction of an event using the M_{T2}^W variable helps discriminate signal from the dominant dilepton $t\bar{t}$ background. For large mass differences between the top squark and the neutralino, the $M_{T2}^W > 200$ GeV requirement significantly reduces the background while maintaining reasonable signal efficiency. In contrast, for small- Δm models, such a requirement results in a significant loss in signal efficiency. To preserve sensitivity to both high- and low- Δm scenarios, we subdivide the search sample into two event categories with $M_{T2}^W > 200$ GeV and ≤ 200 GeV. The M_{T2}^W distribution for events with at least four jets is shown in Fig. 4 (left).

In signals with a large difference in mass between the top squark and the neutralino, a significant fraction of events can contain two quarks that merge into a single jet as a result of the large boost of the top quark or W boson that decay into jets. These events would fail the four-jet requirement. To recover acceptance for such topologies, we define an additional SR in events with three jets. Since this region targets large Δm signal scenarios, only events with $M_{T2}^W > 200$ GeV are considered.

To increase the sensitivity of this analysis to a mixed decay scenario (Fig. 1c) when the chargino and neutralino are nearly degenerate in mass, SRs with exactly two jets are added. In events with low jet multiplicity the modified topness variable (t_{mod}) [69] provides improved dilepton

$t\bar{t}$ rejection:

$$t_{\text{mod}} = \ln(\min S), \text{ with } S(\vec{p}_W, p_z, \nu) = \frac{(m_W^2 - (p_\nu + p_\ell)^2)^2}{a_W^4} + \frac{(m_t^2 - (p_b + p_W)^2)^2}{a_t^4}. \quad (7)$$

This equation uses the mass constraints for the particles and also the assumption that $\vec{p}_T^{\text{miss}} = \vec{p}_{T,W} + \vec{p}_{T,\nu}$. The first term constrains the W boson whose lepton decay product is the detected lepton, while the second term constrains the top quark for which the lepton from the W boson decay is lost in the reconstruction. Once again, we consider all possible pairings of b jet candidates with up to three jets with highest CSV discriminator values. The calculation of modified topness uses the resolution parameters $a_W = 5 \text{ GeV}$ and $a_t = 15 \text{ GeV}$, which determine the relative weighting of the mass shell conditions. We select events with $t_{\text{mod}} > 6.4$. The definition of topness used in this analysis is modified from the one originally proposed in Ref. [69]: namely, the terms corresponding to the detected leptonic top quark decay and the centre-of-mass energy are dropped since in events with low jet multiplicity the second b jet is often not identified. In these cases, the discriminating power of the topness variable is reduced when a light-flavour jet is used instead in the calculation. The modified topness is more robust against such effects and provides better signal sensitivity in these SRs than the M_{T2}^W variable. The distribution of modified topness for events with at least two jets is shown in Fig. 4 (right).

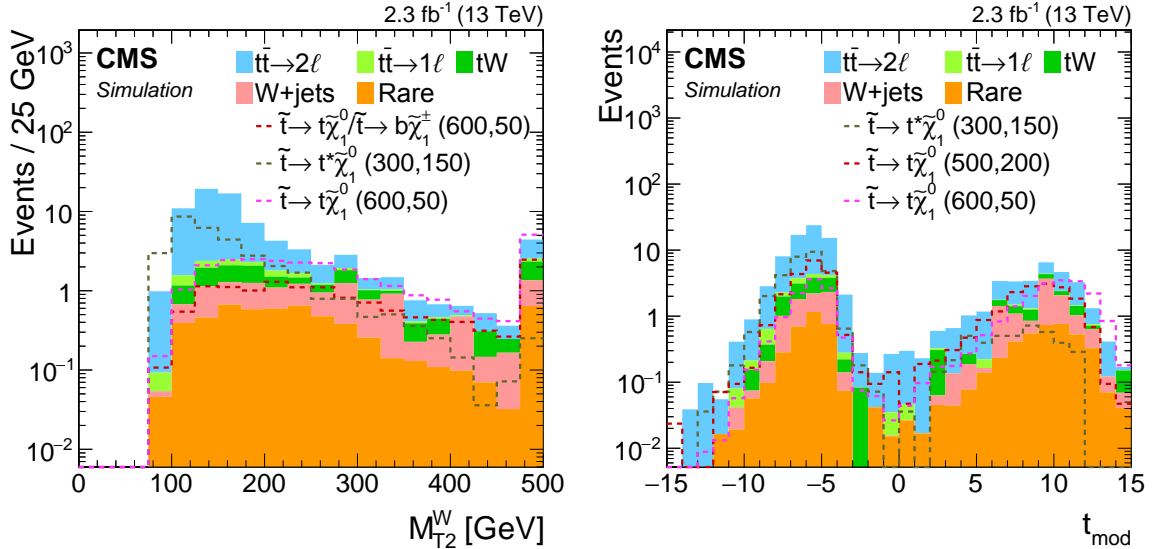


Figure 4: The M_{T2}^W (left) and t_{mod} (right) distributions for signal and backgrounds after the preselection are shown. The M_{T2}^W variable is shown for events with four or more jets, while t_{mod} is shown for events with at least two jets. Signal models with different top squark and neutralino mass hypotheses are shown for comparison.

Finally, events in each of the categories described above are further classified into different SRs based on the value of E_T^{miss} . This results in a total of nine exclusive SRs as summarized in Table 3.

5.2 Background estimation

Three categories of backgrounds originating from SM processes remain after the preselection described in Section 5.1. The dominant contribution arises from backgrounds with a lost lepton, primarily from the dilepton $t\bar{t}$ process. A second class of background events originates from SM processes with a single leptonically decaying W boson. Preselection requirements of $E_T^{\text{miss}} >$

Table 3: Summary of the SR definitions for the single-lepton search.

Targeted models	N_j	M_{T2}^W [GeV]	t_{mod}	E_T^{miss} [GeV]		
Low- Δm	≥ 4	≤ 200		250–325	> 325	
High- Δm	≥ 4	> 200		250–350	350–450	> 450
Boosted high- Δm	$= 3$	> 200		250–350	> 350	
Degenerate $\tilde{\chi}_1^\pm$ and $\tilde{\chi}_1^0$	$= 2$		> 6.4	250–350	> 350	

250 GeV and $M_T > 150$ GeV strongly suppress this background. The suppression is much stronger for events with a W boson originating from the decay of a top quark than for direct W boson production, as the mass of the top quark imposes a constraint on M_W . As a result, large values of M_T in semileptonic $t\bar{t}$ events are dominated by E_T^{miss} resolution effects, while for events in which the W boson is produced directly (W+jets) they are mainly a function of the width of the W boson. The third class of background events includes rare SM processes such as W Z and $t\bar{t}Z$ (where the Z boson decays to neutrinos), with smaller contributions from $t\bar{t}W$, $t\bar{t}\gamma$, and processes with two or three electroweak vector bosons. The QCD background is negligible in this search due to requirements on the presence of a high- p_T isolated lepton, large E_T^{miss} , and large M_T .

5.2.1 Lost-lepton background

The lost-lepton background is estimated from data in dilepton CRs, where we require the presence of a second lepton passing the rejection requirements but with $p_T > 10$ GeV, an isolated track, or a τ_h candidate. This is done again by extrapolating the data in the dilepton CRs to the SRs using transfer factors obtained from simulation. We use the same preselection requirements on E_T^{miss} and M_T as in the search regions. We remove the subdivision in E_T^{miss} and the separation of the three and at least four jet regions to increase the statistical power of the CRs, and arrive at three CRs: exactly two jets and $t_{\text{mod}} > 6.4$, at least three jets and $M_{T2}^W \leq 200$ GeV, and at least three jets and $M_{T2}^W > 200$ GeV. These control regions have a purity in dilepton events of $> 97\%$. Additional transfer factors are therefore needed to account for the extrapolation in jet multiplicity and E_T^{miss} requirements; these are derived from simulation. The background estimate can be written as follows:

$$N_{\text{LL}}^{\text{pred}} = N_{2\ell}^{\text{data}} T_{\text{LL}} T_{E_T^{\text{miss}}, N_j}, \quad T_{\text{LL}} = \frac{N_{1\ell}^{\text{sim}}}{N_{2\ell}^{\text{sim}}}, \quad T_{E_T^{\text{miss}}, N_j} = \frac{N_{1\ell}^{\text{sim}}(E_T^{\text{miss}}, N_j)}{N_{1\ell}^{\text{sim}}}, \quad (8)$$

where $N_{2\ell}^{\text{data}}$ is the number of events observed in data in the dilepton CR. The largest systematic uncertainty in the background estimate is due to the statistical uncertainties of the event yields in data CRs and the estimates from simulated samples (10–30%). The signal contamination in this CR is around 10% for the bulk of the studied parameter space and is taken into account in the final interpretation. The transfer factor T_{LL} is obtained from simulation, and estimates the probability that a lepton is not identified in the detector, accounting for the kinematic acceptance and the efficiency of the lepton selection criteria. The second transfer factor, $T_{E_T^{\text{miss}}, N_j}$, extrapolates the inclusive estimate to individual SR bins. This transfer factor, also obtained from simulation, is validated by checking the modelling of the jet multiplicity and of the E_T^{miss} spectrum in dedicated data CRs, which will be described in the following paragraphs.

The dilepton $t\bar{t}$ background contributes to the SRs with three or more jets only if jets from ISR or final-state radiation (FSR) are also present, or when a τ_h decay is misidentified as an additional jet. The modelling of jet multiplicity is checked in a high-purity dedicated dilepton data control sample with one electron and one muon, at least two b-tagged jets, and $E_T^{\text{miss}} > 250$ GeV. The differences between data and simulation are used to estimate scale factors relative to the

baseline selection of events with at least two jets. The scale factors are 1.10 ± 0.06 for three-jet events and 0.94 ± 0.06 for events with at least four jets. Within statistical uncertainties, these factors display no E_T^{miss} dependence. The scale factors are applied to the dilepton $t\bar{t}$ simulation when extrapolating the inclusive background prediction into the specified jet multiplicity bins. The statistical uncertainties in these scale factors are also propagated to the predictions in the SRs. The uncertainty in the modelling of the jet multiplicity ranges up to 3%.

The extrapolation in E_T^{miss} is carried out through simulation, and it must be verified that its resolution is accurately modelled. Changing the resolution can lead to a different E_T^{miss} spectrum. In this analysis we are interested in the effect of the E_T^{miss} resolution in events containing intrinsic E_T^{miss} because of the presence of neutrinos in the events. This effect is estimated by comparing a γ +jets sample in data with simulation. The events are selected using a single-photon trigger with $p_T > 165$ GeV and $|\eta| < 2.4$. Photons are required to pass stringent identification criteria. We use the photons to mimic the neutrinos in the event, with the photon momentum serving as an estimate of the sum of the neutrino momenta.

The photon p_T spectrum in data and in simulation is reweighted to match that of the neutrinos in the background-simulation sample. For dilepton $t\bar{t}$ events, this corresponds to the $\nu\nu$ - p_T spectrum. To model the E_T^{miss} resolution, the transverse momentum of the photon system is added vectorially to the \vec{p}_T^{miss} and the resulting E_T^{miss} spectrum is compared between data and simulation. We use this modified E_T^{miss} definition to calculate our discriminants. For this CR, we then apply selection criteria close to the SR criteria, except that selections related to the lepton are dropped, the presence of a well-identified photon is required, and the requirement of a b-tagged jet is reversed so as to suppress effects related to semileptonic heavy-flavour decays. Corrections for the observed differences, which can go up to 15%, are applied to events in the simulated samples and the uncertainties propagated to the final background estimate, resulting in an uncertainty of 1–4% in the lost-lepton background prediction.

5.2.2 One-lepton background

In SRs with a high M_{T2}^W or modified topness requirement, the W+jets background is estimated using a data control sample containing no b-tagged jets. For SRs with a low- M_{T2}^W requirement, this background constitutes less than 10% of the total SM background. In these SRs we do not employ an estimate based on data, but instead use the W+jets background estimate directly from simulation. The semileptonic $t\bar{t}$ background is also estimated from simulation.

The CRs used to extract the W+jets background in the SRs with a high M_{T2}^W or modified topness requirement are again not subdivided in E_T^{miss} to have a sufficient number of events to carry out the prediction. We therefore use three CRs for this background estimate: exactly two jets with $t_{\text{mod}} > 6.4$, exactly three jets with $M_{T2}^W > 200$ GeV, and at least four jets with $M_{T2}^W > 200$ GeV. We extrapolate the yields from the CRs to the SRs by applying transfer factors from simulation for the extrapolation in E_T^{miss} and number of b-tagged jets:

$$N_{W+jets}^{\text{pred}} = (N_{N_b=0}^{\text{data}} - N_{N_b=0}^{\text{non-W+jets}}) T_{E_T^{\text{miss}}} T_{N_b}, \quad (9)$$

with $N_{N_b=0}^{\text{data}} - N_{N_b=0}^{\text{non-W+jets}}$ representing the event yield in the CR after subtracting the estimated contribution from other SM background processes. The non- 1ℓ contribution in the CRs, $N_{N_b=0}^{\text{non-W+jets}}$, is estimated from simulation and amounts to roughly 25–35%. A 50% uncertainty is assigned to the subtraction. The largest source of uncertainty is again the limited size of the data and simulation samples. The statistical uncertainty of these samples results in an uncertainty of 20–40% in the W+jets background estimate.

The transfer factor $T_{E_T^{\text{miss}}}$ extrapolates the yields from the inclusive CR with $E_T^{\text{miss}} > 50 \text{ GeV}$ to the exclusive E_T^{miss} regions. The main uncertainties in this extrapolation factor can be attributed to the modelling of the neutrino p_T spectrum, the W boson width, and the E_T^{miss} resolution. The neutrino p_T spectrum is checked in a data sample enriched in W+jets, with no b-tagged jets and $60 < M_T < 120 \text{ GeV}$. No large mismodelling of E_T^{miss} is observed. Therefore, we do not apply any corrections to the neutrino p_T spectrum but only propagate the statistical limitation of this study as the uncertainty (6–22%) in the modelling of the neutrino p_T spectrum. The uncertainty in the W boson width (3% [70]) is estimated by scaling the four-vectors of the W boson decay products appropriately. The E_T^{miss} resolution effects on this background are studied using the same method as described in Section 5.2.1, giving rise to a 1–3% uncertainty.

The other transfer factor, T_{N_b} , performs the extrapolation in the number of b-tagged jets for each E_T^{miss} bin. Scale factors are applied to the simulation to match the b tagging efficiency in data. The largest uncertainty in this transfer factor is the fraction of the heavy-flavour component in the W+jets sample; we assign a 50% uncertainty to this component. We performed a dedicated cross-check in a CR with one or two jets and at least 50 GeV of E_T^{miss} . Data and simulation were found to be in agreement in the b jet multiplicity within uncertainties. After taking into consideration the additional sources of systematic uncertainty described in Section 7, the total uncertainty in the W+jets estimate varies from 50% to 70%.

The semileptonic $t\bar{t}$ background is never larger than 10% of the total background estimate. We rely on simulation to estimate it. The main source of uncertainty in this estimate is the modelling of the E_T^{miss} resolution because poor resolution can enhance the contributions at large M_T . The studies of E_T^{miss} resolution presented in Section 5.2.1 indicate that it could be mismodelled by about 10% in simulation. Changes in the simulated E_T^{miss} resolution by a corresponding amount provide an uncertainty of 100% in the semileptonic $t\bar{t}$ estimate.

5.2.3 Rare standard model backgrounds

The “rare” background category includes $t\bar{t}$ production in association with a vector boson (W, Z, or γ), diboson, and triboson events. Within this category, W Z events dominate the SRs with two jets, and $t\bar{t}Z$ events with the Z boson decaying into a pair of neutrinos ($Z \rightarrow \nu\bar{\nu}$) dominate regions of higher jet multiplicity. The expected contributions from these backgrounds are small, and the simulation is expected to model the kinematics of these processes well in the regions of phase space relevant to the SRs. The rare backgrounds are therefore estimated using simulation. We assess the theoretical and experimental uncertainties affecting the estimates as described in Section 7, resulting in a total uncertainty of 15–26%, depending on the SR.

5.3 Results

The background expectations and the corresponding yields for each SR are summarized in Table 4 and in Fig. 5. Overall, the observed and predicted yields agree within two standard deviations in all SRs. For signals of top squark pair production for different mass hypotheses, the maximum observed significance obtained by combining the results in different SRs is 1.2 standard deviations for a top squark mass of $\approx 400 \text{ GeV}$ and a massless LSP hypothesis. We therefore find no evidence for top squark pair production.

Table 4: Background estimates from data and simulation, and observed data yields for the single-lepton top squark analysis using 2.3 fb^{-1} of data collected during 2015 pp collisions. The uncertainties are the quadratic sums of statistical and systematic uncertainties.

E_T^{miss} [GeV]	Lost-lepton	1ℓ (not from top)	$t\bar{t} \rightarrow 1\ell$	$Z \rightarrow \nu\bar{\nu}$	Total background	Data
Degenerate $\tilde{\chi}_1^\pm$ and $\tilde{\chi}_1^0$: 2 jets, $t_{\text{mod}} > 6.4$						
250–350	4.4 ± 1.4	2.61 ± 0.99	0.09 ± 0.09	0.60 ± 0.12	7.7 ± 1.7	8
>350	0.62 ± 0.23	0.98 ± 0.47	<0.03	0.36 ± 0.13	1.96 ± 0.54	5
Boosted high Δm : 3 jets, $M_{T2}^W > 200 \text{ GeV}$						
250–350	2.83 ± 0.73	0.92 ± 0.52	0.12 ± 0.12	0.64 ± 0.13	4.51 ± 0.91	8
>350	0.74 ± 0.21	0.88 ± 0.50	0.05 ± 0.05	0.41 ± 0.09	2.08 ± 0.55	2
Low Δm : ≥ 4 jets, $M_{T2}^W \leq 200 \text{ GeV}$						
250–325	23.0 ± 3.2	0.61 ± 0.61	0.88 ± 0.88	0.74 ± 0.17	25.2 ± 3.4	14
>325	7.9 ± 1.5	0.45 ± 0.45	0.40 ± 0.40	0.30 ± 0.11	9.0 ± 1.6	8
High Δm : ≥ 4 jets, $M_{T2}^W > 200 \text{ GeV}$						
250–350	3.29 ± 0.91	0.92 ± 0.46	0.78 ± 0.78	0.76 ± 0.19	5.8 ± 1.3	13
350–450	0.94 ± 0.27	0.54 ± 0.34	0.18 ± 0.18	0.46 ± 0.14	2.13 ± 0.48	4
>450	0.57 ± 0.21	0.55 ± 0.36	0.07 ± 0.07	0.52 ± 0.17	1.71 ± 0.45	0

6 Search for pair production of bottom squarks or of top squarks decaying to charm quarks

This search is motivated by the production of pairs of bottom or top squarks, in which each \tilde{b}_1 or \tilde{t}_1 decays, respectively, into a bottom or a charm quark and a neutralino. In the latter search, the difference between the \tilde{t}_1 and $\tilde{\chi}_1^0$ masses is assumed to be less than 80 GeV, and the only top squark decay mode considered is through a flavour changing neutral current to $c\tilde{\chi}_1^0$. Small mass splittings $\Delta m = m_{\tilde{t}_1} - m_{\tilde{\chi}_1^0}$ or $\Delta m = m_{\tilde{b}_1} - m_{\tilde{\chi}_1^0}$ between the top or bottom squark and the neutralino leave little visible energy in the detector, making signal events difficult to distinguish from SM background. However, events with an energetic ISR jet recoiling against the \vec{p}_T^{miss} originating from the neutralino can provide a distinct topology for signals with compressed mass spectra, i.e. with small Δm . We thus perform a search for events with an ISR jet and significant E_T^{miss} .

6.1 Analysis strategy

Events in the search sample are recorded using the same trigger as that for the top squark search in the all-jet final state, requiring the presence of large E_T^{miss} and at least two energetic jets within the tracker acceptance. After applying an offline selection requiring $E_T^{\text{miss}} > 250 \text{ GeV}$ and at least two jets with $p_T > 60 \text{ GeV}$, we find the trigger efficiency to be greater than 97%. We veto events that have at least four jets with p_T above 50 GeV. The veto and its threshold are motivated by the harder p_T spectrum of the fourth jet in semileptonic $t\bar{t}$ events compared to the signal, in which extra jets originate from ISR or FSR. To reduce the SM background from processes with a leptonically decaying W boson, we reject events containing isolated electrons or muons with $I_{\text{rel}} < 0.1$ and $|\eta| < 2.5$, or $I_{\text{rel}} < 0.2$ and $|\eta| < 2.4$, respectively, and with $p_T > 10 \text{ GeV}$. The contribution containing τ_h decays is reduced by placing a veto on events containing charged-hadron PF candidates with $p_T > 10 \text{ GeV}$, $|\eta| < 2.5$, and an isolation sum smaller than 10% of the candidate p_T .

The dominant SM background sources are Z+jets production with $Z \rightarrow \nu\bar{\nu}$, and the lost-lepton background originating from W+jets, $t\bar{t}$, and single top quark processes with leptonic W bo-

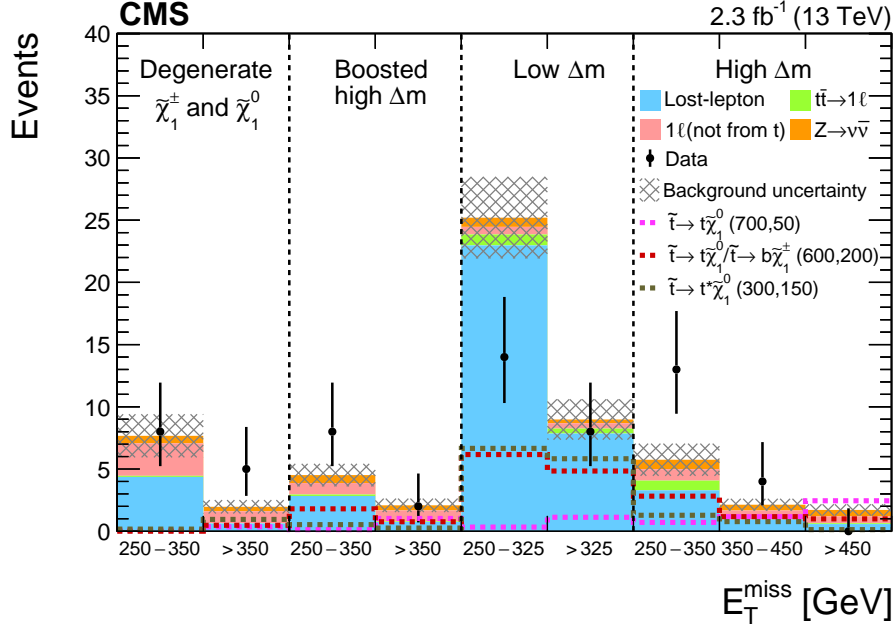


Figure 5: Background estimates from data and simulation, together with the observed yields in the SRs of the single-lepton analysis, described in Table 3. The uncertainties, which are the quadratic sums of statistical and systematic uncertainties, are indicated by the cross-hatched areas. The SM background predictions shown do not include the effects of the maximum likelihood fit to the data. Three signal hypotheses are overlaid. The hypothesis $\tilde{t}_1 \rightarrow t\tilde{\chi}_1^0/\tilde{t}_1 \rightarrow b\tilde{\chi}_1^\pm$ has branching fractions $\mathcal{B}(\tilde{t}_1 \rightarrow t\tilde{\chi}_1^0) = \mathcal{B}(\tilde{t}_1 \rightarrow b\tilde{\chi}_1^\pm) = 0.5$.

son decays. A smaller background contribution comes from QCD events in which large E_T^{miss} originates from jet mismeasurements and the direction of \vec{p}_T^{miss} is often aligned with one of the jets. To suppress this background we require that the absolute difference in azimuthal angle between the \vec{p}_T^{miss} and the closest of the three leading jets ($\Delta\phi_{123}$) is greater than 0.4. Two sets of SRs are defined to optimize the sensitivity for signal models with either compressed or noncompressed mass spectra.

In addition to the criteria discussed above, for regions targeting noncompressed scenarios we require that the p_T of the leading jet be above 100 GeV and that the event contain at least one additional jet with p_T above 75 GeV. We also require that the two highest- p_T jets be identified as b jets. These requirements suppress events originating from W and Z boson production, for which the leading jets have a softer p_T spectrum since they are produced by ISR or FSR. To maintain a stable b tagging efficiency as a function of jet p_T , both the loose and medium working points of the b tagging algorithm are used to identify b jets. The b tagging efficiency of the medium working point depends strongly on the jet p_T and degrades by about 20–30% for jets with p_T above 500 GeV, while the efficiency of the loose working point is more stable with increasing jet p_T . Specifically, we use the loose working point to identify b-tagged jets when the leading jet has p_T above 500 GeV, and the medium working point otherwise. Since such high- p_T jets are less likely to occur in SM processes, the higher misidentification rate of the loose working point results in only a small increase in the SM background.

The distribution of $M_T(j_{1,2}, \vec{p}_T^{\text{miss}}) \equiv \min[M_T(j_1, \vec{p}_T^{\text{miss}}), M_T(j_2, \vec{p}_T^{\text{miss}})]$, where j_1, j_2 are the two highest- p_T jets, is expected to have a kinematic endpoint at the mass of the top quark when \vec{p}_T^{miss} and the closest jet originate from the semileptonic decay of a top quark. In the noncompressed search sample we require $M_T(j_{1,2}, \vec{p}_T^{\text{miss}})$ to be greater than 250 GeV. Events in this

sample are then categorized by $H_{T,12}$, defined for the purposes of this analysis as the scalar sum of the p_T of the two leading jets, and the m_{CT} kinematic variable. The boost-corrected cotransverse mass [71, 72], m_{CT} , is defined by:

$$m_{CT}^2(j_1, j_2) = 2p_T(j_1)p_T(j_2)[1 + \cos \Delta\phi(j_1, j_2)]. \quad (10)$$

For scenarios in which two particles are pair-produced and have the same decay chain, the m_{CT} distribution has an endpoint determined by the masses of the parent and decay-product particles. For $\tilde{b}_1 \rightarrow b\tilde{\chi}_1^0$ this endpoint is at $(m(\tilde{b}_1)^2 - m(\tilde{\chi}_1^0)^2)/m(\tilde{b}_1)$.

For signals with compressed mass spectra, high- p_T ISR is required to be able to reconstruct the quarks as jets and obtain a large value of E_T^{miss} . Compressed SRs require therefore a leading jet with $p_T > 250$ GeV that is back-to-back relative to the \vec{p}_T^{miss} ($\Delta\phi(j_1, \vec{p}_T^{\text{miss}}) > 2.3$). Since such ISR jets are not expected to originate from b quarks, we require that the leading jet fail the loose b-tagging requirement.

We relax the thresholds on the second jet p_T and on the $M_T(j_{1,2}, \vec{p}_T^{\text{miss}})$ to 60 and 200 GeV, respectively, and categorize events in the search sample according to the number of b-tagged jets. The m_{CT} observable loses its discriminating power for these compressed signal models due to the small mass splitting between the parent particle and $\tilde{\chi}_1^0$. The E_T^{miss} is therefore used as the main discriminant, with different E_T^{miss} thresholds applied to define the final SRs.

The baseline selections for both noncompressed and compressed regions are summarized in Table 5, while the definitions of the two sets of SRs are described in Table 6.

Table 5: A summary of the baseline selections used for the noncompressed and compressed \tilde{b}_1 and $\tilde{t}_1 \rightarrow c\tilde{\chi}_1^0$ compressed SRs.

Selection	Noncompressed	Compressed
N_j	$2 \leq N_j \leq 3$	$2 \leq N_j \leq 3$
First jet p_T	> 100 GeV	> 250 GeV
Second jet p_T	> 75 GeV	> 60 GeV
Veto fourth jet	$p_T > 50$ GeV	$p_T > 50$ GeV
Lepton and isolated track veto	$p_T > 10$ GeV	$p_T > 10$ GeV
b tagging	First and second jets are b-tagged	Leading jet is not b-tagged
E_T^{miss}	> 250 GeV	> 250 GeV
$\Delta\phi_{123}$	> 0.4	> 0.4
$\Delta\phi(j_1, \vec{p}_T^{\text{miss}})$	—	> 2.3
$M_T(j_{1,2}, \vec{p}_T^{\text{miss}})$	> 250 GeV	> 200 GeV
$H_{T,12}$	> 200 GeV	—
m_{CT}	> 250 GeV	—

6.2 Background estimation

The SM background contributions originating from $Z \rightarrow \nu\bar{\nu}$, lost-lepton, and QCD processes are estimated from dedicated data CRs as discussed below. Smaller contributions from other SM processes, such as diboson (VV) processes, are estimated from simulation, and an uncertainty of 50% is assigned to these contributions.

6.2.1 Estimation of the $Z \rightarrow \nu\bar{\nu}$ background

The $Z \rightarrow \nu\bar{\nu}$ background is estimated from a high-purity data sample of $Z \rightarrow \mu^+\mu^-$ events in which we remove the muons and recalculate the relevant kinematic variables to emulate

226 Search for pair production of bottom squarks or of top squarks decaying to charm quarks

Table 6: The categorization in $H_{T,12}$ and m_{CT} for the SRs targeting noncompressed signal scenarios, and in N_b and E_T^{miss} for those targeting compressed signal scenarios.

Noncompressed SRs							
$H_{T,12}[\text{GeV}]$		$m_{\text{CT}} [\text{GeV}]$					
250–500		250–350		350–500		>500	
>500		250–350		350–500		>500	
Compressed SRs							
N_b	$E_{\text{T}}^{\text{miss}} [\text{GeV}]$						
0	250–350	350–450	450–550	550–700	700–850	850–1000	>1000
1	250–350	350–450	450–550	550–700	>700		
2	>250						

$Z \rightarrow \nu\bar{\nu}$ events. The trigger used to collect this CR requires the presence of a high- p_T muon with $|\eta| < 2.1$. In keeping with the trigger constraints, the sample is selected by requiring the presence of two isolated muons in the event with $p_T > 50$ (10) GeV and $|\eta| < 2.1$ (2.4) for the leading (trailing) muon. The invariant mass of the dimuon pair is required to be within 15 GeV of the Z boson mass [70]. Each muon is required to be separated from jets in the event by $\Delta R > 0.3$.

Apart from the lepton selection, we apply the same object and event selection criteria as described in Section 6.1 to this sample, with the exception that b jets are selected using the loose working point of the b tagging algorithm to improve the statistical power of the data CR. Events in the selected sample are subdivided into CRs corresponding to the noncompressed and compressed SRs. The observed events in these data CRs, $N_{\mu\mu}^{\text{data}}$, are translated into an estimation of the $Z \rightarrow \nu\bar{\nu}$ contribution in the SRs with the help of simulation, as follows:

$$N_{Z \rightarrow \nu\bar{\nu}}^{\text{pred}} = \frac{N_{\mu\mu}^{\text{data}} - N_{\mu\mu}^{\text{non-Z}}}{A \epsilon} R_Z^{\mu\mu \rightarrow \nu\nu} \kappa, \quad (11)$$

where $N_{\mu\mu}^{\text{non-Z}}$, representing the small contamination in the CRs due to $t\bar{t}$, W+jets, single top quark, and diboson processes, is estimated from simulation. The corrected dimuon event yield is scaled by the kinematic and detector acceptance of muons from Z bosons, A , and the muon reconstruction, identification, and isolation efficiency ϵ . The acceptance and efficiency are determined from simulation. Efficiency scale factors are applied to correct for differences between data and simulation. These scale factors are determined with a “tag-and-probe” method in $Z \rightarrow \mu^+\mu^-$ events [53]. The product of the muon acceptance and efficiency, $A\epsilon$, varies from 0.6 in the low- m_{CT} and low- E_T^{miss} regions to 0.9 in the high- m_{CT} and high- E_T^{miss} regions. The correction factor $R_Z^{\mu\mu \rightarrow \nu\nu} = 5.942 \pm 0.019$ [70] represents the ratio of the Z boson branching fractions to neutrinos and leptons. The remaining term, κ , accounts for differences in the b tagging efficiency and misidentification rate between the CRs and SRs, resulting from the use of different b tagging working points. These κ factors are determined from $Z \rightarrow \ell\ell$ simulation and corrected for known differences in the performance of the b tagging algorithm between data and simulation as measured in samples of multijet and $t\bar{t}$ events [44]. The value of the b tagging κ factor ranges from 0.10 to 0.15 for the noncompressed SRs, and from 0.20 to 0.25 for the $N_b = 1$ compressed SRs, while it is about 0.15 for the $N_b = 2$ compressed SR.

The largest uncertainty in the $Z \rightarrow \nu\bar{\nu}$ background estimate arises from the limited event yields in the dimuon CR, corresponding to a 10–100% uncertainty in the $Z \rightarrow \nu\bar{\nu}$ prediction. We correct for the estimated contributions to the CR from SM processes other than $Z \rightarrow \mu^+\mu^-$ using simulation samples with an assigned uncertainty of 50% in their normalization. This leads

to an uncertainty of 2–20% in the background estimate. Other experimental and theoretical sources of uncertainty, to be discussed in Section 7, result in an additional 2–8% uncertainty in $A\epsilon$, and a 2% uncertainty is assigned in all SRs to account for the uncertainty in the Z boson branching fractions. The uncertainty in the b tagging κ factors is assessed by varying the data-to-simulation b tagging correction factors according to their measured uncertainties. Additionally, the dependence of κ on the heavy-flavour content in Z boson events is evaluated by varying the $Z+b\bar{b}$ and $Z+c\bar{c}$ fractions in simulation by 20% based on the uncertainty in the CMS $Z+b\bar{b}$ measurement [73], resulting in an additional uncertainty of 10–20% in the $Z \rightarrow \nu\bar{\nu}$ estimate.

6.2.2 Estimation of the lost-lepton background

The lost-lepton background in each SR is estimated from a single-lepton CR in data selected by inverting the electron and muon vetoes in events collected with the same trigger as used to record the signal sample. We relax the b tagging requirement in the CRs using the loose working point in the noncompressed selection, while keeping the same requirement as in the SRs for the compressed regions. In all other respects, the CRs are defined through the same selection criteria as the corresponding SRs, including requirements on the $H_{T,12}$, m_{CT} , N_b , and E_T^{miss} , to remove any dependence of the prediction on the modelling of these kinematic variables in simulation. The possible contamination from signal in the single-lepton CR is negligible, less than 1%, so no extra requirement on $M_T(\ell, \vec{p}_T^{\text{miss}})$ is made. The lost-lepton component of the SM background in each SR, N_{LL}^{pred} , is estimated once again from the corresponding data via a transfer factor, T_{LL} , determined from simulation:

$$N_{LL}^{\text{pred}} = N_{1\ell}^{\text{data}} T_{LL}, \quad T_{LL} = \frac{N_{0\ell}^{\text{sim}}}{N_{1\ell}^{\text{sim}}}, \quad (12)$$

where $N_{1\ell}^{\text{data}}$ is the observed event yield in the single-lepton CR. The transfer factor T_{LL} accounts for effects related to lepton acceptance and efficiency.

The largest uncertainty in the lost-lepton estimate is, as in the previous analyses, due to the statistical uncertainty in the event yields, ranging from 3 to 50%, depending on the SR. Contributions to the CRs from $Z \rightarrow \ell\ell$ and diboson processes are subtracted using estimates from simulation, and a 50% uncertainty is applied to this subtraction, which leads to an uncertainty of 3–10% in the lost-lepton prediction. The limited event counts in the simulation sample result in a 2–12% uncertainty, while uncertainties related to discrepancies between the lepton selection efficiency in data and simulation give rise to a 3–4% uncertainty in the final estimate. An additional uncertainty of 7% in the τ_h component accounts for differences in isolation efficiency between muons and single-prong τ_h decays, as determined from studies with simulated samples of W +jets and $t\bar{t}$ events. A systematic uncertainty of 5–10% is found for the uncertainties in the b tagging scale factors that are applied to the simulation for the differences in b tagging performance between data and simulation and the different b tagging working points. Finally, we estimate a systematic uncertainty in the transfer factor to account for differences in the $t\bar{t}$ and W +jets admixture in the search and control regions. This results in a 20–30% uncertainty in the final prediction.

6.2.3 Estimation of the QCD background

The $\Delta\phi_{123} > 0.4$ requirement reduces the QCD contribution to a small fraction of the total background in all SRs for both compressed and noncompressed models. We estimate this contribution for each SR by applying a transfer factor to the number of events observed in a CR

enriched in QCD events. The CRs are obtained by inverting the $\Delta\phi_{123}$ requirement. The transfer factor, T_{QCD} , is measured in a sideband region in data with $E_{\text{T}}^{\text{miss}} \in [200, 250]$ GeV and the same requirements on the other variables as in the SRs. This factor is the ratio between the number of QCD events in the $\Delta\phi_{123} > 0.4$ and $\Delta\phi_{123} < 0.4$ subsets of this sideband region. The estimated contribution of other SM processes ($t\bar{t}$, W +jets, single top quark, and diboson production) based on simulated samples is subtracted from the event yields in the CR and each subset of the sideband.

The transfer factor for the noncompressed regions does not vary significantly as a function of $H_{\text{T},12}$ and m_{CT} . Therefore, we extract the value of T_{QCD} used for the noncompressed SRs from a sideband selected with an inclusive requirement on $H_{\text{T},12}$ and m_{CT} to reduce the statistical uncertainty in the transfer factor. The transfer factors for the compressed SRs are obtained from sidebands that are subdivided according to the number of b-tagged jets into $N_{\text{b}} = 0$ and $N_{\text{b}} \geq 1$ regions, with the latter used to extract the QCD predictions for the $N_{\text{b}} = 1$ and $N_{\text{b}} \geq 2$ SRs.

The statistical uncertainties due to the limited number of events in the data CRs and the non-QCD simulated samples are propagated to the final QCD estimate, ranging from 10 to 100%. The main uncertainty in T_{QCD} also originates from the statistical uncertainty of the observed and simulated event yields in the sideband region. We assign additional uncertainties for differences in b tagging efficiency between data and simulation and for the subtraction of the non-QCD background contribution in the sideband. The total systematic uncertainty in the QCD prediction varies between 27% and 76% in the compressed SRs, but can be as large as 550% in the noncompressed SRs due to the small event samples in the corresponding sideband in data.

6.3 Results

The expected SM background yields and the number of events observed in data are summarized in Table 7 and shown in Fig. 6. The observed yields agree well with the predicted SM background.

7 Systematic uncertainties

Several categories of systematic uncertainties apply to all three analyses. These include uncertainties arising from the limited event counts in control samples, uncertainties related to the use of simulation in SM background predictions, and a 2.7% uncertainty in integrated luminosity [74] that applies to the estimated signal yields and contributions from rare background processes that are taken directly from simulation, without the use of data control samples.

The limited number of simulated events surviving the stringent requirements on jets and $E_{\text{T}}^{\text{miss}}$ in all three searches can lead to a significant statistical uncertainty in background predictions. In the case of background predictions that rely on simulation for accurate modelling of the relevant event kinematics, we assess theoretical uncertainties, primarily those associated with missing higher-order corrections, in the simulated samples by varying the renormalization and factorization scales up and down by a factor of two [75, 76] and by variations of PDFs. The PDF uncertainties are defined by the standard deviation obtained from 100 variations of the NNPDF3.0 [57] PDFs. The uncertainties are then propagated to the final background estimates.

When the simulation of the detector response does not adequately describe the data, correction factors are applied to account for the observed discrepancies. Differences in the efficiencies for selecting isolated leptons between simulation and data are measured in $Z \rightarrow \ell\ell$ events in the

Table 7: Observed number of events and background prediction in the different SRs for the \tilde{b}_1 and $\tilde{t}_1 \rightarrow c\tilde{\chi}_1^0$ searches. The total uncertainty in the background predictions is also shown.

	$Z \rightarrow \nu\bar{\nu}$	Lost-lepton	QCD	Rare SM	Total SM	Data
m_{CT} [GeV]	$200 \text{ GeV} < H_{T,12} \leq 500 \text{ GeV}$					
250–350	12.5 ± 6.3	5.3 ± 2.0	$0.6^{+3.3}_{-0.6}$	1.09 ± 0.54	$19.4^{+7.4}_{-6.6}$	12
>350	$0.9^{+1.1}_{-0.9}$	1.28 ± 0.46	< 0.34	0.18 ± 0.09	$2.4^{+1.3}_{-1.1}$	3
m_{CT} [GeV]	$H_{T,12} > 500 \text{ GeV}$					
250–350	< 1.5	1.34 ± 0.78	< 0.34	< 0.12	1.34 ± 0.78	1
350–500	0.84 ± 0.94	0.67 ± 0.35	< 0.34	< 0.12	1.51 ± 0.98	1
>500	2.0 ± 1.6	0.34 ± 0.20	$0.2^{+1.6}_{-0.2}$	< 0.12	$2.3^{+2.2}_{-1.6}$	0
E_T^{miss} [GeV]	$N_b = 0$					
250–350	680 ± 78	530 ± 120	86 ± 25	14.2 ± 7.1	1310 ± 150	1250
350–450	454 ± 63	270 ± 64	24.9 ± 8.8	11.0 ± 5.5	760 ± 89	802
450–550	226 ± 42	82 ± 52	$0.8^{+2.7}_{-0.8}$	4.8 ± 2.4	314 ± 67	305
550–700	94 ± 27	27 ± 21	< 0.95	1.75 ± 0.87	122 ± 34	137
700–850	26 ± 14	7.0 ± 6.1	1.6 ± 1.4	0.43 ± 0.21	35 ± 15	37
850–1000	$7.2^{+7.6}_{-7.2}$	$1.6^{+1.8}_{-1.6}$	< 0.95	0.13 ± 0.06	$7.3^{+7.9}_{-7.3}$	13
>1000	< 2.0	$0.48^{+0.51}_{-0.48}$	$0.12^{+0.53}_{-0.12}$	0.11 ± 0.05	$0.71^{+0.71}_{-0.52}$	1
E_T^{miss} [GeV]	$N_b = 1$					
250–350	29.2 ± 5.0	43 ± 11	5.1 ± 4.2	1.32 ± 0.65	79 ± 13	93
350–450	27.7 ± 4.7	17.1 ± 4.9	< 0.47	0.99 ± 0.49	45.8 ± 6.8	47
450–550	10.8 ± 2.0	4.9 ± 2.0	< 0.47	0.41 ± 0.20	16.2 ± 2.8	18
550–700	6.0 ± 1.3	1.82 ± 0.96	< 0.47	0.23 ± 0.11	8.1 ± 1.6	8
> 700	3.07 ± 0.64	0.59 ± 0.47	< 0.47	< 0.12	3.66 ± 0.80	2
E_T^{miss} [GeV]	$N_b = 2$					
>250	1.6 ± 1.6	4.7 ± 2.5	$0.32^{+0.40}_{-0.32}$	0.19 ± 0.09	6.5 ± 2.9	11

case of electrons and muons and in a $t\bar{t}$ -enriched sample for hadronically decaying τ leptons. The observed deviations are accounted for in the form of corrections to the simulation, and the corresponding uncertainties are propagated to the predicted SM yields in the SRs. Correction factors and uncertainties based on measurements of b tagging performance in data and simulation [44] are also applied. They are parameterized by jet kinematics and flavour. We also assess an uncertainty related to the modelling of additional interactions in the simulation. For the rare SM backgrounds with top quarks, predominantly from $t\bar{t}$ production in association with a Z boson, where the Z boson decays to a pair of neutrinos, an extra uncertainty is estimated to account for the possible mismodelling of the top quark p_T spectrum. The efficiency and misidentification rates for the top quark tagging algorithm are compared between data and simulation in CRs as a function of the key kinematic variables. The correction factors are found not to be strongly dependent on the different kinematic variables. The efficiency estimated in simulation agrees with the measured efficiency while the misidentification rate has to be corrected by 30%. Both correction factors have a 10% uncertainty, estimated from the variations of the efficiency measurement.

All these uncertainties are propagated to the different signal and background estimates to which they apply. The background predictions from control samples in data are affected through the transfer factors that are calculated from simulation corrected to reproduce data. In general these uncertainties are subdominant and the uncertainty in the final background estimate is dominated by the statistical uncertainty of the data control sample.

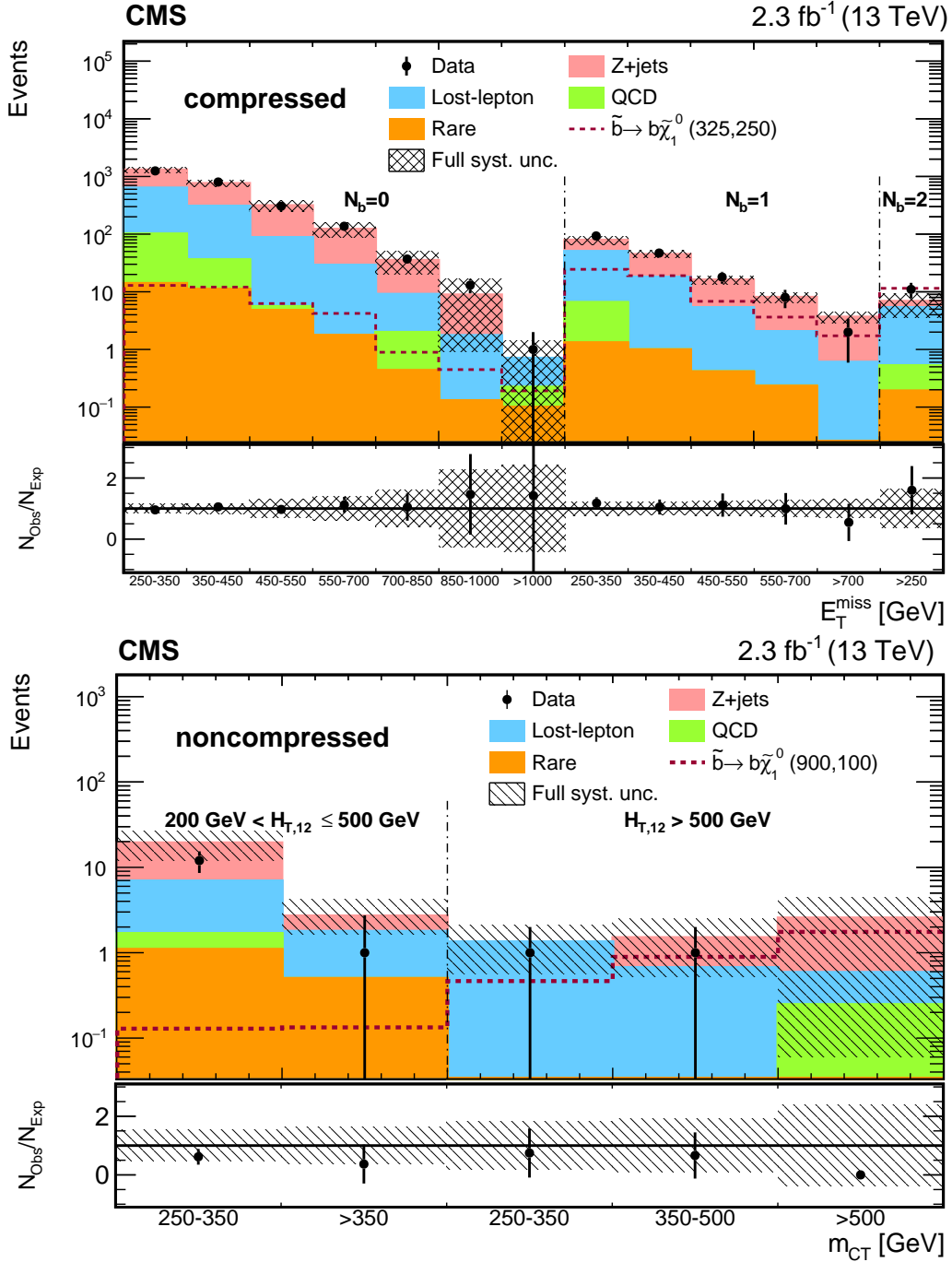


Figure 6: Observed events and estimated SM background and signal yields for the compressed (top) and noncompressed (bottom) SRs for the bottom squark search in the all-jet final state. The observed data yield is shown as black points and the total background predictions are shown in solid area. The SM background predictions shown do not include the effects of the maximum likelihood fit to the data. The bottom panel shows the ratio of data to the total background prediction in each search bin. Only statistical uncertainties are propagated to the ratio.

For the signal samples differences between the fast simulation and the full GEANT4-based model are also taken into account. Lepton selection efficiencies and b tagging performance are found to be different in the fast simulation. We derive appropriate corrections for the fast

simulation and propagate the corresponding uncertainties to the predicted signal yields. We also assess an additional uncertainty for the difference in E_T^{miss} resolution between the fast simulation and the full GEANT4-based model. This difference in E_T^{miss} resolution has the largest impact on signal models with small intrinsic E_T^{miss} , as is the case for compressed mass spectra. The modelling of the ISR plays an important role in cases where the top squark and $\tilde{\chi}_1^0$ masses are very similar. The uncertainty is determined by comparing the simulated and observed p_T spectra of the system recoiling against the ISR jets in $t\bar{t}$ events, using the method described in Ref. [21]. The effect is generally found to be small, although in scenarios with a compressed mass spectrum the effect can be as large as 30%.

The uncertainties in the signal modelling are determined in each analysis for every SR. The dominant uncertainties in the predicted signal yield arise from the size of the simulated samples in some of the SRs (1–100%), jet energy scale corrections (1–50%), b tagging efficiency corrections used to scale simulation to data (1–35%), and ISR (1–30%). The largest uncertainties are in SRs that have small signal acceptance to a specific model.

The statistical uncertainties of the signal samples are uncorrelated, whereas all other signal systematic uncertainties are considered to be fully correlated among the different SRs and analyses. Since the three analyses predict the backgrounds with different CRs, the treatment of systematic uncertainties is mostly uncorrelated among analyses, except for the estimates based on simulation. Here only the statistical component of the uncertainty is treated as uncorrelated. Systematic uncertainties due to jet energy scale corrections, b tagging efficiency and selection efficiencies are treated as correlated among the different background estimates.

8 Interpretation

The data in all three searches are consistent with the background expected from SM processes. The results are interpreted as limits on supersymmetric particle masses in the context of simplified models [77–80] of top or bottom squark pair production.

Different decay modes are considered for top squark pair production. For mass splittings Δm larger than the W boson mass, we consider two decay modes for the top squark: to a top quark and a neutralino, or to a bottom quark and a chargino, where the chargino decays to an LSP. Scenarios with $\tilde{t}_1 \rightarrow t^{(*)}\tilde{\chi}_1^0$ branching fractions of 50 or 100% are considered. The results of the top squark searches in the all-jet and single-lepton final states are combined for these interpretations. For Δm smaller than the W boson mass, only the decay of top squarks to a charm quark and an LSP is considered in this paper. For the pair production of bottom squarks, all bottom squarks are assumed to decay to a bottom quark and an LSP.

The signal yield is corrected for signal contamination of data CRs for each mass hypothesis and each analysis. Typical values are around 5–10%, except for compressed mass spectra, where it can vary between 10 and 50%. The signal contamination is most significant for the top squark production models with a 100% $\tilde{t}_1 \rightarrow t^{(*)}\tilde{\chi}_1^0$ branching fraction, a light LSP, and Δm close to the top quark mass. The 95% confidence level (CL) upper limits on SUSY production cross sections are calculated using a modified frequentist approach with the CL_s criterion [81, 82] and asymptotic results for the test statistic [83, 84].

The SRs and CRs for top squark searches in the all-jet and single-lepton final states are mutually exclusive. We combine the results of the two searches, treating the systematic uncertainties assigned to the predicted signal and background yields as correlated or uncorrelated depending on the source, as detailed in Section 7.

Figure 7 shows 95% CL exclusion limits for $pp \rightarrow \tilde{t}_1 \tilde{t}_1 \rightarrow t^{(*)} \tilde{\chi}_1^0 t^{(*)} \tilde{\chi}_1^0$, assuming the top quarks in the decay to be unpolarized, together with the upper limit at 95% CL on the excluded signal cross section. All top squarks are assumed to decay to a top quark and an LSP. For $\Delta m < m_t$ the signal samples assume a three-body decay without an off-shell top quark as intermediate particle. The expected exclusion is given by the dashed red line, with the one standard deviation (s.d.) experimental uncertainty. The observed exclusion curve is shown as a solid black line together with the 1 s.d. uncertainty in the theoretical cross section. We do not interpret in the region near $\Delta m \approx m_t$ when $\tilde{\chi}_1^0$ is very light because of the difficulty in modelling rapidly varying kinematics in this region. In this region an indirect search for top squark pair production can be performed by looking for a small excess in the measured $t\bar{t}$ cross section compared to the SM expectation [20, 85]. We exclude top squark masses from 280 GeV to 830 GeV for a massless LSP and LSP masses up to 260 GeV for 675 GeV top squarks. At 8 TeV top squark masses were excluded up to 780 GeV for a massless LSP [25]. For models with heavy top squarks and light LSPs, the sensitivity is driven by the top squark analysis in the all-jet final state of Section 4, which is more sensitive than the single-lepton analysis (Section 5) because of the larger acceptance for signal. The combination extends the expected reach in top squark mass by about 45 GeV. When the LSP is heavier, the cleaner search in the single-lepton final state becomes more important. Both analyses have similar sensitivity in this area of parameter space, and combining them extends the reach in LSP mass by about 30 GeV.

Figure 8 shows the 95% CL exclusion limits for $\tilde{t}_1 \tilde{t}_1$ production, assuming equal probabilities for the decay modes $\tilde{t}_1 \rightarrow t^{(*)} \tilde{\chi}_1^0$ and $\tilde{t}_1 \rightarrow b \tilde{\chi}_1^\pm$. The chargino in the latter mode decays to a W boson and an LSP. In this model, the chargino is considered to be nearly mass-degenerate with the LSP ($m_{\tilde{\chi}_1^\pm} = m_{\tilde{\chi}_1^0} + 5$ GeV). The W boson decay products originating from the chargino decay are very soft because of the small mass splitting, and might not be detectable. For intermediate LSP masses, top squark masses are probed up to 725 GeV. The LSP masses up to 210 GeV are probed for a top squark mass of around 500 GeV. Here, the single-lepton analysis does not contribute much to the combination because of the larger acceptance in the all-jet final state, except at low LSP masses. In most of the mass parameter space the combination reaches ≈ 15 GeV higher than the analysis in the all-jet final state.

The compressed SRs from the bottom squark analysis in the all-jet final state (Section 6) are used to set upper limits on the top squark cross sections when the mass splitting between the top squark and the LSP is smaller than the mass of the W boson. Figure 9 shows the expected and observed 95% CL upper limits on the top squark cross sections in the $m_{\tilde{t}_1} - m_{\tilde{\chi}_1^0}$ plane assuming the top squark always decays to a charm quark and an LSP. Top squarks with masses below 240 GeV are probed in this model, when the mass splitting between the top squark and the LSP is close to 10 GeV. At 8 TeV top squark masses up to 270 GeV were probed for the same Δm [20].

Figure 10 shows the expected and observed 95% CL upper limits on the bottom squark cross sections in the $m_{\tilde{b}_1} - m_{\tilde{\chi}_1^0}$ plane using both the compressed and noncompressed SRs of the bottom squark analysis. We probe bottom squark masses up to 890 GeV for small LSP masses. With 8 TeV data bottom squark masses below 650 GeV were excluded. [20, 24].

9 Summary

Results are presented from three complementary searches for top or bottom squark-antisquark pairs in data collected with the CMS detector in proton-proton collisions at a centre-of-mass energy of 13 TeV, corresponding to an integrated luminosity of 2.3 fb^{-1} . The search for top squarks is carried out in the all-jet and single-lepton final states, which are combined for the

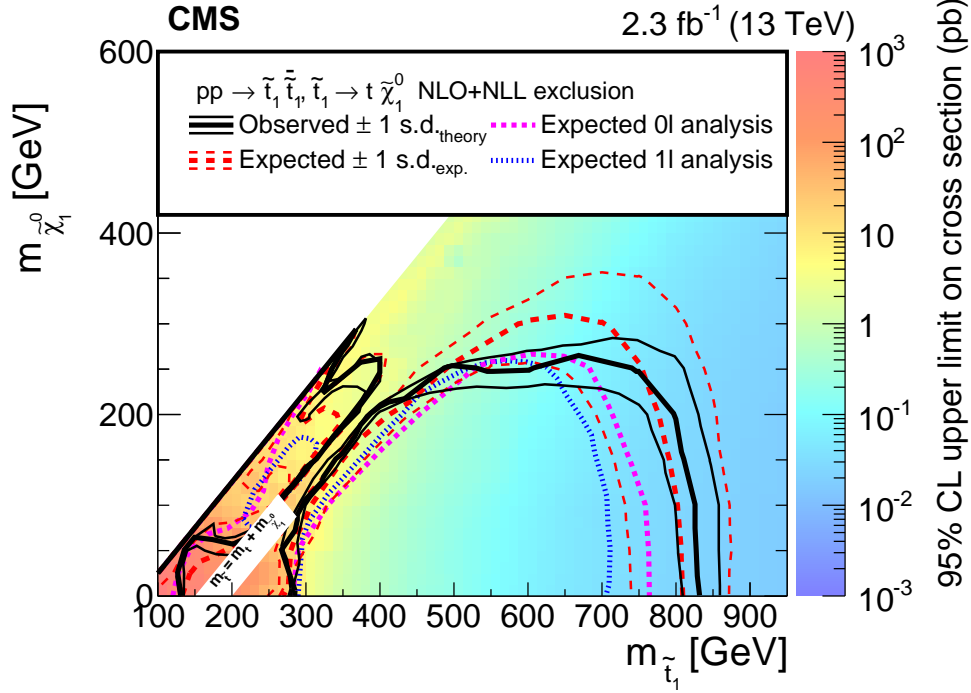


Figure 7: Exclusion limits at 95% CL for direct top squark pair production for the decay mode $\tilde{t}_1 \rightarrow t^{(*)} \tilde{\chi}_1^0$. The interpretation is performed in the two-dimensional space of $m_{\tilde{t}_1}$ vs. $m_{\tilde{\chi}_1^0}$. The color indicates the 95% CL upper limit on the product of cross section and branching fraction at each point in the $m_{\tilde{t}_1}$ - $m_{\tilde{\chi}_1^0}$ plane. The regions enclosed by the thick black curves represent the observed exclusion at 95% CL, while the dashed red lines indicate the expected limits at 95% CL and their ± 1 s.d. experimental uncertainties. The thin black lines show the impact of the ± 1 s.d. theoretical uncertainties in the signal cross section. The magenta short-dashed curve and the blue dotted curve show the expected limits for the analysis in the all-jet (Section 4) and single-lepton (Section 5) final states, respectively. The limits in the region $\Delta m \approx m_t$ and low $\tilde{\chi}_1^0$ mass are not shown due to the difficulty in modelling rapidly varying kinematics in this region.

final result. A second search in all-jet events is designed for bottom squark pairs and for top squarks decaying to charm quarks through a flavour changing neutral current process. No statistically significant excess of events is observed above the expected standard model background, and exclusion limits are set at 95% confidence level in the context of simplified models of direct top and bottom squark pair production. Limits for top squark masses of 830 GeV are established for a massless lightest supersymmetric particle (LSP), and for LSP masses up to 260 GeV for a 675 GeV top squark mass, when all top squarks are assumed to decay to a top quark and an LSP. When the top squarks can also decay to a bottom quark and a chargino, this reach is reduced. Assuming a mass splitting between the top squark and the LSP close to 10 GeV, and top squarks that decay to a charm quark and an LSP, top squark mass limits up to 240 GeV are established. Finally, bottom squark mass limits up to 890 GeV are established for small LSP masses. The results extend the reach with respect to previous limits obtained from LHC Run 1 data in most of the parameter space.

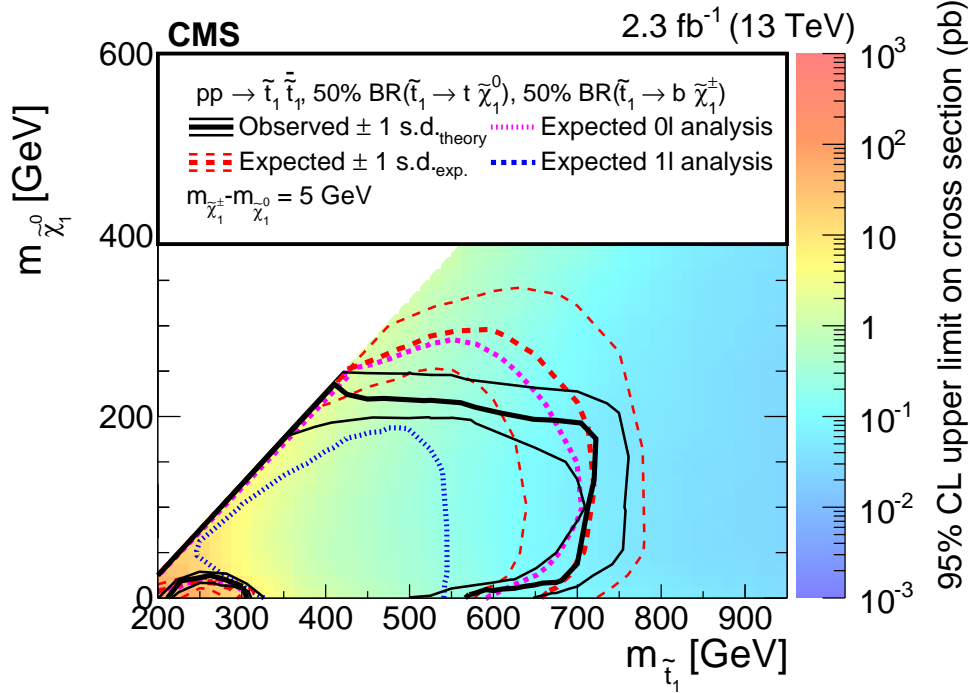


Figure 8: Exclusion limits at 95% CL for direct top squark pair production assuming equal branching fractions for the decays $\tilde{t}_1 \rightarrow t^{(*)} \tilde{\chi}_1^0$ and $\tilde{t}_1 \rightarrow b \tilde{\chi}_1^\pm$. The interpretation is performed in the two-dimensional space of $m_{\tilde{t}_1}$ vs. $m_{\tilde{\chi}_1^0}$. The chargino is considered to be nearly mass-degenerate with the LSP ($m_{\tilde{\chi}_1^\pm} = m_{\tilde{\chi}_1^0} + 5$ GeV). The caption of Fig. 7 explains the use of lines and colors in detail.

Acknowledgments

We congratulate our colleagues in the CERN accelerator departments for the excellent performance of the LHC and thank the technical and administrative staffs at CERN and at other CMS institutes for their contributions to the success of the CMS effort. In addition, we gratefully acknowledge the computing centres and personnel of the Worldwide LHC Computing Grid for delivering so effectively the computing infrastructure essential to our analyses. Finally, we acknowledge the enduring support for the construction and operation of the LHC and the CMS detector provided by the following funding agencies: the Austrian Federal Ministry of Science, Research and Economy and the Austrian Science Fund; the Belgian Fonds de la Recherche Scientifique, and Fonds voor Wetenschappelijk Onderzoek; the Brazilian Funding Agencies (CNPq, CAPES, FAPERJ, and FAPESP); the Bulgarian Ministry of Education and Science; CERN; the Chinese Academy of Sciences, Ministry of Science and Technology, and National Natural Science Foundation of China; the Colombian Funding Agency (COLCIENCIAS); the Croatian Ministry of Science, Education and Sport, and the Croatian Science Foundation; the Research Promotion Foundation, Cyprus; the Secretariat for Higher Education, Science, Technology and Innovation, Ecuador; the Ministry of Education and Research, Estonian Research Council via IUT23-4 and IUT23-6 and European Regional Development Fund, Estonia; the Academy of Finland, Finnish Ministry of Education and Culture, and Helsinki Institute of Physics; the Institut National de Physique Nucléaire et de Physique des Particules / CNRS, and Commissariat à l'Énergie Atomique et aux Énergies Alternatives / CEA, France; the Bundesministerium für Bildung und Forschung, Deutsche Forschungsgemeinschaft, and Helmholtz-Gemeinschaft Deutscher Forschungszentren, Germany; the General Secretariat for Research and Technology, Greece; the National Scientific Research Foundation, and National Innova-

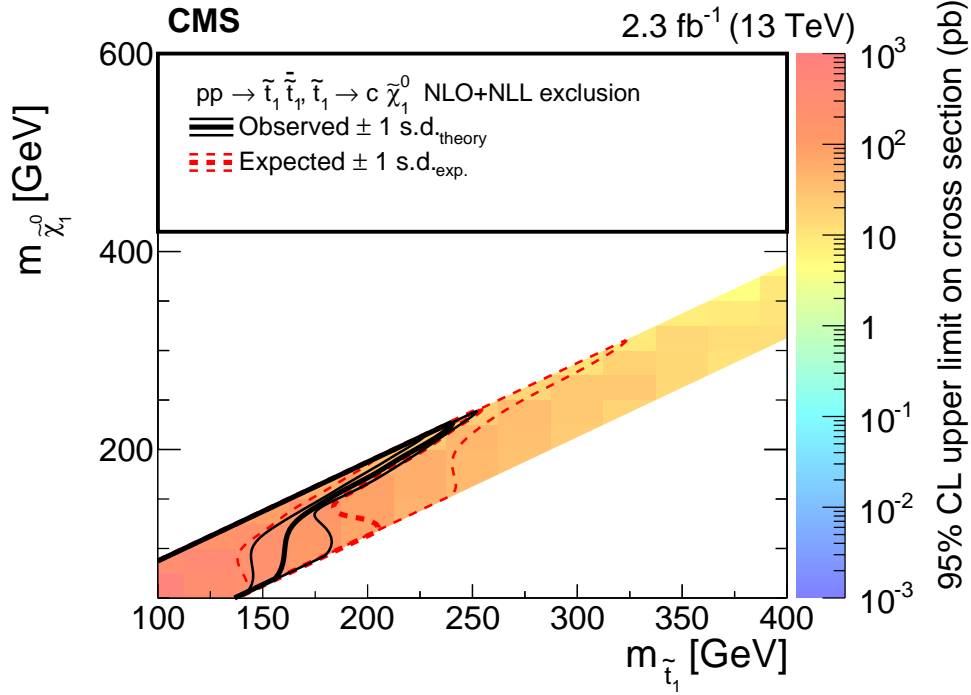


Figure 9: Exclusion limits at 95% CL for direct top squark pair production with decay $\tilde{t}_1 \rightarrow c\tilde{\chi}_1^0$ using the compressed SRs of the bottom squark analysis (Section 6). The interpretation is done in the two-dimensional space of $m_{\tilde{t}_1}$ vs. $m_{\tilde{\chi}_1^0}$. The caption of Fig. 7 explains the use of lines and colors in detail.

tion Office, Hungary; the Department of Atomic Energy and the Department of Science and Technology, India; the Institute for Studies in Theoretical Physics and Mathematics, Iran; the Science Foundation, Ireland; the Istituto Nazionale di Fisica Nucleare, Italy; the Ministry of Science, ICT and Future Planning, and National Research Foundation (NRF), Republic of Korea; the Lithuanian Academy of Sciences; the Ministry of Education, and University of Malaya (Malaysia); the Mexican Funding Agencies (BUAP, CINVESTAV, CONACYT, LNS, SEP, and UASLP-FAI); the Ministry of Business, Innovation and Employment, New Zealand; the Pakistan Atomic Energy Commission; the Ministry of Science and Higher Education and the National Science Centre, Poland; the Fundação para a Ciência e a Tecnologia, Portugal; JINR, Dubna; the Ministry of Education and Science of the Russian Federation, the Federal Agency of Atomic Energy of the Russian Federation, Russian Academy of Sciences, the Russian Foundation for Basic Research and the Russian Competitiveness Program of NRNU MEPhI (M.H.U.); the Ministry of Education, Science and Technological Development of Serbia; the Secretaría de Estado de Investigación, Desarrollo e Innovación and Programa Consolider-Ingenio 2010, Spain; the Swiss Funding Agencies (ETH Board, ETH Zurich, PSI, SNF, UniZH, Canton Zurich, and SER); the Ministry of Science and Technology, Taipei; the Thailand Center of Excellence in Physics, the Institute for the Promotion of Teaching Science and Technology of Thailand, Special Task Force for Activating Research and the National Science and Technology Development Agency of Thailand; the Scientific and Technical Research Council of Turkey, and Turkish Atomic Energy Authority; the National Academy of Sciences of Ukraine, and State Fund for Fundamental Researches, Ukraine; the Science and Technology Facilities Council, UK; the US Department of Energy, and the US National Science Foundation.

Individuals have received support from the Marie-Curie programme and the European Research Council and EPLANET (European Union); the Leventis Foundation; the A. P. Sloan

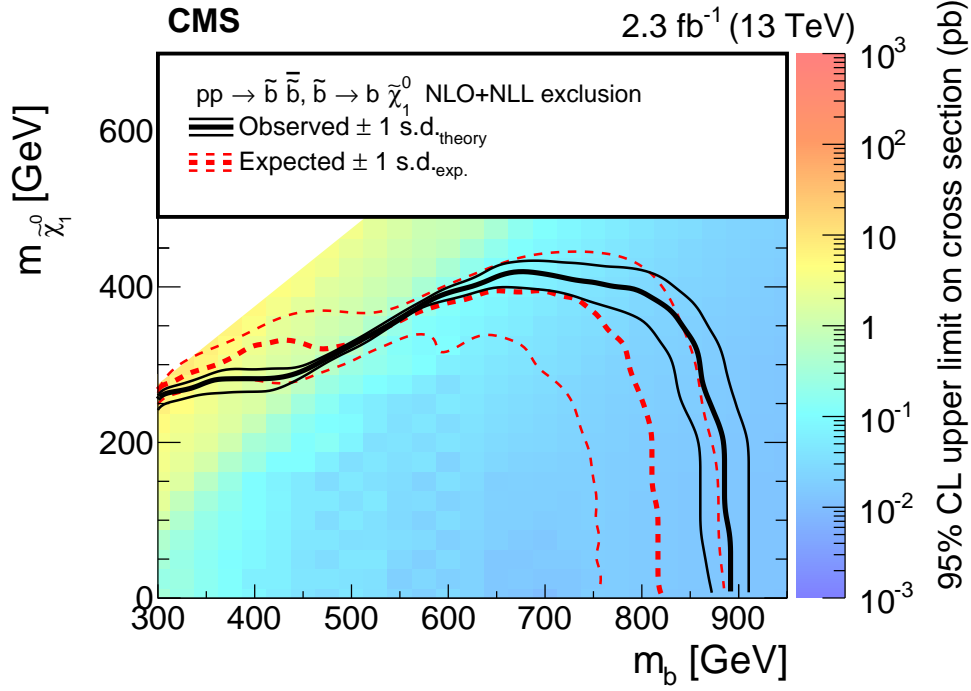


Figure 10: Exclusion limits at 95% CL for direct bottom squark pair production with decay $\tilde{b}_1 \rightarrow b \tilde{\chi}_1^0$. The interpretation is performed in the two-dimensional space of $m_{\tilde{b}_1}$ vs. $m_{\tilde{\chi}_1^0}$ using the results of the bottom squark analysis (Section 6). The caption of Fig. 7 explains the use of lines and colors in detail.

Foundation; the Alexander von Humboldt Foundation; the Belgian Federal Science Policy Office; the Fonds pour la Formation à la Recherche dans l'Industrie et dans l'Agriculture (FRIA-Belgium); the Agentschap voor Innovatie door Wetenschap en Technologie (IWT-Belgium); the Ministry of Education, Youth and Sports (MEYS) of the Czech Republic; the Council of Science and Industrial Research, India; the HOMING PLUS programme of the Foundation for Polish Science, cofinanced from European Union, Regional Development Fund, the Mobility Plus programme of the Ministry of Science and Higher Education, the National Science Center (Poland), contracts Harmonia 2014/14/M/ST2/00428, Opus 2014/13/B/ST2/02543, 2014/15/B/ST2/03998, and 2015/19/B/ST2/02861, Sonata-bis 2012/07/E/ST2/01406; the Thalís and Aristeia programmes cofinanced by EU-ESF and the Greek NSRF; the National Priorities Research Program by Qatar National Research Fund; the Programa Clarín-COFUND del Principado de Asturias; the Rachadapisek Sompot Fund for Postdoctoral Fellowship, Chulalongkorn University and the Chulalongkorn Academic into Its 2nd Century Project Advancement Project (Thailand); and the Welch Foundation, contract C-1845.

References

- [1] G. 't Hooft, “Naturalness, chiral symmetry, and spontaneous chiral symmetry breaking”, *NATO Sci. Ser. B* **59** (1980) 135.
- [2] E. Witten, “Dynamical breaking of supersymmetry”, *Nucl. Phys. B* **188** (1981) 513, doi:10.1016/0550-3213(81)90006-7.
- [3] M. Dine, W. Fischler, and M. Srednicki, “Supersymmetric technicolor”, *Nucl. Phys. B* **189** (1981) 575, doi:10.1016/0550-3213(81)90582-4.

- [4] S. Dimopoulos and S. Raby, “Supercolor”, *Nucl. Phys. B* **192** (1981) 353, doi:10.1016/0550-3213(81)90430-2.
- [5] S. Dimopoulos and H. Georgi, “Softly broken supersymmetry and SU(5)”, *Nucl. Phys. B* **193** (1981) 150, doi:10.1016/0550-3213(81)90522-8.
- [6] R. K. Kaul and P. Majumdar, “Cancellation of quadratically divergent mass corrections in globally supersymmetric spontaneously broken gauge theories”, *Nucl. Phys. B* **199** (1982) 36, doi:10.1016/0550-3213(82)90565-X.
- [7] J. Wess and B. Zumino, “Supergauge transformations in four-dimensions”, *Nucl. Phys. B* **70** (1974) 39, doi:10.1016/0550-3213(74)90355-1.
- [8] G. R. Farrar and P. Fayet, “Phenomenology of the Production, Decay, and Detection of New Hadronic States Associated with Supersymmetry”, *Phys. Lett. B* **76** (1978) 575, doi:10.1016/0370-2693(78)90858-4.
- [9] C. Boehm, A. Djouadi, and M. Drees, “Light scalar top quarks and supersymmetric dark matter”, *Phys. Rev. D* **62** (2000) 035012, doi:10.1103/PhysRevD.62.035012, arXiv:hep-ph/9911496.
- [10] C. Balázs, M. Carena, and C. E. M. Wagner, “Dark matter, light stops and electroweak baryogenesis”, *Phys. Rev. D* **70** (2004) 015007, doi:10.1103/PhysRevD.70.015007, arXiv:hep-ph/403224.
- [11] G. Jungman, M. Kamionkowski, and K. Griest, “Supersymmetric dark matter”, *Phys. Rept.* **267** (1996) 195, doi:10.1016/0370-1573(95)00058-5, arXiv:hep-ph/9506380.
- [12] ATLAS Collaboration, “Search for a supersymmetric partner to the top quark in final states with jets and missing transverse momentum at $\sqrt{s} = 7$ TeV with the ATLAS detector”, *Phys. Rev. Lett.* **109** (2012) 211802, doi:10.1103/PhysRevLett.109.211802, arXiv:1208.1447.
- [13] ATLAS Collaboration, “Search for direct top squark pair production in final states with one isolated lepton, jets, and missing transverse momentum in $\sqrt{s} = 7$ TeV pp collisions using 4.7 fb⁻¹ of ATLAS data”, *Phys. Rev. Lett.* **109** (2012) 211803, doi:10.1103/PhysRevLett.109.211803, arXiv:1208.2590.
- [14] ATLAS Collaboration, “Search for a heavy top-quark partner in final states with two leptons with the ATLAS detector at the LHC”, *JHEP* **11** (2012) 094, doi:10.1007/JHEP11(2012)094, arXiv:1209.4186.
- [15] ATLAS Collaboration, “Search for direct top-squark pair production in final states with two leptons in pp collisions at $\sqrt{s} = 8$ TeV with the ATLAS detector”, *JHEP* **06** (2014) 124, doi:10.1007/JHEP06(2014)124, arXiv:1403.4853.
- [16] ATLAS Collaboration, “Search for direct third-generation squark pair production in final states with missing transverse momentum and two b-jets in $\sqrt{s} = 8$ TeV pp collisions with the ATLAS detector”, *JHEP* **10** (2013) 189, doi:10.1007/JHEP10(2013)189, arXiv:1308.2631.

- [17] ATLAS Collaboration, “Measurement of Spin Correlation in Top-Antitop Quark Events and Search for Top Squark Pair Production in pp Collisions at $\sqrt{s} = 8$ TeV Using the ATLAS Detector”, *Phys. Rev. Lett.* **114** (2015) 142001, doi:10.1103/PhysRevLett.114.142001, arXiv:1412.4742.
- [18] ATLAS Collaboration, “Search for pair-produced third-generation squarks decaying via charm quarks or in compressed supersymmetric scenarios in pp collisions at $\sqrt{s} = 8$ TeV with the ATLAS detector”, *Phys. Rev. D* **90** (2014) 052008, doi:10.1103/PhysRevD.90.052008, arXiv:1407.0608.
- [19] ATLAS Collaboration, “Search for direct pair production of the top squark in all-hadronic final states in proton–proton collisions at $\sqrt{s} = 8$ TeV with the ATLAS detector”, *JHEP* **09** (2014) 015, doi:10.1007/JHEP09(2014)015, arXiv:1406.1122.
- [20] ATLAS Collaboration, “ATLAS Run 1 searches for direct pair production of third-generation squarks at the Large Hadron Collider”, *Eur. Phys. J. C* **75** (2015) 510, doi:10.1140/epjc/s10052-015-3726-9, arXiv:1506.08616.
- [21] CMS Collaboration, “Search for top-squark pair production in the single-lepton final state in pp collisions at $\sqrt{s} = 8$ TeV”, *Eur. Phys. J. C* **73** (2013) 2677, doi:10.1140/epjc/s10052-013-2677-2, arXiv:1308.1586.
- [22] CMS Collaboration, “Search for supersymmetry in hadronic final states with missing transverse energy using the variables α_T and b -quark multiplicity in pp collisions at $\sqrt{s} = 8$ TeV”, *Eur. Phys. J. C* **73** (2013) 2568, doi:10.1140/epjc/s10052-013-2568-6, arXiv:1303.2985.
- [23] CMS Collaboration, “Search for supersymmetry using razor variables in events with b -tagged jets in pp collisions at $\sqrt{s} = 8$ TeV”, *Phys. Rev. D* **91** (2015) 052018, doi:10.1103/PhysRevD.91.052018, arXiv:1502.00300.
- [24] CMS Collaboration, “Searches for third-generation squark production in fully hadronic final states in proton-proton collisions at $\sqrt{s} = 8$ TeV”, *JHEP* **06** (2015) 116, doi:10.1007/JHEP06(2015)116, arXiv:1503.08037.
- [25] CMS Collaboration, “Search for direct pair production of supersymmetric top quarks decaying to all-hadronic final states in pp collisions at $\sqrt{s} = 8$ TeV”, *Eur. Phys. J. C* **76** (2016) 460, doi:10.1140/epjc/s10052-016-4292-5, arXiv:1603.00765.
- [26] D0 Collaboration, “Search for 3- and 4-body decays of the scalar top quark in $p\bar{p}$ collisions at $\sqrt{s} = 1.8$ TeV”, *Phys. Lett. B* **581** (2004) 147, doi:10.1016/j.physletb.2003.12.001.
- [27] D0 Collaboration, “Search for pair production of the scalar top quark in muon+tau final states”, *Phys. Lett. B* **710** (2012) 578, doi:10.1016/j.physletb.2012.03.028, arXiv:1202.1978.
- [28] D0 Collaboration, “Search for the lightest scalar top quark in events with two leptons in $p\bar{p}$ collisions at $\sqrt{s} = 1.96$ TeV”, *Phys. Lett. B* **659** (2008) 500, doi:10.1016/j.physletb.2007.11.086, arXiv:0707.2864.
- [29] CDF Collaboration, “Search for the supersymmetric partner of the top quark in $p\bar{p}$ collisions at $\sqrt{s} = 1.96$ TeV”, *Phys. Rev. D* **82** (2010) 092001, doi:10.1103/PhysRevD.82.092001, arXiv:1009.0266.

- [30] CDF Collaboration, “Search for the supersymmetric partner of the top quark in dilepton events from $p\bar{p}$ collisions at $\sqrt{s} = 1.8$ TeV”, *Phys. Rev. Lett.* **90** (2003) 251801, doi:10.1103/PhysRevLett.90.251801, arXiv:hep-ex/0302009.
- [31] C. Borschensky et al., “Squark and gluino production cross sections in pp collisions at $\sqrt{s} = 13, 14, 33$ and 100 TeV”, *Eur. Phys. J. C* **74** (2014) 3174, doi:10.1140/epjc/s10052-014-3174-y, arXiv:1407.5066.
- [32] LHC SUSY Cross Section Working Group, “SUSY cross sections twiki”, 2015.
- [33] CMS Collaboration, “Search for new physics in the all-hadronic final state with the M_{T2} variable”, *JHEP* **10** (2016) 006, doi:10.1007/JHEP10(2016)006, arXiv:1603.04053.
- [34] CMS Collaboration, “Inclusive search for supersymmetry using razor variables in pp collisions at $\sqrt{s} = 13$ TeV”, *Phys. Rev. D* **95** (2017) 012003, doi:10.1103/PhysRevD.95.012003, arXiv:1609.07658.
- [35] CMS Collaboration, “A search for new phenomena in pp collisions at $\sqrt{s} = 13$ TeV in final states with missing transverse momentum and at least one jet using the α_T variable”, *Eur. Phys. J. C* **77** (2017) 294, doi:10.1140/epjc/s10052-017-4787-8, arXiv:1611.00338.
- [36] ATLAS Collaboration, “Search for top squarks in final states with one isolated lepton, jets, and missing transverse momentum in $\sqrt{s} = 13$ TeV collisions with the ATLAS detector”, *Phys. Rev. D* **94** (2016) 052009, doi:10.1103/PhysRevD.94.052009, arXiv:1606.03903.
- [37] CMS Collaboration, “The CMS experiment at the CERN LHC”, *JINST* **3** (2008) S08004, doi:10.1088/1748-0221/3/08/S08004.
- [38] CMS Collaboration, “Particle-Flow Event Reconstruction in CMS and Performance for Jets, Taus, and E_T^{miss} ”, CMS Physics Analysis Summary CMS-PAS-PFT-09-001, 2009.
- [39] CMS Collaboration, “Commissioning of the Particle-flow Event Reconstruction with the first LHC collisions recorded in the CMS detector”, CMS Physics Analysis Summary CMS-PAS-PFT-10-001, 2010.
- [40] M. Cacciari, G. P. Salam, and G. Soyez, “The anti- k_t jet clustering algorithm”, *JHEP* **04** (2008) 063, doi:10.1088/1126-6708/2008/04/063, arXiv:0802.1189.
- [41] M. Cacciari, G. P. Salam, and G. Soyez, “FastJet user manual”, *Eur. Phys. J. C* **72** (2012) 1896, doi:10.1140/epjc/s10052-012-1896-2, arXiv:1111.6097.
- [42] CMS Collaboration, “Study of pileup removal algorithms for jets”, CMS Physics Analysis Summary CMS-PAS-JME-14-001, 2014.
- [43] CMS Collaboration, “Identification of b-quark jets with the CMS experiment”, *JINST* **8** (2013) P04013, doi:10.1088/1748-0221/8/04/P04013, arXiv:1211.4462.
- [44] CMS Collaboration, “Identification of b quark jets at the CMS Experiment in the LHC Run 2”, CMS Physics Analysis Summary CMS-PAS-BTV-15-001, 2016.
- [45] CMS Collaboration, “Boosted Top Jet Tagging at CMS”, CMS Physics Analysis Summary CMS-PAS-JME-13-007, 2014.

- [46] CMS Collaboration, “Top Tagging with New Approaches”, CMS Physics Analysis Summary CMS-PAS-JME-15-002, 2016.
- [47] D. E. Kaplan, K. Rehermann, M. D. Schwartz, and B. Tweedie, “Top Tagging: A Method for Identifying Boosted Hadronically Decaying Top Quarks”, *Phys. Rev. Lett.* **101** (2008) 142001, doi:10.1103/PhysRevLett.101.142001, arXiv:0806.0848.
- [48] M. Dasgupta, A. Fregoso, S. Marzani, and G. P. Salam, “Towards an understanding of jet substructure”, *JHEP* **09** (2013) 029, doi:10.1007/JHEP09(2013)029, arXiv:1307.0007.
- [49] M. Cacciari and G. P. Salam, “Dispelling the N^3 myth for the k_t jet-finder”, *Phys. Lett. B* **641** (2006) 57, doi:10.1016/j.physletb.2006.08.037, arXiv:hep-ph/0512210.
- [50] Y. L. Dokshitzer, G. D. Leder, S. Moretti, and B. R. Webber, “Better jet clustering algorithms”, *JHEP* **08** (1997) 001, doi:10.1088/1126-6708/1997/08/001, arXiv:hep-ph/9707323.
- [51] M. Wobisch and T. Wengler, “Hadronization corrections to jet cross sections in deep-inelastic scattering”, (1998). arXiv:hep-ph/9907280.
- [52] CMS Collaboration, “Performance of electron reconstruction and selection with the CMS detector in proton-proton collisions at $\sqrt{s} = 8$ TeV”, *JINST* **10** (2015) P06005, doi:10.1088/1748-0221/10/06/P06005, arXiv:1502.02701.
- [53] CMS Collaboration, “Performance of CMS muon reconstruction in pp collision events at $\sqrt{s} = 7$ TeV”, *JINST* **7** (2012) P10002, doi:10.1088/1748-0221/7/10/P10002, arXiv:1206.4071.
- [54] CMS Collaboration, “Reconstruction and identification of τ lepton decays to hadrons and ν_τ at CMS”, *JINST* **11** (2016) P01019, doi:10.1088/1748-0221/11/01/P01019, arXiv:1510.07488.
- [55] CMS Collaboration, “Performance of photon reconstruction and identification with the CMS detector in proton-proton collisions at $\sqrt{s} = 8$ TeV”, *JINST* **10** (2015) P08010, doi:10.1088/1748-0221/10/08/P08010.
- [56] J. Alwall et al., “The automated computation of tree-level and next-to-leading order differential cross sections, and their matching to parton shower simulations”, *JHEP* **07** (2014) 079, doi:10.1007/JHEP07(2014)079, arXiv:1405.0301.
- [57] NNPDF Collaboration, “Parton distributions for the LHC Run II”, *JHEP* **04** (2015) 040, doi:10.1007/JHEP04(2015)040, arXiv:1410.8849.
- [58] P. Nason, “A new method for combining NLO QCD with shower Monte Carlo algorithms”, *JHEP* **11** (2004) 040, doi:10.1088/1126-6708/2004/11/040, arXiv:hep-ph/0409146.
- [59] S. Frixione, P. Nason, and C. Oleari, “Matching NLO QCD computations with Parton Shower simulations: the POWHEG method”, *JHEP* **11** (2007) 070, doi:10.1088/1126-6708/2007/11/070, arXiv:0709.2092.
- [60] S. Alioli, P. Nason, C. Oleari, and E. Re, “A general framework for implementing NLO calculations in shower Monte Carlo programs: the POWHEG BOX”, *JHEP* **06** (2010) 043, doi:10.1007/JHEP06(2010)043, arXiv:1002.2581.

- [61] E. Re, “Single-top Wt -channel production matched with parton showers using the POWHEG method”, *Eur. Phys. J. C* **71** (2011) 1547, doi:10.1140/epjc/s10052-011-1547-z, arXiv:1009.2450.
- [62] T. Sjöstrand et al., “An introduction to PYTHIA 8.2”, *Comput. Phys. Commun.* **191** (2015) 159, doi:10.1016/j.cpc.2015.01.024, arXiv:1410.3012.
- [63] GEANT4 Collaboration, “GEANT4 — a simulation toolkit”, *Nucl. Instrum. Meth. A* **506** (2003) 250, doi:10.1016/S0168-9002(03)01368-8.
- [64] S. Abdullin et al., “The fast simulation of the CMS detector at LHC”, *J. Phys. Conf. Ser.* **331** (2011) 032049, doi:10.1088/1742-6596/331/3/032049.
- [65] CMS Collaboration, “Differential cross section measurements for the production of a W boson in association with jets in proton-proton collisions at $\sqrt{s} = 7$ TeV”, *Phys. Lett. B* **741** (2015) 12, doi:10.1016/j.physletb.2014.12.003, arXiv:1406.7533.
- [66] CMS Collaboration, “Measurement of differential cross sections for top quark pair production using the lepton+jets final state in proton-proton collisions at 13 TeV”, (2016). arXiv:1610.04191. Submitted to *Phys. Rev. D*.
- [67] CMS Collaboration, “Observation of top quark pairs produced in association with a vector boson in pp collisions at $\sqrt{s} = 8$ TeV”, *JHEP* **01** (2016) 096, doi:10.1007/JHEP01(2016)096, arXiv:1510.01131.
- [68] Y. Bai, H.-C. Cheng, J. Gallicchio, and J. Gu, “Stop the top background of the stop search”, *JHEP* **07** (2012) 110, doi:10.1007/JHEP07(2012)110, arXiv:1203.4813.
- [69] M. L. Graesser and J. Shelton, “Hunting Mixed Top Squark Decays”, *Phys. Rev. Lett.* **111** (2013) 121802, doi:10.1103/PhysRevLett.111.121802, arXiv:1212.4495.
- [70] Particle Data Group, K. A. Olive et al., “Review of Particle Physics”, *Chin. Phys. C* **38** (2014) 090001, doi:10.1088/1674-1137/38/9/090001.
- [71] G. Polesello and D. Tovey, “Supersymmetric particle mass measurement with boost-corrected constransverse mass”, *JHEP* **03** (2010) 030, doi:10.1007/JHEP03(2010)030, arXiv:0910.0174.
- [72] D. Tovey, “On measuring the masses of pair-produced semi-invisibly decaying particles at hadron colliders”, *JHEP* **04** (2008) 034, doi:10.1088/1126-6708/2008/04/034, arXiv:0802.2879.
- [73] CMS Collaboration, “Measurement of the production cross sections for a Z boson and one or more b jets in pp collisions at $\sqrt{s} = 7$ TeV”, *JHEP* **06** (2014) 120, doi:10.1007/JHEP06(2014)120, arXiv:1402.1521.
- [74] CMS Collaboration, “CMS Luminosity Measurement for the 2015 Data Taking Period”, CMS Physics Analysis Summary CMS-PAS-LUM-15-001, 2016.
- [75] S. Catani, D. de Florian, M. Grazzini, and P. Nason, “Soft gluon resummation for Higgs boson production at hadron colliders”, *JHEP* **07** (2003) 028, doi:10.1088/1126-6708/2003/07/028, arXiv:hep-ph/0306211.
- [76] M. Cacciari et al., “The $t\bar{t}$ cross-section at 1.8 TeV and 1.96 TeV: a study of the systematics due to parton densities and scale dependence”, *JHEP* **04** (2004) 068, doi:10.1088/1126-6708/2004/04/068, arXiv:hep-ph/0303085.

- [77] CMS Collaboration, “Interpretation of searches for supersymmetry with simplified models”, *Phys. Rev. D* **88** (2013) 052017, doi:10.1103/PhysRevD.88.052017, arXiv:1301.2175.
- [78] J. Alwall, P. Schuster, and N. Toro, “Simplified Models for a First Characterization of New Physics at the LHC”, *Phys. Rev. D* **79** (2009) 075020, doi:10.1103/PhysRevD.79.075020.
- [79] J. Alwall, M.-P. Le, M. Lisanti, and J. Wacker, “Model-independent jets plus missing energy searches”, *Phys. Rev. D* **79** (2009) 015005, doi:10.1103/PhysRevD.79.015005.
- [80] LHC New Physics Working Group, D. Alves et al., “Simplified Models for LHC new physics searches”, *J. Phys. G* **39** (2012) 105005, doi:10.1088/0954-3899/39/10/105005, arXiv:1105.2838.
- [81] T. Junk, “Confidence level computation for combining searches with small statistics”, *Nucl. Instrum. Meth. A* **434** (1999) 435, doi:10.1016/S0168-9002(99)00498-2, arXiv:hep-ex/9902006.
- [82] A. L. Read, “Presentation of search results: the CL_S technique”, *J. Phys. G* **28** (2002) 2693, doi:10.1088/0954-3899/28/10/313.
- [83] ATLAS and CMS Collaborations, LHC Higgs Combination Group, “Procedure for the LHC Higgs boson search combination in Summer 2011”, Technical Report ATL-PHYS-PUB 2011-11, CMS NOTE 2011/005, 2011.
- [84] G. Cowan, K. Cranmer, E. Gross, and O. Vitells, “Asymptotic formulae for likelihood-based tests of new physics”, *Eur. Phys. J. C* **71** (2011) 1554, doi:10.1140/epjc/s10052-011-1554-0, arXiv:1007.1727. [Erratum: doi:10.1140/epjc/s10052-013-2501-z].
- [85] CMS Collaboration, “Measurement of the $t\bar{t}$ production cross section in the $e\mu$ channel in proton-proton collisions at $\sqrt{s} = 7$ and 8 TeV”, *JHEP* **08** (2016) 029, doi:10.1007/JHEP08(2016)029, arXiv:1603.02303.

A The CMS Collaboration

Yerevan Physics Institute, Yerevan, Armenia

A.M. Sirunyan, A. Tumasyan

Institut für Hochenergiephysik, Wien, Austria

W. Adam, E. Asilar, T. Bergauer, J. Brandstetter, E. Brondolin, M. Dragicevic, J. Erö, M. Flechl, M. Friedl, R. Frühwirth¹, V.M. Ghete, C. Hartl, N. Hörmann, J. Hrubec, M. Jeitler¹, A. König, I. Krätschmer, D. Liko, T. Matsushita, I. Mikulec, D. Rabadý, N. Rad, B. Rahbaran, H. Rohringer, J. Schieck¹, J. Strauss, W. Waltenberger, C.-E. Wulz¹

Institute for Nuclear Problems, Minsk, Belarus

V. Chekhovsky, O. Dvornikov, Y. Dydyshka, I. Emelianchik, A. Litomin, V. Makarenko, V. Mossolov, R. Stefanovitch, J. Suarez Gonzalez, V. Zykunov

National Centre for Particle and High Energy Physics, Minsk, Belarus

N. Shumeiko

Universiteit Antwerpen, Antwerpen, Belgium

S. Alderweireldt, E.A. De Wolf, X. Janssen, J. Lauwers, M. Van De Klundert, H. Van Haevermaet, P. Van Mechelen, N. Van Remortel, A. Van Spilbeeck

Vrije Universiteit Brussel, Brussel, Belgium

S. Abu Zeid, F. Blekman, J. D'Hondt, N. Daci, I. De Bruyn, K. Deroover, S. Lowette, S. Moortgat, L. Moreels, A. Olbrechts, Q. Python, K. Skovpen, S. Tavernier, W. Van Doninck, P. Van Mulders, I. Van Parijs

Université Libre de Bruxelles, Bruxelles, Belgium

H. Brun, B. Clerbaux, G. De Lentdecker, H. Delannoy, G. Fasanella, L. Favart, R. Goldouzian, A. Grebenyuk, G. Karapostoli, T. Lenzi, A. Léonard, J. Luetic, T. Maerschalk, A. Marinov, A. Randle-conde, T. Seva, C. Vander Velde, P. Vanlaer, D. Vannerom, R. Yonamine, F. Zenoni, F. Zhang²

Ghent University, Ghent, Belgium

A. Cimmino, T. Cornelis, D. Dobur, A. Fagot, M. Gul, I. Khvastunov, D. Poyraz, S. Salva, R. Schöfbeck, M. Tytgat, W. Van Driessche, E. Yazgan, N. Zaganidis

Université Catholique de Louvain, Louvain-la-Neuve, Belgium

H. Bakhshiansohi, C. Beluffi³, O. Bondu, S. Brochet, G. Bruno, A. Caudron, S. De Visscher, C. Delaere, M. Delcourt, B. Francois, A. Giammanco, A. Jafari, M. Komm, G. Krintiras, V. Lemaitre, A. Magitteri, A. Mertens, M. Musich, K. Piotrkowski, L. Quertenmont, M. Selvaggi, M. Vidal Marono, S. Wertz

Université de Mons, Mons, Belgium

N. Beliy

Centro Brasileiro de Pesquisas Fisicas, Rio de Janeiro, Brazil

W.L. Aldá Júnior, F.L. Alves, G.A. Alves, L. Brito, C. Hensel, A. Moraes, M.E. Pol, P. Rebello Teles

Universidade do Estado do Rio de Janeiro, Rio de Janeiro, Brazil

E. Belchior Batista Das Chagas, W. Carvalho, J. Chinellato⁴, A. Custódio, E.M. Da Costa, G.G. Da Silveira⁵, D. De Jesus Damiao, C. De Oliveira Martins, S. Fonseca De Souza, L.M. Huertas Guativa, H. Malbouisson, D. Matos Figueiredo, C. Mora Herrera, L. Mundim,

H. Nogima, W.L. Prado Da Silva, A. Santoro, A. Sznajder, E.J. Tonelli Manganote⁴, A. Vilela Pereira

Universidade Estadual Paulista ^a, Universidade Federal do ABC ^b, São Paulo, Brazil

S. Ahuja^a, C.A. Bernardes^a, S. Dogra^a, T.R. Fernandez Perez Tomei^a, E.M. Gregores^b, P.G. Mercadante^b, C.S. Moon^a, S.F. Novaes^a, Sandra S. Padula^a, D. Romero Abad^b, J.C. Ruiz Vargas^a

Institute for Nuclear Research and Nuclear Energy, Sofia, Bulgaria

A. Aleksandrov, R. Hadjiiska, P. Iaydjiev, M. Rodozov, S. Stoykova, G. Sultanov, M. Vutova

University of Sofia, Sofia, Bulgaria

A. Dimitrov, I. Glushkov, L. Litov, B. Pavlov, P. Petkov

Beihang University, Beijing, China

W. Fang⁶

Institute of High Energy Physics, Beijing, China

M. Ahmad, J.G. Bian, G.M. Chen, H.S. Chen, M. Chen, Y. Chen⁷, T. Cheng, C.H. Jiang, D. Leggat, Z. Liu, F. Romeo, M. Ruan, S.M. Shaheen, A. Spiezia, J. Tao, C. Wang, Z. Wang, H. Zhang, J. Zhao

State Key Laboratory of Nuclear Physics and Technology, Peking University, Beijing, China

Y. Ban, G. Chen, Q. Li, S. Liu, Y. Mao, S.J. Qian, D. Wang, Z. Xu

Universidad de Los Andes, Bogota, Colombia

C. Avila, A. Cabrera, L.F. Chaparro Sierra, C. Florez, J.P. Gomez, C.F. González Hernández, J.D. Ruiz Alvarez, J.C. Sanabria

University of Split, Faculty of Electrical Engineering, Mechanical Engineering and Naval Architecture, Split, Croatia

N. Godinovic, D. Lelas, I. Puljak, P.M. Ribeiro Cipriano, T. Sculac

University of Split, Faculty of Science, Split, Croatia

Z. Antunovic, M. Kovac

Institute Rudjer Boskovic, Zagreb, Croatia

V. Brigljevic, D. Ferencek, K. Kadija, B. Mesic, T. Susa

University of Cyprus, Nicosia, Cyprus

A. Attikis, G. Mavromanolakis, J. Mousa, C. Nicolaou, F. Ptochos, P.A. Razis, H. Rykaczewski, D. Tsiakkouri

Charles University, Prague, Czech Republic

M. Finger⁸, M. Finger Jr.⁸

Universidad San Francisco de Quito, Quito, Ecuador

E. Carrera Jarrin

Academy of Scientific Research and Technology of the Arab Republic of Egypt, Egyptian Network of High Energy Physics, Cairo, Egypt

E. El-khateeb⁹, S. Elgammal¹⁰, A. Mohamed¹¹

National Institute of Chemical Physics and Biophysics, Tallinn, Estonia

M. Kadastik, L. Perrini, M. Raidal, A. Tiko, C. Veelken

Department of Physics, University of Helsinki, Helsinki, Finland

P. Eerola, J. Pekkanen, M. Voutilainen

Helsinki Institute of Physics, Helsinki, Finland

J. Härkönen, T. Järvinen, V. Karimäki, R. Kinnunen, T. Lampén, K. Lassila-Perini, S. Lehti, T. Lindén, P. Luukka, J. Tuominiemi, E. Tuovinen, L. Wendland

Lappeenranta University of Technology, Lappeenranta, Finland

J. Talvitie, T. Tuuva

IRFU, CEA, Université Paris-Saclay, Gif-sur-Yvette, France

M. Besancon, F. Couderc, M. Dejardin, D. Denegri, B. Fabbro, J.L. Faure, C. Favaro, F. Ferri, S. Ganjour, S. Ghosh, A. Givernaud, P. Gras, G. Hamel de Monchenault, P. Jarry, I. Kucher, E. Locci, M. Machet, J. Malcles, J. Rander, A. Rosowsky, M. Titov

Laboratoire Leprince-Ringuet, Ecole Polytechnique, IN2P3-CNRS, Palaiseau, France

A. Abdulsalam, I. Antropov, S. Baffioni, F. Beaudette, P. Busson, L. Cadamuro, E. Chapon, C. Charlot, O. Davignon, R. Granier de Cassagnac, M. Jo, S. Lisniak, P. Miné, M. Nguyen, C. Ochando, G. Ortona, P. Paganini, P. Pigard, S. Regnard, R. Salerno, Y. Sirois, T. Strebler, Y. Yilmaz, A. Zabi, A. Zghiche

Institut Pluridisciplinaire Hubert Curien (IPHC), Université de Strasbourg, CNRS-IN2P3

J.-L. Agram¹², J. Andrea, A. Aubin, D. Bloch, J.-M. Brom, M. Buttignol, E.C. Chabert, N. Chanon, C. Collard, E. Conte¹², X. Coubez, J.-C. Fontaine¹², D. Gelé, U. Goerlach, M. Jansová, A.-C. Le Bihan, P. Van Hove

Centre de Calcul de l'Institut National de Physique Nucleaire et de Physique des Particules, CNRS/IN2P3, Villeurbanne, France

S. Gadrat

Université de Lyon, Université Claude Bernard Lyon 1, CNRS-IN2P3, Institut de Physique Nucléaire de Lyon, Villeurbanne, France

S. Beauceron, C. Bernet, G. Boudoul, C.A. Carrillo Montoya, R. Chierici, D. Contardo, B. Courbon, P. Depasse, H. El Mamouni, J. Fan, J. Fay, S. Gascon, M. Gouzevitch, G. Grenier, B. Ille, F. Lagarde, I.B. Laktineh, M. Lethuillier, L. Mirabito, A.L. Pequegnot, S. Perries, A. Popov¹³, D. Sabes, V. Sordini, M. Vander Donckt, P. Verdier, S. Viret

Georgian Technical University, Tbilisi, Georgia

T. Toriashvili¹⁴

Tbilisi State University, Tbilisi, Georgia

Z. Tsamalaidze⁸

RWTH Aachen University, I. Physikalisches Institut, Aachen, Germany

C. Autermann, S. Beranek, L. Feld, M.K. Kiesel, K. Klein, M. Lipinski, M. Preuten, C. Schomakers, J. Schulz, T. Verlage, V. Zhukov¹³

RWTH Aachen University, III. Physikalisches Institut A, Aachen, Germany

A. Albert, M. Brodski, E. Dietz-Laursonn, D. Duchardt, M. Endres, M. Erdmann, S. Erdweg, T. Esch, R. Fischer, A. Güth, M. Hamer, T. Hebbeker, C. Heidemann, K. Hoepfner, S. Knutzen, M. Merschmeyer, A. Meyer, P. Millet, S. Mukherjee, M. Olschewski, K. Padeken, T. Pook, M. Radziej, H. Reithler, M. Rieger, F. Scheuch, L. Sonnenschein, D. Teyssier, S. Thüer

RWTH Aachen University, III. Physikalisches Institut B, Aachen, Germany

V. Cherepanov, G. Flügge, B. Kargoll, T. Kress, A. Künsken, J. Lingemann, T. Müller, A. Nehrkorn, A. Nowack, C. Pistone, O. Pooth, A. Stahl¹⁵

Deutsches Elektronen-Synchrotron, Hamburg, Germany

M. Aldaya Martin, T. Arndt, C. Asawatangtrakuldee, K. Beernaert, O. Behnke, U. Behrens, A.A. Bin Anuar, K. Borras¹⁶, A. Campbell, P. Connor, C. Contreras-Campana, F. Costanza, C. Diez Pardos, G. Dolinska, G. Eckerlin, D. Eckstein, T. Eichhorn, E. Eren, E. Gallo¹⁷, J. Garay Garcia, A. Geiser, A. Gizhko, J.M. Grados Luyando, A. Grohsjean, P. Gunnellini, A. Harb, J. Hauk, M. Hempel¹⁸, H. Jung, A. Kalogeropoulos, O. Karacheban¹⁸, M. Kasemann, J. Keaveney, C. Kleinwort, I. Korol, D. Krücker, W. Lange, A. Lelek, J. Leonard, K. Lipka, A. Lobanov, W. Lohmann¹⁸, R. Mankel, I.-A. Melzer-Pellmann, A.B. Meyer, G. Mittag, J. Mnich, A. Mussgiller, E. Ntomari, D. Pitzl, R. Placakyte, A. Raspereza, B. Roland, M.Ö. Sahin, P. Saxena, T. Schoerner-Sadenius, C. Seitz, S. Spannagel, N. Stefaniuk, G.P. Van Onsem, R. Walsh, C. Wissing

University of Hamburg, Hamburg, Germany

V. Blobel, M. Centis Vignali, A.R. Draeger, T. Dreyer, E. Garutti, D. Gonzalez, J. Haller, M. Hoffmann, A. Junkes, R. Klanner, R. Kogler, N. Kovalchuk, T. Lapsien, T. Lenz, I. Marchesini, D. Marconi, M. Meyer, M. Niedziela, D. Nowatschin, F. Pantaleo¹⁵, T. Peiffer, A. Perieanu, J. Poehlsen, C. Sander, C. Scharf, P. Schleper, A. Schmidt, S. Schumann, J. Schwandt, H. Stadie, G. Steinbrück, F.M. Stober, M. Stöver, H. Tholen, D. Troendle, E. Usai, L. Vanelderen, A. Vanhoefer, B. Vormwald

Institut für Experimentelle Kernphysik, Karlsruhe, Germany

M. Akbiyik, C. Barth, S. Baur, C. Baus, J. Berger, E. Butz, R. Caspart, T. Chwalek, F. Colombo, W. De Boer, A. Dierlamm, S. Fink, B. Freund, R. Friese, M. Giffels, A. Gilbert, P. Goldenzweig, D. Haitz, F. Hartmann¹⁵, S.M. Heindl, U. Husemann, I. Katkov¹³, S. Kudella, H. Mildner, M.U. Mozer, Th. Müller, M. Plagge, G. Quast, K. Rabbertz, S. Röcker, F. Roscher, M. Schröder, I. Shvetsov, G. Sieber, H.J. Simonis, R. Ulrich, S. Wayand, M. Weber, T. Weiler, S. Williamson, C. Wöhrmann, R. Wolf

Institute of Nuclear and Particle Physics (INPP), NCSR Demokritos, Aghia Paraskevi, Greece

G. Anagnostou, G. Daskalakis, T. Gerasis, V.A. Giakoumopoulou, A. Kyriakis, D. Loukas, I. Topsis-Giotis

National and Kapodistrian University of Athens, Athens, Greece

S. Kesisoglou, A. Panagiotou, N. Saoulidou, E. Tziaferi

University of Ioánnina, Ioánnina, Greece

I. Evangelou, G. Flouris, C. Foudas, P. Kokkas, N. Loukas, N. Manthos, I. Papadopoulos, E. Paradas

MTA-ELTE Lendület CMS Particle and Nuclear Physics Group, Eötvös Loránd University, Budapest, Hungary

N. Filipovic

Wigner Research Centre for Physics, Budapest, Hungary

G. Bencze, C. Hajdu, D. Horvath¹⁹, F. Sikler, V. Veszpremi, G. Vesztergombi²⁰, A.J. Zsigmond

Institute of Nuclear Research ATOMKI, Debrecen, Hungary

N. Beni, S. Czellar, J. Karancsi²¹, A. Makovec, J. Molnar, Z. Szillasi

Institute of Physics, University of Debrecen

M. Bartók²⁰, P. Raics, Z.L. Trocsanyi, B. Ujvari

National Institute of Science Education and Research, Bhubaneswar, India

S. Bahinipati, S. Choudhury²², P. Mal, K. Mandal, A. Nayak²³, D.K. Sahoo, N. Sahoo, S.K. Swain

Panjab University, Chandigarh, India

S. Bansal, S.B. Beri, V. Bhatnagar, R. Chawla, U. Bhawandeep, A.K. Kalsi, A. Kaur, M. Kaur, R. Kumar, P. Kumari, A. Mehta, M. Mittal, J.B. Singh, G. Walia

University of Delhi, Delhi, India

Ashok Kumar, A. Bhardwaj, B.C. Choudhary, R.B. Garg, S. Keshri, S. Malhotra, M. Naimuddin, N. Nishu, K. Ranjan, R. Sharma, V. Sharma

Saha Institute of Nuclear Physics, Kolkata, India

R. Bhattacharya, S. Bhattacharya, K. Chatterjee, S. Dey, S. Dutt, S. Dutta, S. Ghosh, N. Majumdar, A. Modak, K. Mondal, S. Mukhopadhyay, S. Nandan, A. Purohit, A. Roy, D. Roy, S. Roy Chowdhury, S. Sarkar, M. Sharan, S. Thakur

Indian Institute of Technology Madras, Madras, India

P.K. Behera

Bhabha Atomic Research Centre, Mumbai, India

R. Chudasama, D. Dutta, V. Jha, V. Kumar, A.K. Mohanty¹⁵, P.K. Netrakanti, L.M. Pant, P. Shukla, A. Topkar

Tata Institute of Fundamental Research-A, Mumbai, India

T. Aziz, S. Dugad, G. Kole, B. Mahakud, S. Mitra, G.B. Mohanty, B. Parida, N. Sur, B. Sutar

Tata Institute of Fundamental Research-B, Mumbai, India

S. Banerjee, S. Bhowmik²⁴, R.K. Dewanjee, S. Ganguly, M. Guchait, Sa. Jain, S. Kumar, M. Maity²⁴, G. Majumder, K. Mazumdar, T. Sarkar²⁴, N. Wickramage²⁵

Indian Institute of Science Education and Research (IISER), Pune, India

S. Chauhan, S. Dube, V. Hegde, A. Kapoor, K. Kothekar, S. Pandey, A. Rane, S. Sharma

Institute for Research in Fundamental Sciences (IPM), Tehran, Iran

S. Chenarani²⁶, E. Eskandari Tadavani, S.M. Etesami²⁶, M. Khakzad, M. Mohammadi Najafabadi, M. Naseri, S. Paktinat Mehdiabadi²⁷, F. Rezaei Hosseinabadi, B. Safarzadeh²⁸, M. Zeinali

University College Dublin, Dublin, Ireland

M. Felcini, M. Grunewald

INFN Sezione di Bari ^a, Università di Bari ^b, Politecnico di Bari ^c, Bari, Italy

M. Abbrescia^{a,b}, C. Calabria^{a,b}, C. Caputo^{a,b}, A. Colaleo^a, D. Creanza^{a,c}, L. Cristella^{a,b}, N. De Filippis^{a,c}, M. De Palma^{a,b}, L. Fiore^a, G. Iaselli^{a,c}, G. Maggi^{a,c}, M. Maggi^a, G. Miniello^{a,b}, S. My^{a,b}, S. Nuzzo^{a,b}, A. Pompili^{a,b}, G. Pugliese^{a,c}, R. Radogna^{a,b}, A. Ranieri^a, G. Selvaggi^{a,b}, A. Sharma^a, L. Silvestris^{a,15}, R. Venditti^{a,b}, P. Verwilligen^a

INFN Sezione di Bologna ^a, Università di Bologna ^b, Bologna, Italy

G. Abbiendi^a, C. Battilana, D. Bonacorsi^{a,b}, S. Braibant-Giacomelli^{a,b}, L. Brigliadori^{a,b}, R. Campanini^{a,b}, P. Capiluppi^{a,b}, A. Castro^{a,b}, F.R. Cavallo^a, S.S. Chhibra^{a,b}, G. Codispoti^{a,b}, M. Cuffiani^{a,b}, G.M. Dallavalle^a, F. Fabbri^a, A. Fanfani^{a,b}, D. Fasanella^{a,b}, P. Giacomelli^a, C. Grandi^a, L. Guiducci^{a,b}, S. Marcellini^a, G. Masetti^a, A. Montanari^a, F.L. Navarria^{a,b}, A. Perrotta^a, A.M. Rossi^{a,b}, T. Rovelli^{a,b}, G.P. Siroli^{a,b}, N. Tosi^{a,b,15}

INFN Sezione di Catania ^a, Università di Catania ^b, Catania, Italy

S. Albergo^{a,b}, S. Costa^{a,b}, A. Di Mattia^a, F. Giordano^{a,b}, R. Potenza^{a,b}, A. Tricomi^{a,b}, C. Tuve^{a,b}

INFN Sezione di Firenze ^a, Università di Firenze ^b, Firenze, Italy

G. Barbagli^a, V. Ciulli^{a,b}, C. Civinini^a, R. D'Alessandro^{a,b}, E. Focardi^{a,b}, P. Lenzi^{a,b}, M. Meschini^a, S. Paoletti^a, L. Russo^{a,29}, G. Sguazzoni^a, D. Strom^a, L. Viliani^{a,b,15}

INFN Laboratori Nazionali di Frascati, Frascati, Italy

L. Benussi, S. Bianco, F. Fabbri, D. Piccolo, F. Primavera¹⁵

INFN Sezione di Genova ^a, Università di Genova ^b, Genova, Italy

V. Calvelli^{a,b}, F. Ferro^a, M.R. Monge^{a,b}, E. Robutti^a, S. Tosi^{a,b}

INFN Sezione di Milano-Bicocca ^a, Università di Milano-Bicocca ^b, Milano, Italy

L. Brianza^{a,b,15}, F. Brivio^{a,b}, V. Ciriolo, M.E. Dinardo^{a,b}, S. Fiorendi^{a,b,15}, S. Gennai^a, A. Ghezzi^{a,b}, P. Govoni^{a,b}, M. Malberti^{a,b}, S. Malvezzi^a, R.A. Manzoni^{a,b}, D. Menasce^a, L. Moroni^a, M. Paganoni^{a,b}, D. Pedrini^a, S. Pigazzini^{a,b}, S. Ragazzi^{a,b}, T. Tabarelli de Fatis^{a,b}

INFN Sezione di Napoli ^a, Università di Napoli 'Federico II' ^b, Napoli, Italy, Università della Basilicata ^c, Potenza, Italy, Università G. Marconi ^d, Roma, Italy

S. Buontempo^a, N. Cavallo^{a,c}, G. De Nardo, S. Di Guida^{a,d,15}, M. Esposito^{a,b}, F. Fabozzi^{a,c}, F. Fienga^{a,b}, A.O.M. Iorio^{a,b}, G. Lanza^a, L. Lista^a, S. Meola^{a,d,15}, P. Paolucci^{a,15}, C. Sciacca^{a,b}, F. Thyssen^a

INFN Sezione di Padova ^a, Università di Padova ^b, Padova, Italy, Università di Trento ^c, Trento, Italy

P. Azzi^{a,15}, N. Bacchetta^a, M. Bellato^a, L. Benato^{a,b}, M. Biasotto^{a,30}, D. Bisello^{a,b}, A. Boletti^{a,b}, P. Checchia^a, M. Dall'Osso^{a,b}, P. De Castro Manzano^a, U. Dosselli^a, F. Gasparini^{a,b}, U. Gasparini^{a,b}, A. Gozzelino^a, S. Lacaprara^a, M. Margoni^{a,b}, A.T. Meneguzzo^{a,b}, J. Pazzini^{a,b}, N. Pozzobon^{a,b}, P. Ronchese^{a,b}, F. Simonetto^{a,b}, E. Torassa^a, S. Ventura^a, M. Zanetti^{a,b}, P. Zotto^{a,b}, G. Zumerle^{a,b}

INFN Sezione di Pavia ^a, Università di Pavia ^b, Pavia, Italy

A. Braghieri^a, F. Fallavollita^{a,b}, A. Magnani^{a,b}, P. Montagna^{a,b}, S.P. Ratti^{a,b}, V. Re^a, C. Riccardi^{a,b}, P. Salvini^a, I. Vai^{a,b}, P. Vitulo^{a,b}

INFN Sezione di Perugia ^a, Università di Perugia ^b, Perugia, Italy

L. Alunni Solestizi^{a,b}, G.M. Bilei^a, D. Ciangottini^{a,b}, L. Fanò^{a,b}, P. Lariccia^{a,b}, R. Leonardi^{a,b}, G. Mantovani^{a,b}, M. Menichelli^a, A. Saha^a, A. Santocchia^{a,b}

INFN Sezione di Pisa ^a, Università di Pisa ^b, Scuola Normale Superiore di Pisa ^c, Pisa, Italy

K. Androsov^{a,29}, P. Azzurri^{a,15}, G. Bagliesi^a, J. Bernardini^a, T. Boccali^a, R. Castaldi^a, M.A. Ciocci^{a,29}, R. Dell'Orso^a, S. Donato^{a,c}, G. Fedi, A. Giassi^a, M.T. Grippo^{a,29}, F. Ligabue^{a,c}, T. Lomtadze^a, L. Martini^{a,b}, A. Messineo^{a,b}, F. Palla^a, A. Rizzi^{a,b}, A. Savoy-Navarro^{a,31}, P. Spagnolo^a, R. Tenchini^a, G. Tonelli^{a,b}, A. Venturi^a, P.G. Verdini^a

INFN Sezione di Roma ^a, Università di Roma ^b, Roma, Italy

L. Barone^{a,b}, F. Cavallari^a, M. Cipriani^{a,b}, D. Del Re^{a,b,15}, M. Diemoz^a, S. Gelli^{a,b}, E. Longo^{a,b}, F. Margaroli^{a,b}, B. Marzocchi^{a,b}, P. Meridiani^a, G. Organtini^{a,b}, R. Paramatti^a, F. Preiato^{a,b}, S. Rahatlou^{a,b}, C. Rovelli^a, F. Santanastasio^{a,b}

INFN Sezione di Torino ^a, Università di Torino ^b, Torino, Italy, Università del Piemonte Orientale ^c, Novara, Italy

N. Amapane^{a,b}, R. Arcidiacono^{a,c,15}, S. Argiro^{a,b}, M. Arneodo^{a,c}, N. Bartosik^a, R. Bellan^{a,b}, C. Biino^a, N. Cartiglia^a, F. Cenna^{a,b}, M. Costa^{a,b}, R. Covarelli^{a,b}, A. Degano^{a,b}, N. Demaria^a,

L. Finco^{a,b}, B. Kiani^{a,b}, C. Mariotti^a, S. Maselli^a, E. Migliore^{a,b}, V. Monaco^{a,b}, E. Monteil^{a,b}, M. Monteno^a, M.M. Obertino^{a,b}, L. Pacher^{a,b}, N. Pastrone^a, M. Pelliccioni^a, G.L. Pinna Angioni^{a,b}, F. Ravera^{a,b}, A. Romero^{a,b}, M. Ruspa^{a,c}, R. Sacchi^{a,b}, K. Shchelina^{a,b}, V. Sola^a, A. Solano^{a,b}, A. Staiano^a, P. Traczyk^{a,b}

INFN Sezione di Trieste^a, Università di Trieste^b, Trieste, Italy

S. Belforte^a, M. Casarsa^a, F. Cossutti^a, G. Della Ricca^{a,b}, A. Zanetti^a

Kyungpook National University, Daegu, Korea

D.H. Kim, G.N. Kim, M.S. Kim, S. Lee, S.W. Lee, Y.D. Oh, S. Sekmen, D.C. Son, Y.C. Yang

Chonbuk National University, Jeonju, Korea

A. Lee

Chonnam National University, Institute for Universe and Elementary Particles, Kwangju, Korea

H. Kim

Hanyang University, Seoul, Korea

J.A. Brochero Cifuentes, T.J. Kim

Korea University, Seoul, Korea

S. Cho, S. Choi, Y. Go, D. Gyun, S. Ha, B. Hong, Y. Jo, Y. Kim, K. Lee, K.S. Lee, S. Lee, J. Lim, S.K. Park, Y. Roh

Seoul National University, Seoul, Korea

J. Almond, J. Kim, H. Lee, S.B. Oh, B.C. Radburn-Smith, S.h. Seo, U.K. Yang, H.D. Yoo, G.B. Yu

University of Seoul, Seoul, Korea

M. Choi, H. Kim, J.H. Kim, J.S.H. Lee, I.C. Park, G. Ryu, M.S. Ryu

Sungkyunkwan University, Suwon, Korea

Y. Choi, J. Goh, C. Hwang, J. Lee, I. Yu

Vilnius University, Vilnius, Lithuania

V. Dudenas, A. Juodagalvis, J. Vaitkus

National Centre for Particle Physics, Universiti Malaya, Kuala Lumpur, Malaysia

I. Ahmed, Z.A. Ibrahim, J.R. Komaragiri, M.A.B. Md Ali³², F. Mohamad Idris³³, W.A.T. Wan Abdullah, M.N. Yusli, Z. Zolkapli

Centro de Investigacion y de Estudios Avanzados del IPN, Mexico City, Mexico

H. Castilla-Valdez, E. De La Cruz-Burelo, I. Heredia-De La Cruz³⁴, A. Hernandez-Almada, R. Lopez-Fernandez, R. Magaña Villalba, J. Mejia Guisao, A. Sanchez-Hernandez

Universidad Iberoamericana, Mexico City, Mexico

S. Carrillo Moreno, C. Oropeza Barrera, F. Vazquez Valencia

Benemerita Universidad Autonoma de Puebla, Puebla, Mexico

S. Carpinteyro, I. Pedraza, H.A. Salazar Ibarguen, C. Uribe Estrada

Universidad Autónoma de San Luis Potosí, San Luis Potosí, Mexico

A. Morelos Pineda

University of Auckland, Auckland, New Zealand

D. Krofcheck

University of Canterbury, Christchurch, New Zealand

P.H. Butler

National Centre for Physics, Quaid-I-Azam University, Islamabad, Pakistan

A. Ahmad, M. Ahmad, Q. Hassan, H.R. Hoorani, W.A. Khan, A. Saddique, M.A. Shah, M. Shoaib, M. Waqas

National Centre for Nuclear Research, Swierk, Poland

H. Bialkowska, M. Bluj, B. Boimska, T. Frueboes, M. Górski, M. Kazana, K. Nawrocki, K. Romanowska-Rybinska, M. Szleper, P. Zalewski

Institute of Experimental Physics, Faculty of Physics, University of Warsaw, Warsaw, Poland

K. Bunkowski, A. Byszuk³⁵, K. Doroba, A. Kalinowski, M. Konecki, J. Krolikowski, M. Misiura, M. Olszewski, M. Walczak

Laboratório de Instrumentação e Física Experimental de Partículas, Lisboa, Portugal

P. Bargassa, C. Beirão Da Cruz E Silva, B. Calpas, A. Di Francesco, P. Faccioli, P.G. Ferreira Parracho, M. Gallinaro, J. Hollar, N. Leonardo, L. Lloret Iglesias, M.V. Nemallapudi, J. Rodrigues Antunes, J. Seixas, O. Toldaiev, D. Vadrucio, J. Varela, P. Vischia

Joint Institute for Nuclear Research, Dubna, Russia

V. Alexakhin, P. Bunin, M. Gavrilenko, I. Golutvin, I. Gorbunov, A. Kamenev, V. Karjavin, A. Lanev, A. Malakhov, V. Matveev^{36,37}, V. Palichik, V. Perelygin, M. Savina, S. Shmatov, N. Skatchkov, V. Smirnov, N. Voytishin, A. Zarubin

Petersburg Nuclear Physics Institute, Gatchina (St. Petersburg), Russia

L. Chtchipounov, V. Golovtsov, Y. Ivanov, V. Kim³⁸, E. Kuznetsova³⁹, V. Murzin, V. Oreshkin, V. Sulimov, A. Vorobyev

Institute for Nuclear Research, Moscow, Russia

Yu. Andreev, A. Dermenev, S. Gninenko, N. Golubev, A. Karneyeu, M. Kirsanov, N. Krasnikov, A. Pashenkov, D. Tlisov, A. Toropin

Institute for Theoretical and Experimental Physics, Moscow, Russia

V. Epshteyn, V. Gavrillov, N. Lychkovskaya, V. Popov, I. Pozdnyakov, G. Safronov, A. Spiridonov, M. Toms, E. Vlasov, A. Zhokin

Moscow Institute of Physics and Technology, Moscow, Russia

A. Bylinkin³⁷

National Research Nuclear University 'Moscow Engineering Physics Institute' (MEPhI), Moscow, Russia

O. Markin, E. Popova, E. Zhemchugov

P.N. Lebedev Physical Institute, Moscow, Russia

V. Andreev, M. Azarkin³⁷, I. Dremin³⁷, M. Kirakosyan, A. Leonidov³⁷, A. Terkulov

Skobeltsyn Institute of Nuclear Physics, Lomonosov Moscow State University, Moscow, Russia

A. Baskakov, A. Belyaev, E. Boos, V. Bunichev, M. Dubinin⁴⁰, L. Dudko, A. Ershov, A. Gribushin, V. Klyukhin, O. Kodolova, I. Lokhtin, I. Miagkov, S. Obraztsov, S. Petrushanko, V. Savrin

Novosibirsk State University (NSU), Novosibirsk, Russia

V. Blinov⁴¹, Y. Skovpen⁴¹, D. Shtol⁴¹

State Research Center of Russian Federation, Institute for High Energy Physics, Protvino, Russia

I. Azhgirey, I. Bayshev, S. Bitioukov, D. Elumakhov, V. Kachanov, A. Kalinin, D. Konstantinov, V. Krychkine, V. Petrov, R. Ryutin, A. Sobol, S. Troshin, N. Tyurin, A. Uzunian, A. Volkov

University of Belgrade, Faculty of Physics and Vinca Institute of Nuclear Sciences, Belgrade, Serbia

P. Adzic⁴², P. Cirkovic, D. Devetak, M. Dordevic, J. Milosevic, V. Rekovic

Centro de Investigaciones Energéticas Medioambientales y Tecnológicas (CIEMAT), Madrid, Spain

J. Alcaraz Maestre, M. Barrio Luna, E. Calvo, M. Cerrada, M. Chamizo Llatas, N. Colino, B. De La Cruz, A. Delgado Peris, A. Escalante Del Valle, C. Fernandez Bedoya, J.P. Fernández Ramos, J. Flix, M.C. Fouz, P. Garcia-Abia, O. Gonzalez Lopez, S. Goy Lopez, J.M. Hernandez, M.I. Josa, E. Navarro De Martino, A. Pérez-Calero Yzquierdo, J. Puerta Pelayo, A. Quintario Olmeda, I. Redondo, L. Romero, M.S. Soares

Universidad Autónoma de Madrid, Madrid, Spain

J.F. de Trocóniz, M. Missiroli, D. Moran

Universidad de Oviedo, Oviedo, Spain

J. Cuevas, J. Fernandez Menendez, I. Gonzalez Caballero, J.R. González Fernández, E. Palencia Cortezon, S. Sanchez Cruz, I. Suárez Andrés, J.M. Vizán García

Instituto de Física de Cantabria (IFCA), CSIC-Universidad de Cantabria, Santander, Spain

I.J. Cabrillo, A. Calderon, E. Curras, M. Fernandez, J. Garcia-Ferrero, G. Gomez, A. Lopez Virto, J. Marco, C. Martinez Rivero, F. Matorras, J. Piedra Gomez, T. Rodrigo, A. Ruiz-Jimeno, L. Scodellaro, N. Trevisani, I. Vila, R. Vilar Cortabitarte

CERN, European Organization for Nuclear Research, Geneva, Switzerland

D. Abbaneo, E. Auffray, G. Auzinger, M. Bachtis, P. Baillon, A.H. Ball, D. Barney, P. Bloch, A. Bocci, C. Botta, T. Camporesi, R. Castello, M. Cepeda, G. Cerminara, Y. Chen, D. d'Enterria, A. Dabrowski, V. Daponte, A. David, M. De Gruttola, A. De Roeck, E. Di Marco⁴³, M. Dobson, B. Dorney, T. du Pree, D. Duggan, M. Dünser, N. Dupont, A. Elliott-Peisert, P. Everaerts, S. Fartoukh, G. Franzoni, J. Fulcher, W. Funk, D. Gigi, K. Gill, M. Girone, F. Glege, D. Gulhan, S. Gundacker, M. Guthoff, P. Harris, J. Hegeman, V. Innocente, P. Janot, J. Kieseler, H. Kirschenmann, V. Knünz, A. Kornmayer¹⁵, M.J. Kortelainen, K. Kousouris, M. Krammer¹, C. Lange, P. Lecoq, C. Lourenço, M.T. Lucchini, L. Malgeri, M. Mannelli, A. Martelli, F. Meijers, J.A. Merlin, S. Mersi, E. Meschi, P. Milenovic⁴⁴, F. Moortgat, S. Morovic, M. Mulders, H. Neugebauer, S. Orfanelli, L. Orsini, L. Pape, E. Perez, M. Peruzzi, A. Petrilli, G. Petrucciani, A. Pfeiffer, M. Pierini, A. Racz, T. Reis, G. Rolandi⁴⁵, M. Rovere, H. Sakulin, J.B. Sauvan, C. Schäfer, C. Schwick, M. Seidel, A. Sharma, P. Silva, P. Sphicas⁴⁶, J. Steggemann, M. Stoye, Y. Takahashi, M. Tosi, D. Treille, A. Triossi, A. Tsiros, V. Veckalns⁴⁷, G.I. Veres²⁰, M. Verweij, N. Wardle, H.K. Wöhri, A. Zagozdinska³⁵, W.D. Zeuner

Paul Scherrer Institut, Villigen, Switzerland

W. Bertl, K. Deiters, W. Erdmann, R. Horisberger, Q. Ingram, H.C. Kaestli, D. Kotlinski, U. Langenegger, T. Rohe

Institute for Particle Physics, ETH Zurich, Zurich, Switzerland

F. Bachmair, L. Bäni, L. Bianchini, B. Casal, G. Dissertori, M. Dittmar, M. Donegà, C. Grab, C. Heidegger, D. Hits, J. Hoss, G. Kasieczka, W. Lustermann, B. Mangano, M. Marionneau, P. Martinez Ruiz del Arbol, M. Masciovecchio, M.T. Meinhard, D. Meister, F. Micheli,

P. Musella, F. Nessi-Tedaldi, F. Pandolfi, J. Pata, F. Pauss, G. Perrin, L. Perrozzi, M. Quittnat, M. Rossini, M. Schönenberger, A. Starodumov⁴⁸, V.R. Tavolaro, K. Theofilatos, R. Wallny

Universität Zürich, Zurich, Switzerland

T.K. Aarrestad, C. Amsler⁴⁹, L. Caminada, M.F. Canelli, A. De Cosa, C. Galloni, A. Hinzmann, T. Hreus, B. Kilminster, J. Ngadiuba, D. Pinna, G. Rauco, P. Robmann, D. Salerno, Y. Yang, A. Zucchetta

National Central University, Chung-Li, Taiwan

V. Candelise, T.H. Doan, Sh. Jain, R. Khurana, M. Konyushikhin, C.M. Kuo, W. Lin, Y.J. Lu, A. Pozdnyakov, S.S. Yu

National Taiwan University (NTU), Taipei, Taiwan

Arun Kumar, P. Chang, Y.H. Chang, Y. Chao, K.F. Chen, P.H. Chen, F. Fiori, W.-S. Hou, Y. Hsiung, Y.F. Liu, R.-S. Lu, M. Miñano Moya, E. Paganis, A. Psallidas, J.f. Tsai

Chulalongkorn University, Faculty of Science, Department of Physics, Bangkok, Thailand

B. Asavapibhop, G. Singh, N. Srimanobhas, N. Suwonjandee

Cukurova University - Physics Department, Science and Art Faculty

A. Adiguzel, M.N. Bakirci⁵⁰, S. Cerci⁵¹, S. Damarseckin, Z.S. Demiroglu, C. Dozen, I. Dumanoglu, S. Girgis, G. Gokbulut, Y. Guler, I. Hos⁵², E.E. Kangal⁵³, O. Kara, A. Kayis Topaksu, U. Kiminsu, M. Oglakci, G. Onengut⁵⁴, K. Ozdemir⁵⁵, B. Tali⁵¹, S. Turkcapar, I.S. Zorbakir, C. Zorbilmez

Middle East Technical University, Physics Department, Ankara, Turkey

B. Bilin, S. Bilmis, B. Isildak⁵⁶, G. Karapinar⁵⁷, M. Yalvac, M. Zeyrek

Bogazici University, Istanbul, Turkey

E. Gülmez, M. Kaya⁵⁸, O. Kaya⁵⁹, E.A. Yetkin⁶⁰, T. Yetkin⁶¹

Istanbul Technical University, Istanbul, Turkey

A. Cakir, K. Cankocak, S. Sen⁶²

Institute for Scintillation Materials of National Academy of Science of Ukraine, Kharkov, Ukraine

B. Grynyov

National Scientific Center, Kharkov Institute of Physics and Technology, Kharkov, Ukraine

L. Levchuk, P. Sorokin

University of Bristol, Bristol, United Kingdom

R. Aggleton, F. Ball, L. Beck, J.J. Brooke, D. Burns, E. Clement, D. Cussans, H. Flacher, J. Goldstein, M. Grimes, G.P. Heath, H.F. Heath, J. Jacob, L. Kreczko, C. Lucas, D.M. Newbold⁶³, S. Paramesvaran, A. Poll, T. Sakuma, S. Seif El Nasr-storey, D. Smith, V.J. Smith

Rutherford Appleton Laboratory, Didcot, United Kingdom

K.W. Bell, A. Belyaev⁶⁴, C. Brew, R.M. Brown, L. Calligaris, D. Cieri, D.J.A. Cockerill, J.A. Coughlan, K. Harder, S. Harper, E. Olaiya, D. Petyt, C.H. Shepherd-Themistocleous, A. Thea, I.R. Tomalin, T. Williams

Imperial College, London, United Kingdom

M. Baber, R. Bainbridge, O. Buchmuller, A. Bundock, D. Burton, S. Casasso, M. Citron, D. Colling, L. Corpe, P. Dauncey, G. Davies, A. De Wit, M. Della Negra, R. Di Maria, P. Dunne, A. Elwood, D. Futyan, Y. Haddad, G. Hall, G. Iles, T. James, R. Lane, C. Laner, R. Lucas⁶³, L. Lyons, A.-M. Magnan, S. Malik, L. Mastrolorenzo, J. Nash, A. Nikitenko⁴⁸, J. Pela, B. Penning,

M. Pesaresi, D.M. Raymond, A. Richards, A. Rose, C. Seez, S. Summers, A. Tapper, K. Uchida, M. Vazquez Acosta⁶⁵, T. Virdee¹⁵, J. Wright, S.C. Zenz

Brunel University, Uxbridge, United Kingdom

J.E. Cole, P.R. Hobson, A. Khan, P. Kyberd, I.D. Reid, P. Symonds, L. Teodorescu, M. Turner

Baylor University, Waco, USA

A. Borzou, K. Call, J. Dittmann, K. Hatakeyama, H. Liu, N. Pastika

Catholic University of America

R. Bartek, A. Dominguez

The University of Alabama, Tuscaloosa, USA

S.I. Cooper, C. Henderson, P. Rumerio, C. West

Boston University, Boston, USA

D. Arcaro, A. Avetisyan, T. Bose, D. Gastler, D. Rankin, C. Richardson, J. Rohlf, L. Sulak, D. Zou

Brown University, Providence, USA

G. Benelli, D. Cutts, A. Garabedian, J. Hakala, U. Heintz, J.M. Hogan, O. Jesus, K.H.M. Kwok, E. Laird, G. Landsberg, Z. Mao, M. Narain, S. Piperov, S. Sagir, E. Spencer, R. Syarif

University of California, Davis, Davis, USA

R. Breedon, D. Burns, M. Calderon De La Barca Sanchez, S. Chauhan, M. Chertok, J. Conway, R. Conway, P.T. Cox, R. Erbacher, C. Flores, G. Funk, M. Gardner, W. Ko, R. Lander, C. Mclean, M. Mulhearn, D. Pellett, J. Pilot, S. Shalhout, M. Shi, J. Smith, M. Squires, D. Stolp, K. Tos, M. Tripathi

University of California, Los Angeles, USA

C. Bravo, R. Cousins, A. Dasgupta, A. Florent, J. Hauser, M. Ignatenko, N. Mccoll, D. Saltzberg, C. Schnaible, V. Valuev, M. Weber

University of California, Riverside, Riverside, USA

E. Bouvier, K. Burt, R. Clare, J. Ellison, J.W. Gary, S.M.A. Ghiasi Shirazi, G. Hanson, J. Heilman, P. Jandir, E. Kennedy, F. Lacroix, O.R. Long, M. Olmedo Negrete, M.I. Paneva, A. Shrinivas, W. Si, H. Wei, S. Wimpenny, B. R. Yates

University of California, San Diego, La Jolla, USA

J.G. Branson, G.B. Cerati, S. Cittolin, M. Derdzinski, R. Gerosa, A. Holzner, D. Klein, V. Krutelyov, J. Letts, I. Macneill, D. Olivito, S. Padhi, M. Pieri, M. Sani, V. Sharma, S. Simon, M. Tadel, A. Vartak, S. Wasserbaech⁶⁶, C. Welke, J. Wood, F. Würthwein, A. Yagil, G. Zevi Della Porta

University of California, Santa Barbara - Department of Physics, Santa Barbara, USA

N. Amin, R. Bhandari, J. Bradmiller-Feld, C. Campagnari, A. Dishaw, V. Dutta, M. Franco Sevilla, C. George, F. Golf, L. Gouskos, J. Gran, R. Heller, J. Incandela, S.D. Mullin, A. Ovcharova, H. Qu, J. Richman, D. Stuart, I. Suarez, J. Yoo

California Institute of Technology, Pasadena, USA

D. Anderson, J. Bendavid, A. Bornheim, J. Bunn, J. Duarte, J.M. Lawhorn, A. Mott, H.B. Newman, C. Pena, M. Spiropulu, J.R. Vlimant, S. Xie, R.Y. Zhu

Carnegie Mellon University, Pittsburgh, USA

M.B. Andrews, T. Ferguson, M. Paulini, J. Russ, M. Sun, H. Vogel, I. Vorobiev, M. Weinberg

University of Colorado Boulder, Boulder, USA

J.P. Cumalat, W.T. Ford, F. Jensen, A. Johnson, M. Krohn, T. Mulholland, K. Stenson, S.R. Wagner

Cornell University, Ithaca, USA

J. Alexander, J. Chaves, J. Chu, S. Dittmer, K. McDermott, N. Mirman, G. Nicolas Kaufman, J.R. Patterson, A. Rinkevicius, A. Ryd, L. Skinnari, L. Soffi, S.M. Tan, Z. Tao, J. Thom, J. Tucker, P. Wittich, M. Zientek

Fairfield University, Fairfield, USA

D. Winn

Fermi National Accelerator Laboratory, Batavia, USA

S. Abdullin, M. Albrow, G. Apollinari, A. Apresyan, S. Banerjee, L.A.T. Bauerdick, A. Beretvas, J. Berryhill, P.C. Bhat, G. Bolla, K. Burkett, J.N. Butler, H.W.K. Cheung, F. Chlebana, S. Cihangir[†], M. Cremonesi, V.D. Elvira, I. Fisk, J. Freeman, E. Gottschalk, L. Gray, D. Green, S. Grünendahl, O. Gutsche, D. Hare, R.M. Harris, S. Hasegawa, J. Hirschauer, Z. Hu, B. Jayatilaka, S. Jindariani, M. Johnson, U. Joshi, B. Klima, B. Kreis, S. Lammel, J. Linacre, D. Lincoln, R. Lipton, M. Liu, T. Liu, R. Lopes De Sá, J. Lykken, K. Maeshima, N. Magini, J.M. Marraffino, S. Maruyama, D. Mason, P. McBride, P. Merkel, S. Mrenna, S. Nahn, V. O'Dell, K. Pedro, O. Prokofyev, G. Rakness, L. Ristori, E. Sexton-Kennedy, A. Soha, W.J. Spalding, L. Spiegel, S. Stoynev, J. Strait, N. Strobbe, L. Taylor, S. Tkaczyk, N.V. Tran, L. Uplegger, E.W. Vaandering, C. Vernieri, M. Verzocchi, R. Vidal, M. Wang, H.A. Weber, A. Whitbeck, Y. Wu

University of Florida, Gainesville, USA

D. Acosta, P. Avery, P. Bortignon, D. Bourilkov, A. Brinkerhoff, A. Carnes, M. Carver, D. Curry, S. Das, R.D. Field, I.K. Furic, J. Konigsberg, A. Korytov, J.F. Low, P. Ma, K. Matchev, H. Mei, G. Mitselmakher, D. Rank, L. Shchutska, D. Sperka, L. Thomas, J. Wang, S. Wang, J. Yelton

Florida International University, Miami, USA

S. Linn, P. Markowitz, G. Martinez, J.L. Rodriguez

Florida State University, Tallahassee, USA

A. Ackert, T. Adams, A. Askew, S. Bein, S. Hagopian, V. Hagopian, K.F. Johnson, H. Prosper, A. Santra, R. Yohay

Florida Institute of Technology, Melbourne, USA

M.M. Baarmand, V. Bhopatkar, S. Colafranceschi, M. Hohlmann, D. Noonan, T. Roy, F. Yumiceva

University of Illinois at Chicago (UIC), Chicago, USA

M.R. Adams, L. Apanasevich, D. Berry, R.R. Betts, I. Bucinskaite, R. Cavanaugh, O. Evdokimov, L. Gauthier, C.E. Gerber, D.J. Hofman, K. Jung, I.D. Sandoval Gonzalez, N. Varelas, H. Wang, Z. Wu, M. Zakaria, J. Zhang

The University of Iowa, Iowa City, USA

B. Bilki⁶⁷, W. Clarida, K. Dilsiz, S. Durgut, R.P. Gandrajula, M. Haytmyradov, V. Khristenko, J.-P. Merlo, H. Mermerkaya⁶⁸, A. Mestvirishvili, A. Moeller, J. Nachtman, H. Ogul, Y. Onel, E. Ozok⁶⁹, A. Penzo, C. Snyder, E. Tiras, J. Wetzel, K. Yi

Johns Hopkins University, Baltimore, USA

I. Anderson, B. Blumenfeld, A. Cocoros, N. Eminizer, D. Fehling, L. Feng, A.V. Gritsan, P. Maksimovic, M. Osherson, J. Roskes, U. Sarica, M. Swartz, M. Xiao, Y. Xin, C. You

The University of Kansas, Lawrence, USA

A. Al-bataineh, P. Baringer, A. Bean, S. Boren, J. Bowen, J. Castle, L. Forthomme, R.P. Kenny III, S. Khalil, A. Kropivnitskaya, D. Majumder, W. Mcbrayer, M. Murray, S. Sanders, R. Stringer, J.D. Tapia Takaki, Q. Wang

Kansas State University, Manhattan, USA

A. Ivanov, K. Kaadze, Y. Maravin, A. Mohammadi, L.K. Saini, N. Skhirtladze, S. Toda

Lawrence Livermore National Laboratory, Livermore, USA

F. Rebassoo, D. Wright

University of Maryland, College Park, USA

C. Anelli, A. Baden, O. Baron, A. Belloni, B. Calvert, S.C. Eno, C. Ferraioli, J.A. Gomez, N.J. Hadley, S. Jabeen, R.G. Kellogg, T. Kolberg, J. Kunkle, Y. Lu, A.C. Mignerey, F. Ricci-Tam, Y.H. Shin, A. Skuja, M.B. Tonjes, S.C. Tonwar

Massachusetts Institute of Technology, Cambridge, USA

D. Abercrombie, B. Allen, A. Apyan, V. Azzolini, R. Barbieri, A. Baty, R. Bi, K. Bierwagen, S. Brandt, W. Busza, I.A. Cali, M. D'Alfonso, Z. Demiragli, L. Di Matteo, G. Gomez Ceballos, M. Goncharov, D. Hsu, Y. Iiyama, G.M. Innocenti, M. Klute, D. Kovalskyi, K. Krajczar, Y.S. Lai, Y.-J. Lee, A. Levin, P.D. Luckey, B. Maier, A.C. Marini, C. McGinn, C. Mironov, S. Narayanan, X. Niu, C. Paus, C. Roland, G. Roland, J. Salfeld-Nebgen, G.S.F. Stephans, K. Tatar, M. Varma, D. Velicanu, J. Veverka, J. Wang, T.W. Wang, B. Wyslouch, M. Yang

University of Minnesota, Minneapolis, USA

A.C. Benvenuti, R.M. Chatterjee, A. Evans, P. Hansen, S. Kalafut, S.C. Kao, Y. Kubota, Z. Lesko, J. Mans, S. Nourbakhsh, N. Ruckstuhl, R. Rusack, N. Tambe, J. Turkewitz

University of Mississippi, Oxford, USA

J.G. Acosta, S. Oliveros

University of Nebraska-Lincoln, Lincoln, USA

E. Avdeeva, K. Bloom, D.R. Claes, C. Fangmeier, R. Gonzalez Suarez, R. Kamalieddin, I. Kravchenko, A. Malta Rodrigues, F. Meier, J. Monroy, J.E. Siado, G.R. Snow, B. Stieger

State University of New York at Buffalo, Buffalo, USA

M. Alyari, J. Dolen, A. Godshalk, C. Harrington, I. Iashvili, J. Kaisen, A. Kharchilava, A. Parker, S. Rappoccio, B. Roozbahani

Northeastern University, Boston, USA

G. Alverson, E. Barberis, A. Hortiangtham, A. Massironi, D.M. Morse, D. Nash, T. Orimoto, R. Teixeira De Lima, D. Trocino, R.-J. Wang, D. Wood

Northwestern University, Evanston, USA

S. Bhattacharya, O. Charaf, K.A. Hahn, A. Kumar, N. Mucia, N. Odell, B. Pollack, M.H. Schmitt, K. Sung, M. Trovato, M. Velasco

University of Notre Dame, Notre Dame, USA

N. Dev, M. Hildreth, K. Hurtado Anampa, C. Jessop, D.J. Karmgard, N. Kellams, K. Lannon, N. Marinelli, F. Meng, C. Mueller, Y. Musienko³⁶, M. Planer, A. Reinsvold, R. Ruchti, G. Smith, S. Taroni, M. Wayne, M. Wolf, A. Woodard

The Ohio State University, Columbus, USA

J. Alimena, L. Antonelli, B. Bylsma, L.S. Durkin, S. Flowers, B. Francis, A. Hart, C. Hill, R. Hughes, W. Ji, B. Liu, W. Luo, D. Puigh, B.L. Winer, H.W. Wulsin

Princeton University, Princeton, USA

S. Cooperstein, O. Driga, P. Elmer, J. Hardenbrook, P. Hebda, D. Lange, J. Luo, D. Marlow, T. Medvedeva, K. Mei, J. Olsen, C. Palmer, P. Piroué, D. Stickland, A. Svyatkovskiy, C. Tully

University of Puerto Rico, Mayaguez, USA

S. Malik

Purdue University, West Lafayette, USA

A. Barker, V.E. Barnes, S. Folgueras, L. Gutay, M.K. Jha, M. Jones, A.W. Jung, A. Khatiwada, D.H. Miller, N. Neumeister, J.F. Schulte, X. Shi, J. Sun, F. Wang, W. Xie

Purdue University Calumet, Hammond, USA

N. Parashar, J. Stupak

Rice University, Houston, USA

A. Adair, B. Akgun, Z. Chen, K.M. Ecklund, F.J.M. Geurts, M. Guilbaud, W. Li, B. Michlin, M. Northup, B.P. Padley, J. Roberts, J. Rorie, Z. Tu, J. Zabel

University of Rochester, Rochester, USA

B. Betchart, A. Bodek, P. de Barbaro, R. Demina, Y.t. Duh, T. Ferbel, M. Galanti, A. Garcia-Bellido, J. Han, O. Hindrichs, A. Khukhunaishvili, K.H. Lo, P. Tan, M. Verzetti

Rutgers, The State University of New Jersey, Piscataway, USA

A. Agapitos, J.P. Chou, Y. Gershtein, T.A. Gómez Espinosa, E. Halkiadakis, M. Heindl, E. Hughes, S. Kaplan, R. Kunnawalkam Elayavalli, S. Kyriacou, A. Lath, K. Nash, H. Saka, S. Salur, S. Schnetzer, D. Sheffield, S. Somalwar, R. Stone, S. Thomas, P. Thomassen, M. Walker

University of Tennessee, Knoxville, USA

A.G. Delannoy, M. Foerster, J. Heideman, G. Riley, K. Rose, S. Spanier, K. Thapa

Texas A&M University, College Station, USA

O. Bouhali⁷⁰, A. Celik, M. Dalchenko, M. De Mattia, A. Delgado, S. Dildick, R. Eusebi, J. Gilmore, T. Huang, E. Juska, T. Kamon⁷¹, R. Mueller, Y. Pakhotin, R. Patel, A. Perloff, L. Perniè, D. Rathjens, A. Safonov, A. Tatarinov, K.A. Ulmer

Texas Tech University, Lubbock, USA

N. Akchurin, C. Cowden, J. Damgov, F. De Guio, C. Dragoiu, P.R. Duerdo, J. Faulkner, E. Gurpinar, S. Kunori, K. Lamichhane, S.W. Lee, T. Libeiro, T. Peltola, S. Undleeb, I. Volobouev, Z. Wang

Vanderbilt University, Nashville, USA

S. Greene, A. Gurrola, R. Janjam, W. Johns, C. Maguire, A. Melo, H. Ni, P. Sheldon, S. Tuo, J. Velkovska, Q. Xu

University of Virginia, Charlottesville, USA

M.W. Arenton, P. Barria, B. Cox, J. Goodell, R. Hirosky, A. Ledovskoy, H. Li, C. Neu, T. Sinthuprasith, X. Sun, Y. Wang, E. Wolfe, F. Xia

Wayne State University, Detroit, USA

C. Clarke, R. Harr, P.E. Karchin, J. Sturdy

University of Wisconsin - Madison, Madison, WI, USA

D.A. Belknap, J. Buchanan, C. Caillol, S. Dasu, L. Dodd, S. Duric, B. Gomber, M. Grothe, M. Herndon, A. Hervé, P. Klabbers, A. Lanaro, A. Levine, K. Long, R. Loveless, I. Ojalvo, T. Perry, G.A. Pierro, G. Polese, T. Ruggles, A. Savin, N. Smith, W.H. Smith, D. Taylor, N. Woods

†: Deceased

- 1: Also at Vienna University of Technology, Vienna, Austria
- 2: Also at State Key Laboratory of Nuclear Physics and Technology, Peking University, Beijing, China
- 3: Also at Institut Pluridisciplinaire Hubert Curien (IPHC), Université de Strasbourg, CNRS/IN2P3, Strasbourg, France
- 4: Also at Universidade Estadual de Campinas, Campinas, Brazil
- 5: Also at Universidade Federal de Pelotas, Pelotas, Brazil
- 6: Also at Université Libre de Bruxelles, Bruxelles, Belgium
- 7: Also at Deutsches Elektronen-Synchrotron, Hamburg, Germany
- 8: Also at Joint Institute for Nuclear Research, Dubna, Russia
- 9: Now at Ain Shams University, Cairo, Egypt
- 10: Now at British University in Egypt, Cairo, Egypt
- 11: Also at Zewail City of Science and Technology, Zewail, Egypt
- 12: Also at Université de Haute Alsace, Mulhouse, France
- 13: Also at Skobeltsyn Institute of Nuclear Physics, Lomonosov Moscow State University, Moscow, Russia
- 14: Also at Tbilisi State University, Tbilisi, Georgia
- 15: Also at CERN, European Organization for Nuclear Research, Geneva, Switzerland
- 16: Also at RWTH Aachen University, III. Physikalisches Institut A, Aachen, Germany
- 17: Also at University of Hamburg, Hamburg, Germany
- 18: Also at Brandenburg University of Technology, Cottbus, Germany
- 19: Also at Institute of Nuclear Research ATOMKI, Debrecen, Hungary
- 20: Also at MTA-ELTE Lendület CMS Particle and Nuclear Physics Group, Eötvös Loránd University, Budapest, Hungary
- 21: Also at Institute of Physics, University of Debrecen, Debrecen, Hungary
- 22: Also at Indian Institute of Science Education and Research, Bhopal, India
- 23: Also at Institute of Physics, Bhubaneswar, India
- 24: Also at University of Visva-Bharati, Santiniketan, India
- 25: Also at University of Ruhuna, Matara, Sri Lanka
- 26: Also at Isfahan University of Technology, Isfahan, Iran
- 27: Also at Yazd University, Yazd, Iran
- 28: Also at Plasma Physics Research Center, Science and Research Branch, Islamic Azad University, Tehran, Iran
- 29: Also at Università degli Studi di Siena, Siena, Italy
- 30: Also at Laboratori Nazionali di Legnaro dell'INFN, Legnaro, Italy
- 31: Also at Purdue University, West Lafayette, USA
- 32: Also at International Islamic University of Malaysia, Kuala Lumpur, Malaysia
- 33: Also at Malaysian Nuclear Agency, MOSTI, Kajang, Malaysia
- 34: Also at Consejo Nacional de Ciencia y Tecnología, Mexico city, Mexico
- 35: Also at Warsaw University of Technology, Institute of Electronic Systems, Warsaw, Poland
- 36: Also at Institute for Nuclear Research, Moscow, Russia
- 37: Now at National Research Nuclear University 'Moscow Engineering Physics Institute' (MEPhI), Moscow, Russia
- 38: Also at St. Petersburg State Polytechnical University, St. Petersburg, Russia
- 39: Also at University of Florida, Gainesville, USA
- 40: Also at California Institute of Technology, Pasadena, USA
- 41: Also at Budker Institute of Nuclear Physics, Novosibirsk, Russia
- 42: Also at Faculty of Physics, University of Belgrade, Belgrade, Serbia

- 43: Also at INFN Sezione di Roma; Università di Roma, Roma, Italy
- 44: Also at University of Belgrade, Faculty of Physics and Vinca Institute of Nuclear Sciences, Belgrade, Serbia
- 45: Also at Scuola Normale e Sezione dell'INFN, Pisa, Italy
- 46: Also at National and Kapodistrian University of Athens, Athens, Greece
- 47: Also at Riga Technical University, Riga, Latvia
- 48: Also at Institute for Theoretical and Experimental Physics, Moscow, Russia
- 49: Also at Albert Einstein Center for Fundamental Physics, Bern, Switzerland
- 50: Also at Gaziosmanpasa University, Tokat, Turkey
- 51: Also at Adiyaman University, Adiyaman, Turkey
- 52: Also at Istanbul Aydin University, Istanbul, Turkey
- 53: Also at Mersin University, Mersin, Turkey
- 54: Also at Cag University, Mersin, Turkey
- 55: Also at Piri Reis University, Istanbul, Turkey
- 56: Also at Ozyegin University, Istanbul, Turkey
- 57: Also at Izmir Institute of Technology, Izmir, Turkey
- 58: Also at Marmara University, Istanbul, Turkey
- 59: Also at Kafkas University, Kars, Turkey
- 60: Also at Istanbul Bilgi University, Istanbul, Turkey
- 61: Also at Yildiz Technical University, Istanbul, Turkey
- 62: Also at Hacettepe University, Ankara, Turkey
- 63: Also at Rutherford Appleton Laboratory, Didcot, United Kingdom
- 64: Also at School of Physics and Astronomy, University of Southampton, Southampton, United Kingdom
- 65: Also at Instituto de Astrofísica de Canarias, La Laguna, Spain
- 66: Also at Utah Valley University, Orem, USA
- 67: Also at Argonne National Laboratory, Argonne, USA
- 68: Also at Erzincan University, Erzincan, Turkey
- 69: Also at Mimar Sinan University, Istanbul, Istanbul, Turkey
- 70: Also at Texas A&M University at Qatar, Doha, Qatar
- 71: Also at Kyungpook National University, Daegu, Korea